CHAPTER VI
THE EFFECT OF COMPATIBILIZERS CONTENTS ON MORPHOLOGY, THERMAL, AND MECHANICAL PROPERTIES OF PLA/MODIFIED ETHYLENE(VINYL ACETATE) BLENDS

6.1 Abstract

This study aims to improve the morphology, thermal and mechanical properties of polylactic acid (PLA) by blending it with modified ethylene (vinyl acetate) (mEVA). Then their compatibility is improved by adding a reactive compatibilizers, Ethylene-glycidyl methacrylate copolymer (E-GMA), ethylene-methyl acrylate-glycidyl methacrylate terpolymer (T-GMA), Ethylene-acrylic acid copolymer (PE-AA), and Poly(2-ethyl-2-oxazoline) (Oxa). The PLA/mEVA blends at ratios of 100/0, 90/10, 80/20, 70/30 and 60/40 w/w were prepared in a co-rotating twin-screw extruder with screw speed 30 rpm. The effect of the compatibilizers loading was determined by adding 5, 10, and 15 phr of compatibilizers to the PLA/mEVA blends. The increasing of compatibilizers loading in the PLA/mEVA blends caused an increase in glass transition temperature (T_g) (from 55 °C to 60 °C) and elongation at break of the binary blends. Morphological interpretation through FE-SEM revealed the improved compatibility of the PLA/mEVA blends in the presence of compatibilizers.

Keywords : Catalytic reactive extrusion, Compatibilizer, Ethylene (vinyl acetate) (EVA), Poly(lactic acid) (PLA)

6.2 Introduction

Poly(lactic acid) (PLA), produced from renewable resources (e.g., wheat, rice, sugar or corn), is one of the most important bio-based and biodegradable polymers. It can be biodegraded within 4-5 weeks by heat. Although PLA has several

favorable properties such as, high strength and stiffness at room temperature, the limitation of PLA is brittleness. In recent years, there are several methods to improve PLA properties such as plasticization, copolymerization and blending with various biodegradable and non- biodegradable polymers. For these methods, blending PLA with other polymers is the most effective and convenient way to improve PLA properties. However, phase separation of PLA and other polymers can occur due to thermodynamical incompatibility, resulting in the limitation of toughness improvement.

Ethylene (Vinyl Acetate) (EVA) is the copolymer of ethylene and vinyl acetate. For Vinyl Acetate (VA), it is an extremely elastic material that can be sintered to form a porous material similar to rubber. Therefore, softness and flexibility of EVA can improve properties of PLA and its blend can be processed like other thermoplastics. There are many researches focusing on the improvement in the properties of PLA. Ma et al. (2012) studied compatibility between poly(lactic acid) (PLA) and Ethylene (Vinyl Acetate) (EVA). They found that PLA is miscible with poly(vinyl acetate) (PVAc) but not miscible with polyethylene (PE). As a result, the optimum toughening effect of EVA on the PLA (impact and tensile properties) was obtained at a VA content of 50-60%. This suggests that introduction of hydroxyl groups to EVA chains via catalytic reactive extrusion makes EVA more polar and miscible with polar polymers.

As mentioned above, phase separation of PLA and other polymers can occur due to thermodynamical incompatibility, resulting in the reduction of blend performance. Compatibility of immiscible blends can be done by adding a compatibilizer (third phase) in order to reduce the interfacial tension coefficient and stabilize the desired morphology (Utracki L.A., 2002). As a consequence, mechanical properties and phase morphology of these immiscible blends can be improved.

This chapter studied the effect of compatibilizers contents on morphology, thermal, and mechanical properties by using thermogravimetric analysis (TGA),

differential scanning calorimeter (DSC), dynamic mechanical analyzer (DMA), field emission scanning electron microscope (FE-SEM), the universal testing machine, melt flow indexer, and biodegradability testing.

6.3 Materials

6.3.1 Poly(lactic acid) (PLA) was purchased from BC Polymer. It is an extrusion grade with CAS Number 9002-97-5.

6.3.2 Ethylene(vinyl acetate) (EVA) was purchased from Sigma-Aldrich. It has 18 wt% of vinyl acetate with CAS Number 24937-78-8.

6.3.3 Ethylene-glycidyl methacrylate, or E-GMA(CAS Number 26061-90-5) was purchased from Sigma-Aldrich.

6.3.4 Ethylene-acrylate ester-glycidyl methacrylate terpolymer, or T-GMA (CAS Number 51541-08-3) was purchased from Sigma-Aldrich.

6.3.5 Ethylene-acrylic acid copolymer, or PE-AA (CAS Number 9010-77 – 9) was purchased from Sigma-Aldrich.

6.3.6 Poly(2-ethyl-2-oxazoline), or Oxa (CAS Number 25805-17-8) was purchased from Sigma-Aldrich.

6.4 Methodology

6.4.1 Preparation of PLA/ Modified EVA/compatibilizers blends

PLA/mEVA blends/compatibilizer with different blend ratios shown in Table 6.1, were fed into the twin-screw extruder. Temperature profiles were 140, 150, 160, 165, 165, 165, 165, 165, 165 and 160 °C from feed zone to die. Screw speed was 30 rpm. Then, the blends were dried in vacuum oven at 40°C for 24 hours before characterization by using FE-SEM, FTIR, DSC, DMA, TGA and tensile testing.

Table 6.1 The blend compositions of PLA/Modified EVA/compatibilizer blends

PLA (wt%)	mEVA (wt%)	Compatibilizer	
		Type	Content (phr)
90 80 70 60	10 20 30 40	Ethylene glycidyl methacrylate copolymer	5
			10
			15
		Ethylene-acrylate ester-glycidyl methacrylate terpolymer	5
			10
			15
		Ethylene-acrylic acid copolymer	5
			10
			15
		Poly(2-ethyl-2-oxazoline)	5
			10
			15

6.4.2 Preparation of specimens for testing by Injection molding.

The blends obtained from twin-screw extruder were prepared into dumbbell-shape for tensile test. The operating temperature was 130 °C, screw speed was 160 rpm, molding pressure was 35 bars, mold temperature was 30-40 °C, decompression stoke was 73 mm, pressure for closing mold was 210 bar, holding time in the mold was 5 sec and cool down in dumbbell-shape mold.

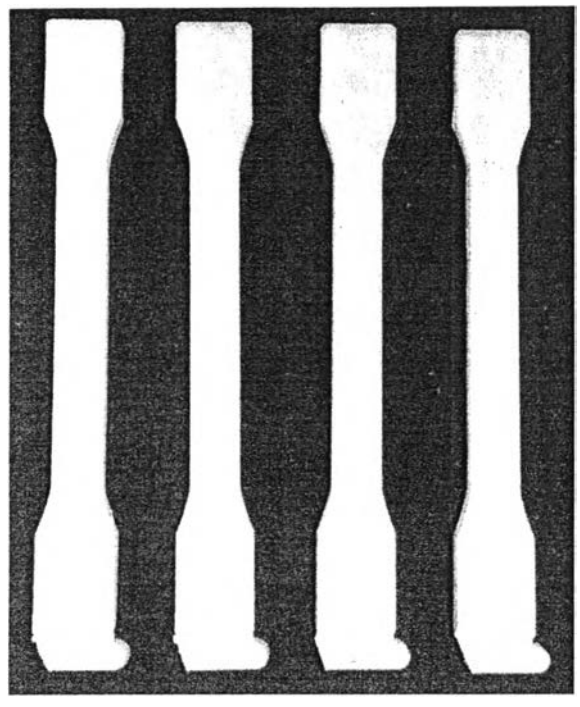

Figure 6.1 Dumbbell-shape samples by injection molding.

6.5 Characterization

6.5.1 Characterizations and mechanical testing of PLA/ Modified EVA/compatibilizer blends

6.5.1.1 Chemical Structure Analysis

The functional groups along the blends backbone were studied by using Thermo Nicolet Nexus 670 Fourier Transform Infrared Spectroscope (FTIR). For sample preparation, the blends were compressed into films. The spectra will be record over the wave number range of 4000 - 400 cm^{-1} with 32 scans at a resolution of 4 cm^{-1}.

6.5.1.2 Thermal Stability Analysis

Thermogravimetric analysis (TGA) was used to determine the degradation temperature (T_d) of the blends by using the temperature range of 30-800 °C and the heating rate of 10 °C/min under nitrogen gas atmosphere.

6.5.1.3 Thermal Properties and Crystallization Behavior Characterization

The glass transition temperature (T_g), melting temperature (T_m), and cold crystallization temperature (T_{cc}) were performed by using differential scanning calorimeter (Mettler Toledo, DSC822). The samples were heated from 30 to 190 °C with the heating rate of 10°C/min. Then they were cooled to -30 °C with the cooling rate of 10°C/min and reheated at the 190 °C at the same condition. Degree of crystallization (χ_c) was calculated by

$$\chi_c = \frac{\Delta H_m - \Delta H_{cc}}{\Delta H_m^0 \times w} \times 100 \qquad (6.1)$$

ΔH_m is the enthalpy of melting, ΔH_{cc} is the enthalpy of cold crystallization, ΔH_m^0 is the enthalpy of melting for 100% crystalline PLA sample, taken as 93.1 J/g (Salamone, J. C., 1996), w is the weight fraction of PLA in the composite.

6.5.1.4 Dynamic Mechanical Properties Test

The storage modulus (E′), the loss modulus (E″), and the dissipation factor (tan δ) of the modified EVA were determined by using Dynamic Mechanical Analyzer (DMA). The tension mode was used in the temperature range from -100 °C to 40 °C. The sample size was 10 mm × 40 mm × 4 mm in width × length × depth. The amplitude was 30.0 μm and the frequency was 1 Hz.

6.5.1.5 Morphology characterization

The fracture surface of samples was coated by Pt and then the phase compatibilization of samples was examined by using the field emission scanning electron microscope (FE-SEM).

6.5.1.6 Physical Properties Testing

The tensile strength, %elongation at break and Young's modulus will be measured by using the universal testing machine.

6.5.1.7 Melt Flow Indexer

The melt flow index of the blends was tested by using Zwick, Model4105 melt flow indexer. The sample which had weight in the range of 5-8 g was melted at 160 °C. The melt was driven through a capillary die using a 1 kg piston, melt time 120 seconds, and cut time 30 seconds. Repeat the entire procedure 5 times and average the results.

6.5.1.8 Biodegradability Testing

The samples (10×40×1 mm^3) were test according to ASTM D5988 – 03 (Standard Test Method for Determining Aerobic Biodegradation in Soil of Plastic Materials or Residual Plastic Materials after Composting). During the course of this testing, weight remaining was measured every week for 8 weeks. The weight loss was evaluated using the follow equation:

$$\text{Weight loss (\%)} = \{(w_0-w_i)/ w_0\}\times 100 \qquad (6.2)$$

Where w_0 and w_i are the sample weight before and after the biodegradation tests, respectively.

6.6 Results and discussion

6.6.1 Ethylene-glycidyl methacrylate copolymer (E-GMA)

6.6.1.1 Chemical analysis

Epoxy group of E-GMA compatibilizer reacts with the carboxylic or hydroxyl end group of PLA and hydroxyl group of mEVA to form ester linkage which is shown in figure 6.2-6.3. From this reaction, it is the cause of

decrease of epoxy, carboxylic and hydroxyl groups. On the contrary, the increment of ester group is observed in the blends.

FTIR spectra of Pure PLA and PLA/mEVA/E-GMA blends with different E-GMA contents are shown in Figures 6.4. FTIR spectra and Table 6.3 show the characteristic peak of pure PLA which compose of C=O stretching at 1730 cm^{-1} corresponding to carboxylic group and carbonyl group of PLA, O-H stretching at 3500 cm^{-1} corresponding to hydroxyl group and C-H stretching at 2850 cm^{-1} corresponding to CH_2 and CH aliphatic, the characteristic peak of mEVA which compose of C=O stretching at 1730 cm^{-1} corresponding to carbonyl group of vinyl acetate, O-H stretching at 3500 cm^{-1} corresponding to hydroxyl group and C-H stretching at 2850 cm^{-1} corresponding to CH_2 and CH aliphatic and the characteristic peak of E-GMA which compose of C-O stretching at 910 cm^{-1} corresponding to epoxy group, C=O stretching at 1730 cm^{-1} corresponding to carbonyl group and C-H stretching at 2850 cm^{-1} corresponding to CH_2 and CH aliphatic [22]. From Table 6.2, the absorbance ratio of the peak at 910/2850 cm^{-1} which is attributed to the epoxy group of E-GMA and the absorbance ratio of the peak at 1200/2850 cm^{-1} which is attributed to the ester linkage of the blend[22,23]. The absorbance ratio of the peak at 910/2850 cm^{-1}, 1730/2850 cm^{-1} and 3500/2850 cm^{-1} decrease however, the absorbance ratio of the peak at 1200/2850 cm^{-1} increase, suggesting the occurrence of chemical reactions between the epoxy groups of E-GMA and carboxylic end groups or hydroxyl end group of PLA and hydroxyl group of mEVA to from ester linkage.

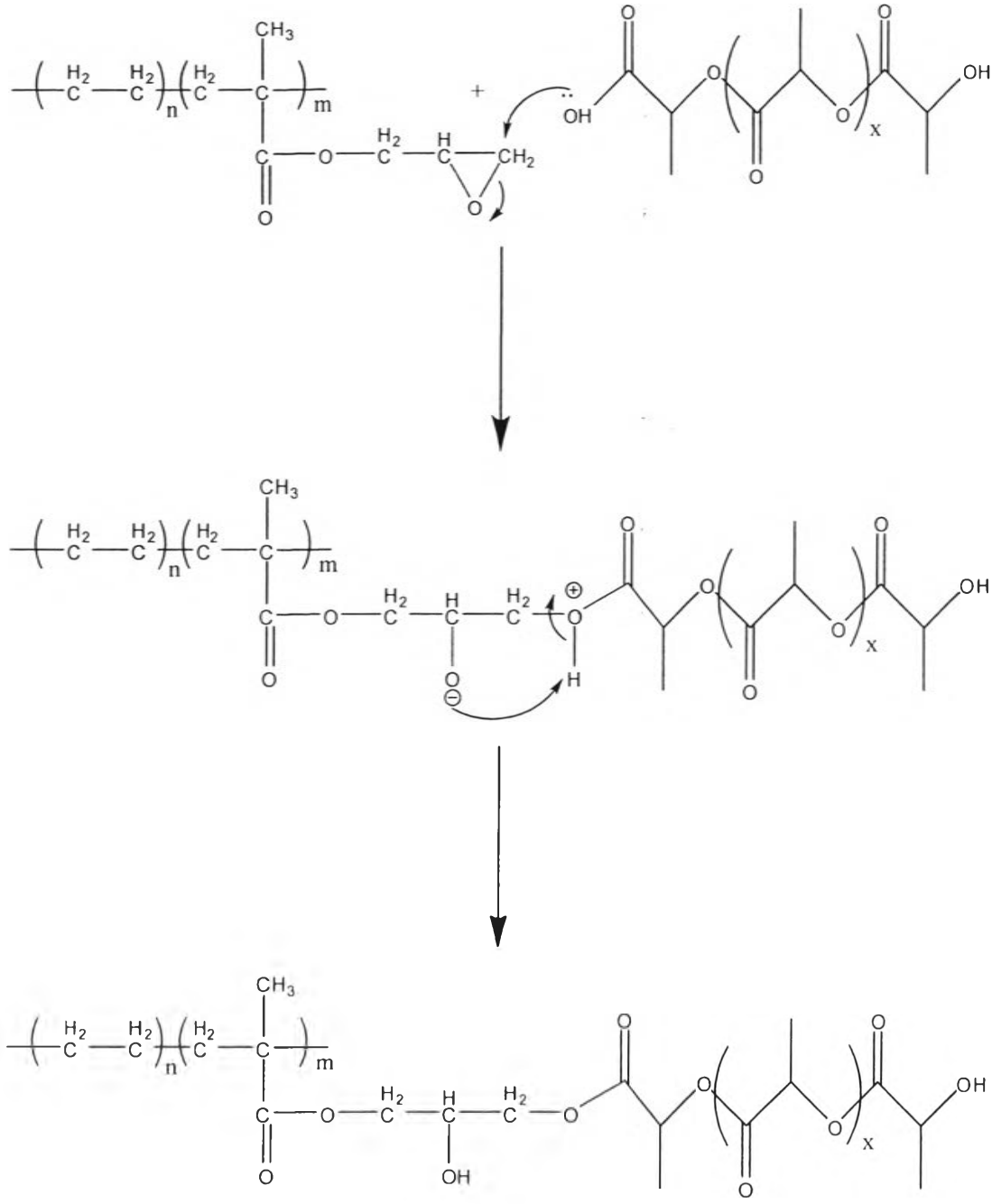

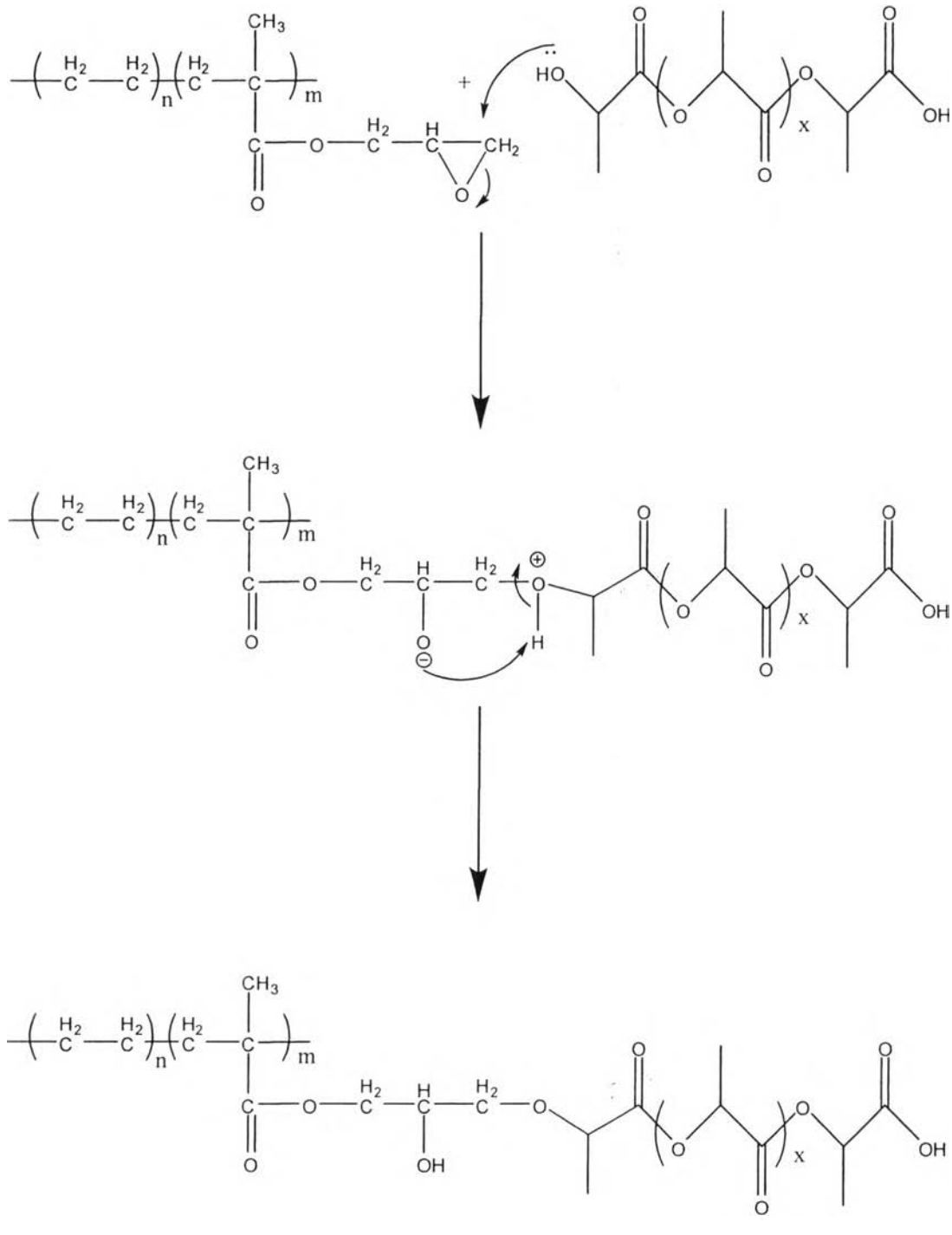

Figure 6.2 Reaction of –COOH and –OH groups of PLA with epoxy group of E-GMA compatibilizer.

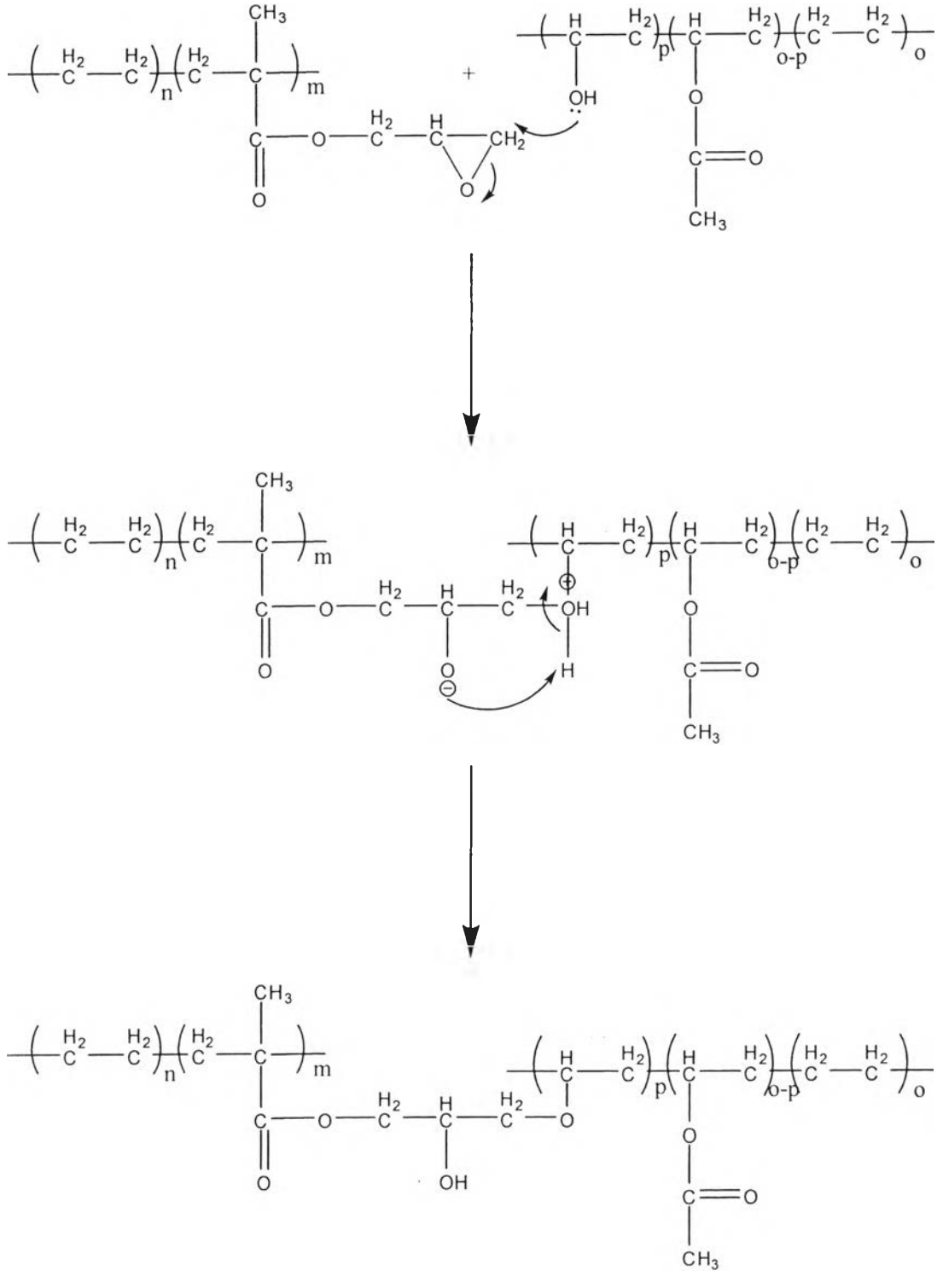

Figure 6.3 Reaction of –OH groups of mEVA with epoxy group of E-GMA compatibilizer.

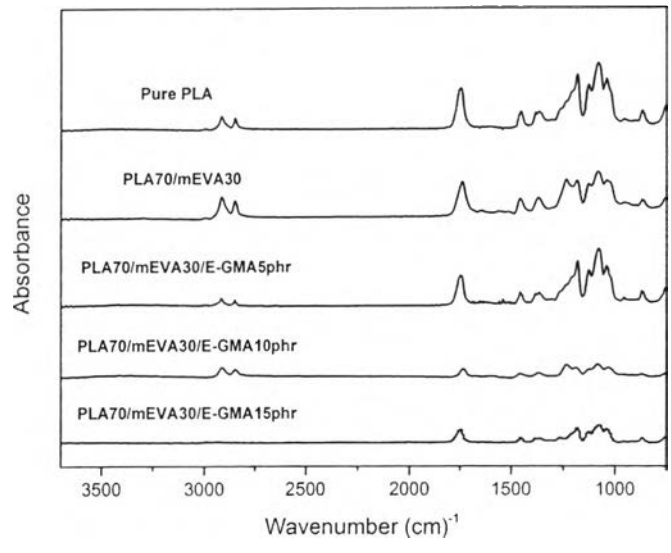

Figure 6.4 FTIR spectra of PLA/mEVA (70/30 w/w) blends at various E-GMA contents.

Table 6.2 Absorbance ratio of pure PLA, PLA/mEVA binary blends and PLA/mEVA/E-GMA blends

absorbance ratio	Pure PLA	PLA/mEVA	PLA/mEVA/ E-GMA 5 phr	PLA/mEVA/ E-GMA 10 phr	PLA/mEVA/ E-GMA 15 phr
910/2850 peak	0.57	0.62	0.72	0.68	0.67
1200/2850 peak	0.81	0.89	0.90	0.99	0.94
1730/2850 peak	0.87	0.89	0.85	0.83	0.80
3500/2850 peak	0.77	0.78	0.75	0.70	0.71

Table 6.3 Assignment of absorbance of PLA, mEVA and E-GMA

Materials	Absorbance (cm^{-1})	Assignment
PLA	1200	C-O stretching of Ester group
	1730	C=O stretching of Carbonyl group and Carboxylic group
	2850	C-H stretching of CH_2 and CH aliphatic
	3500	O-H (H-bonded), usually broad of Hydroxyl group
mEVA	1200	C-O stretching of Ester group
	1730	C=O stretching of Carbonyl group
	2850	C-H stretching of CH_2 and CH aliphatic
	3500	O-H (H-bonded), usually broad of Hydroxyl group
E-GMA	910	C-O stretching of epoxy group
	1200	C-O stretching of Ester group
	1730	C=O stretching of Carbonyl group
	2850	C-H stretching of CH_2 and CH aliphatic

6.6.1.2 Thermal stability

TGA thermograms of PLA/mEVA/E-GMA blends with various E-GMA contents are shown in Figures 6.5-6.8 and Table 6.4. Correspondingly, all PLA/mEVA/E-GMA blends display two steps of degradation as shown in Table 6.4. At the same blend ratio, the decomposition temperatures of PLA/mEVA/E-GMA blends are higher than those of PLA/mEVA binary blend due to the dehydration of hydroxyl group of PLA and thermal cleavage of ester linkage by hydrolysis and scission of C–O and C–C bonds [1]. For addition of E-GMA compatibilizer, the results reveal that the decomposition temperatures of PLA/mEVA/E-GMA blends decline with the additional E-GMA contents.

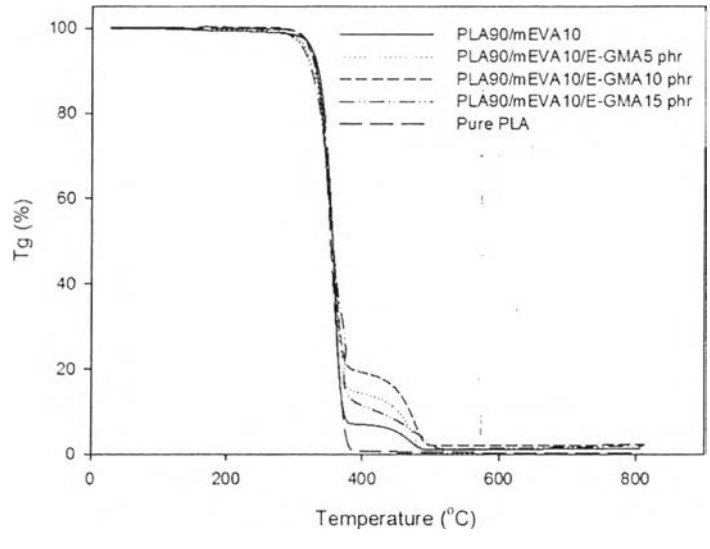

Figure 6.5 TGA thermograms of PLA/mEVA (90/10 w/w) blends at various E-GMA contents.

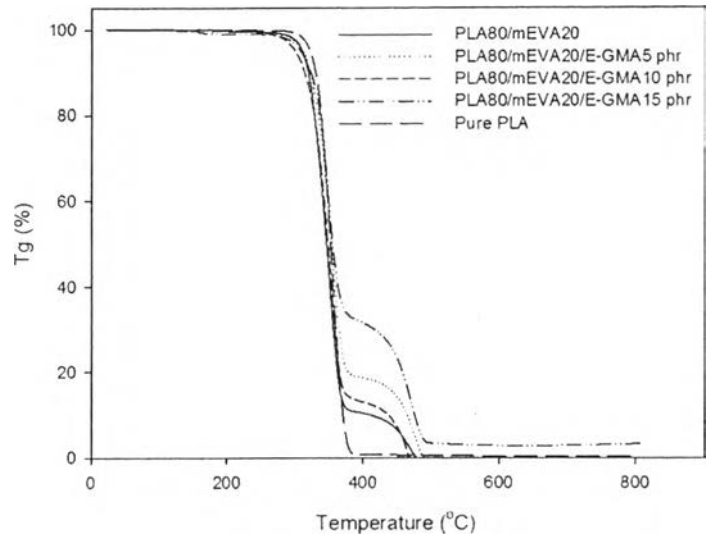

Figure 6.6 TGA thermograms of PLA/mEVA (80/20 w/w) blends at various E-GMA contents.

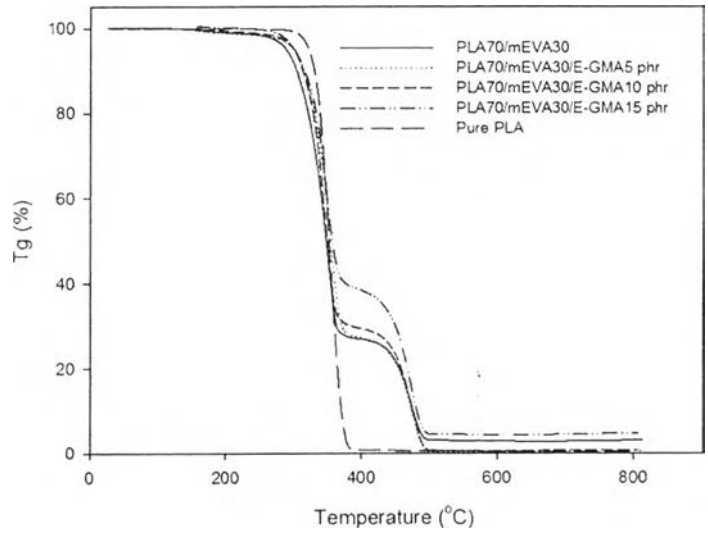

Figure 6.7 TGA thermograms of PLA/mEVA (70/30 w/w) blends at various E-GMA contents.

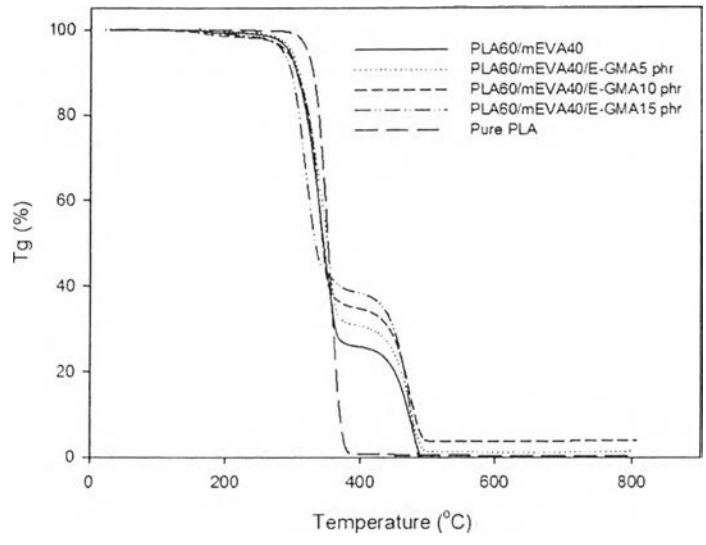

Figure 6.8 TGA thermograms of PLA/mEVA (60/40 w/w) blends at various E-GMA contents.

Table 6.4 Decomposition temperatures of pure PLA, pure mEVA, PLA/mEVA binary blends and PLA/mEVA/E-GMA blends

Blend composition	Decomposition Temperature (°C)	
	1st	2nd
PLA	332.8	-
mEVA	351.5	468.0
PLA90/mEVA10	351.2	471.0
E-GMA 5 phr	359.8	474.8
E-GMA 10 phr	354.0	475.1
E-GMA 15 phr	355.3	476.2
PLA80/mEVA20	351.3	472.1
E-GMA 5 phr	355.1	472.5
E-GMA 10 phr	346.6	471.0
E-GMA 15 phr	347.9	471.8
PLA70/mEVA30	342.9	471.0
E-GMA 5 phr	349.2	472.4
E-GMA 10 phr	343.5	471.3
E-GMA 15 phr	344.4	471.6
PLA60/mEVA40	334.6	469.7
E-GMA 5 phr	343.7	469.8
E-GMA 10 phr	338.9	470.1
E-GMA 15 phr	338.6	470.8

6.6.1.3 Thermal properties

In Figures 6.9-6.12, the thermal properties of PLA/mEVA/E-GMA blends with various E-GMA contents is inspected via DSC curves in which the melting temperature (T_m), cold crystallization temperature (T_{cc}), degree of crystallization (χ_c) and two glass transition temperatures (around -25 °C for mEVA

and around 60 °C for PLA) are clearly exhibited in Table 6.5. The results show that the glass transition temperatures of PLA/mEVA/E-GMA blends increase with the supplement of E-GMA contents due to the hindrance of molecular chain motion which is occurred via the ester linkage reaction between epoxy groups of E-GMA and hydroxyl group of PLA [2]. The melting temperature of PLA/mEVA/E-GMA blends is not significant change from PLA/mEVA binary blends. However, degree of crystallization is higher than those of the binary blends but degree of crystallization decreases with increasing E-GMA contents. This indicates that E-GMA inhibit crystallization of PLA due to steric effect of E-GMA molecule.

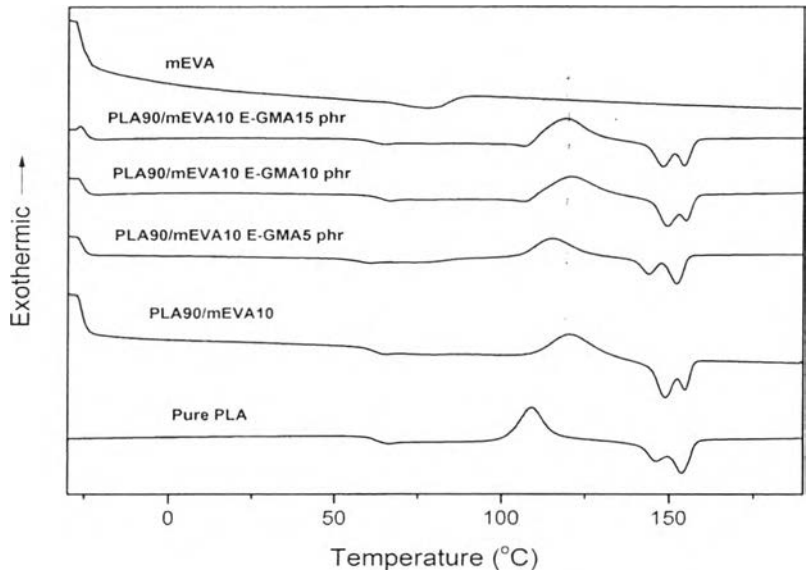

Figure 6.9 DSC thermograms of PLA/mEVA (90/10 w/w) blends at various E-GMA contents.

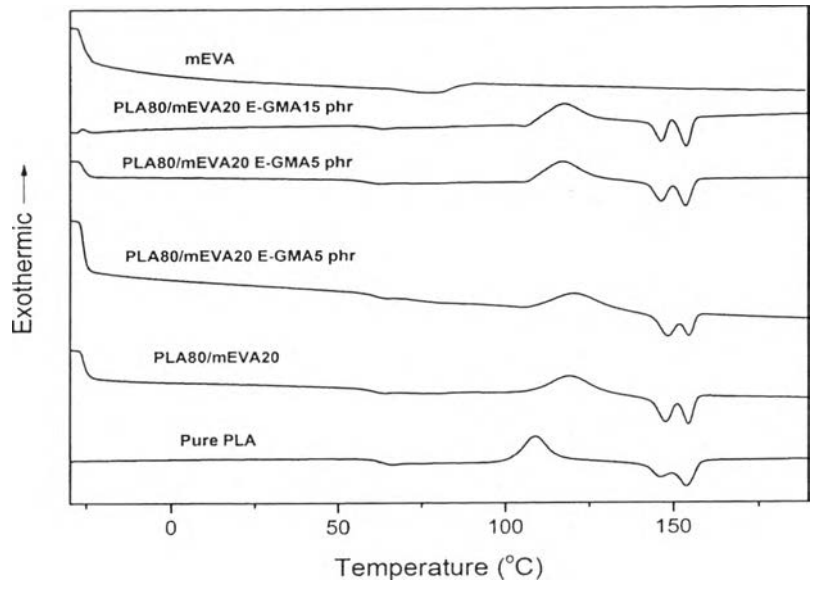

Figure 6.10 DSC thermograms of PLA/mEVA (80/20 w/w) blends at various E-GMA contents.

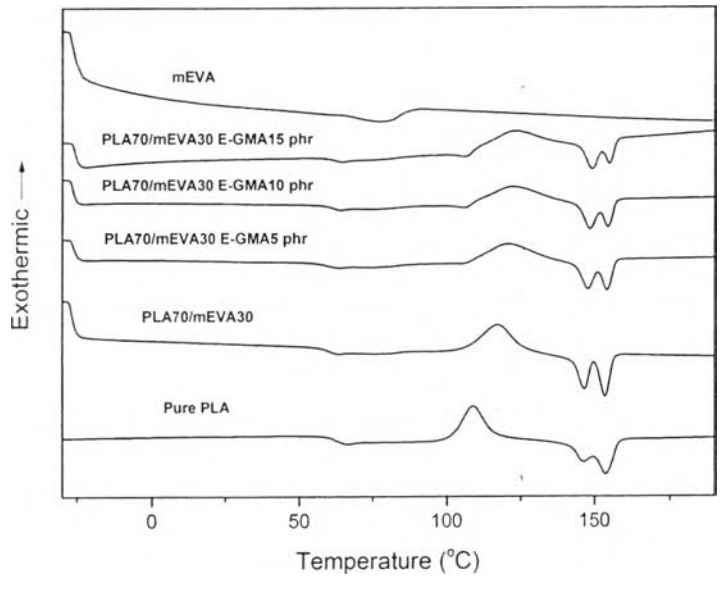

Figure 6.11 DSC thermograms of PLA/mEVA (70/30 w/w) blends at various E-GMA contents.

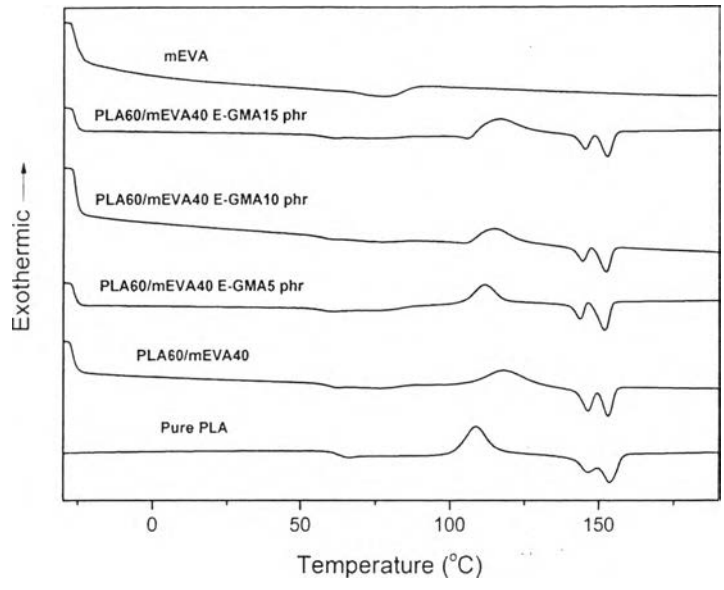

Figure 6.12 DSC thermograms of PLA/mEVA (60/40 w/w) blends at various E-GMA contents.

Table 6.5 Thermal properties of pure PLA, PLA/mEVA binary blends and PLA/mEVA/E-GMA blends

Sample	T_{g1} (°C)	T_{g2} (°C)	T_{cc} (°C)	T_{m1} (°C)	T_{m2} (°C)	ΔH_{cc} (J/g)	ΔH_m (J/g)	$\%\chi_c$
Pure PLA	-	57.9	103.0	146.8	153.7	19.4	24.5	5.45
PLA90/mEVA10	-26.8	58.6	120.3	148.9	154.8	26.9	28.3	1.72
E-GMA5 phr	-26.9	55.1	115.0	149.3	155.0	19.9	21.4	1.81
E-GMA10 phr	-26.5	59.7	120.5	148.0	154.3	23.2	24.7	1.77
E-GMA15 phr	-26.1	60.8	118.5	144.1	152.2	23.0	24.4	1.75
PLA80/mEVA20	-26.6	57.0	119.3	147.8	154.4	26.9	27.9	1.34
E-GMA5 phr	-27.0	56.1	120.7	148.6	154.6	22.4	24.5	2.81
E-GMA10 phr	-27.0	56.1	117.2	146.4	153.6	24.5	26.1	2.08
E-GMA15 phr	-26.2	56.9	117.6	146.6	153.8	22.9	23.4	0.74
PLA70/mEVA30	-27.7	56.4	117.0	146.6	153.7	27.2	27.9	1.15
E-GMA5 phr	-27.2	55.5	120.7	147.7	154.2	18.3	19.5	1.86
E-GMA10 phr	-27.3	58.6	122.3	148.6	154.6	19.4	20.3	1.37
E-GMA15 phr	-26.6	60.0	136.9	149.3	155.1	21.8	22.7	1.40
PLA60/mEVA40	-27.8	55.9	118.3	146.2	159.2	22.3	22.9	1.06
E-GMA5 phr	-27.0	53.7	111.7	143.6	152.0	17.8	18.6	1.41
E-GMA10 phr	-26.9	54.6	125.1	144.6	152.6	16.7	17.4	1.40
E-GMA15 phr	-27.3	56.2	116.8	145.2	152.0	17.7	18.3	0.98

6.6.1.4 Dynamic mechanical properties

The effect of E-GMA compatibilizer on the storage modulus and loss modulus are indicated in Figures 6.13-6.20 and Table 6.6. It is obviously demonstrated that the storage modulus at room temperature (30 °C) of PLA/mEVA/E-GMA blends decreases with the increase in E-GMA contents. As a result of the storage modulus, the excess amount of E-GMA, a very soft material, leads to the reduction in stiffness [3]. Furthermore, the composition of PLA/mEVA/E-GMA blends at 5 phr E-GMA exhibits the optimum storage modulus with the lowest compatibilizer content.

However, PLA/mEVA blends in the presence of E-GMA compatibilizer cause the enrichment in T_g as shown in Figures 6.21-6.24 and Table 6.6. The results imply that the reaction between E-GMA phase and PLA/mEVA

phase obstructs the molecular chain motion. Therefore, the glass transition temperature of PLA/mEVA/E-GMA blends increase with the additional E-GMA contents.

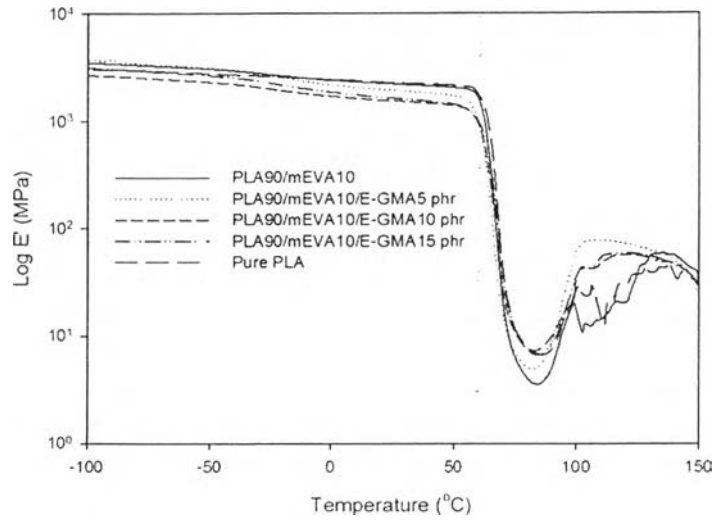

Figure 6.13 Storage Modulus of PLA/mEVA (90/10 w/w) blends at various E-GMA contents.

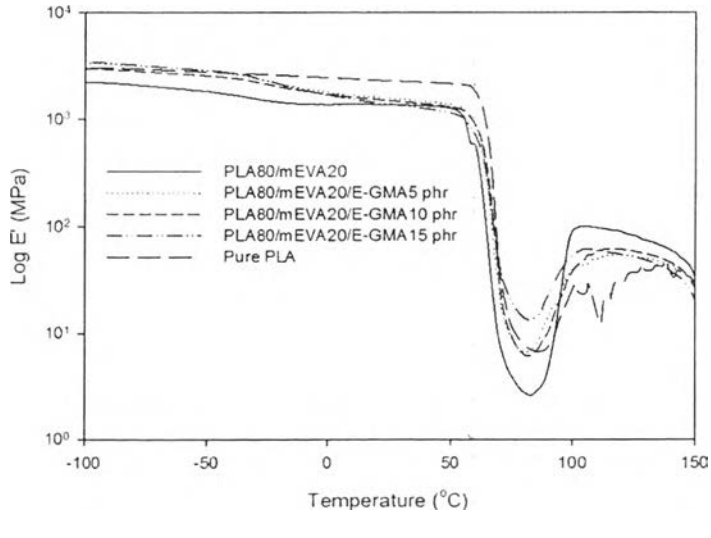

Figure 6.14 Storage Modulus of PLA/mEVA (80/20 w/w) blends at various E-GMA contents.

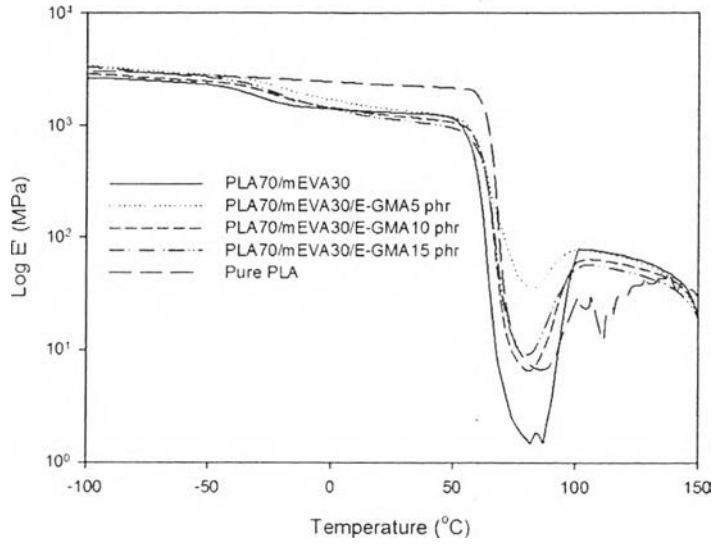

Figure 6.15 Storage Modulus of PLA/mEVA (70/30 w/w) blends at various E-GMA contents.

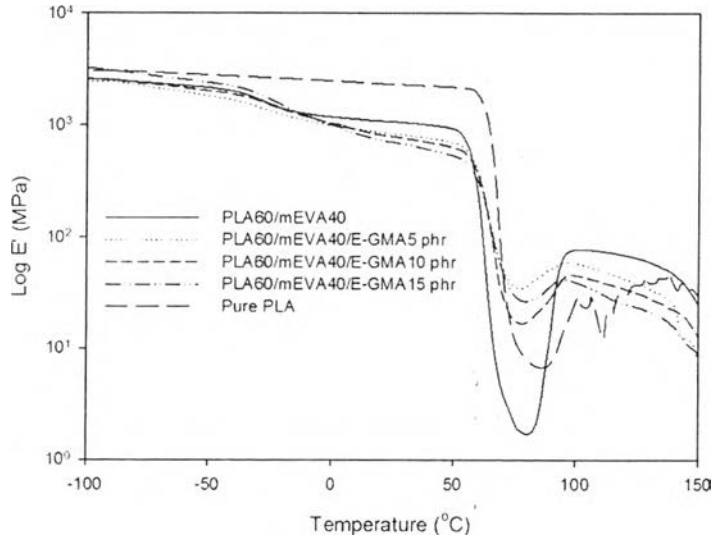

Figure 6.16 Storage Modulus of PLA/mEVA (60/40 w/w) blends at various E-GMA contents.

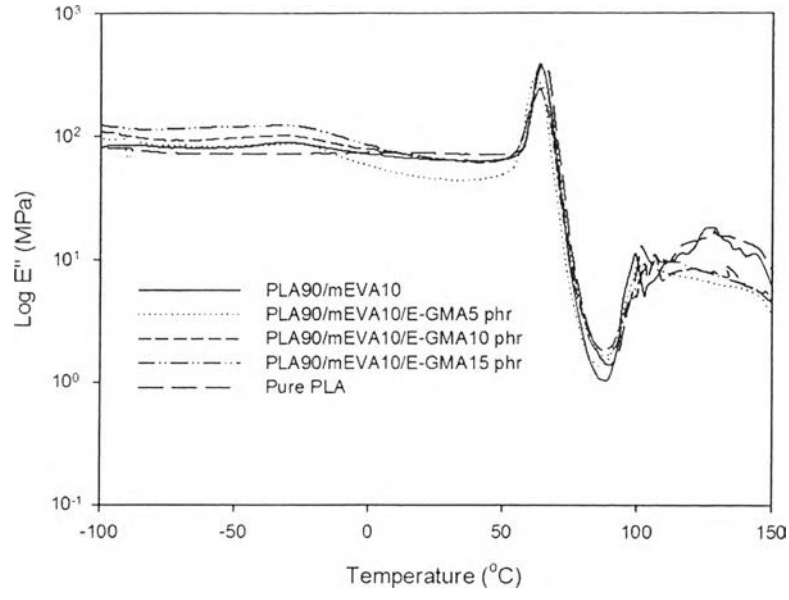

Figure 6.17 Loss Modulus of PLA/mEVA blends (90/10 w/w) at various E-GMA contents.

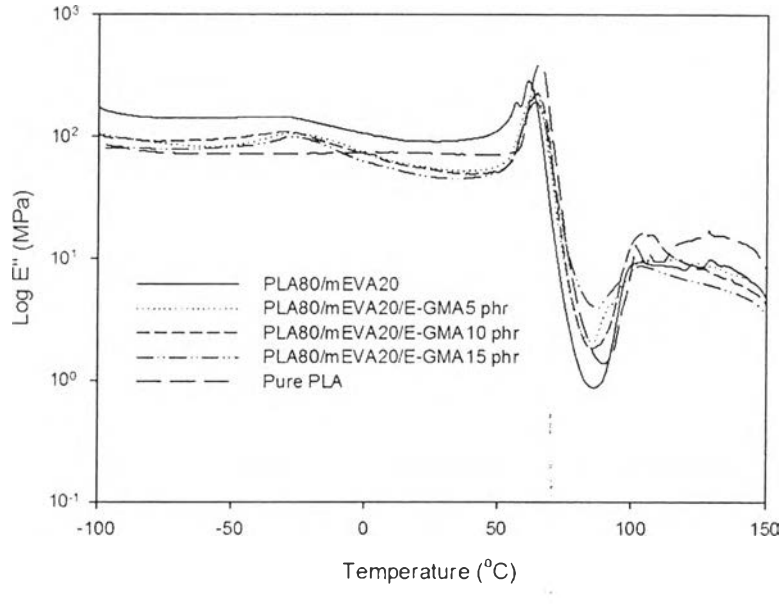

Figure 6.18 Loss Modulus of PLA/mEVA blends (80/20 w/w) at various E-GMA contents.

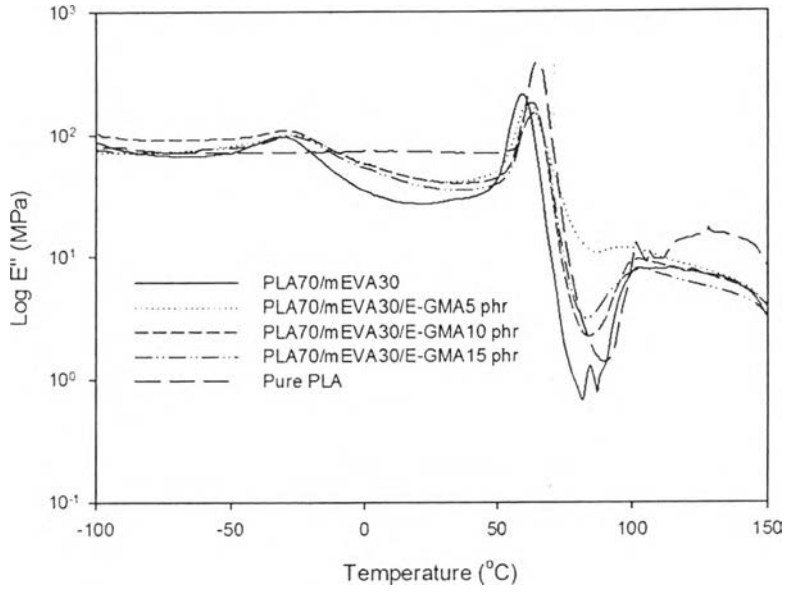

Figure 6.19 Loss Modulus of PLA/mEVA blends (70/30 w/w) at various E-GMA contents.

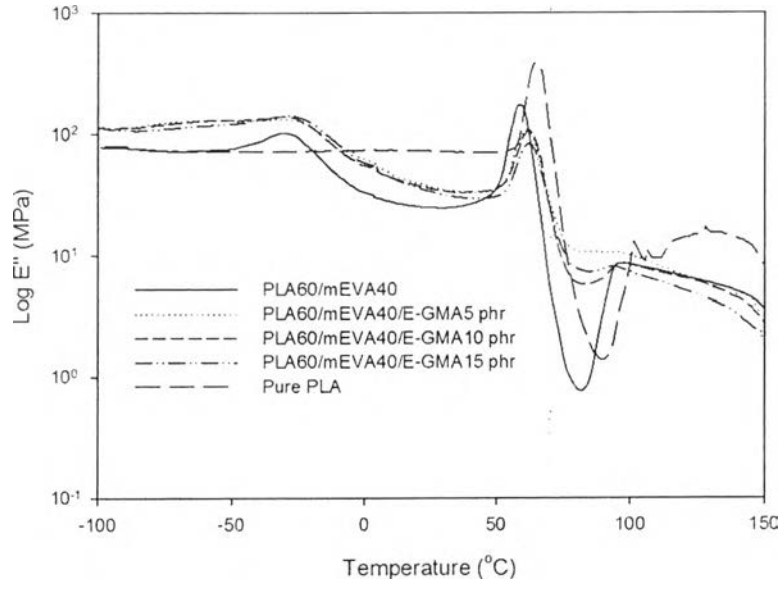

Figure 6.20 Loss Modulus of PLA/mEVA blends (60/40 w/w) at various E-GMA contents.

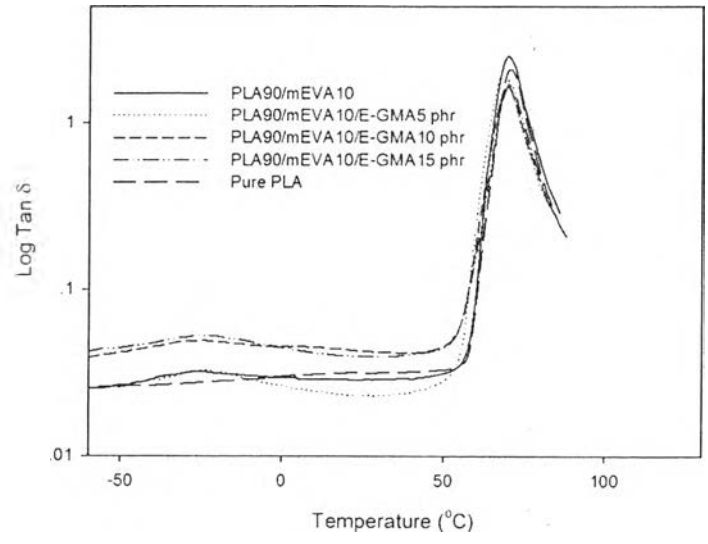

Figure 6.21 Tan δ of PLA/mEVA (90/10 w/w) blends at various E-GMA contents.

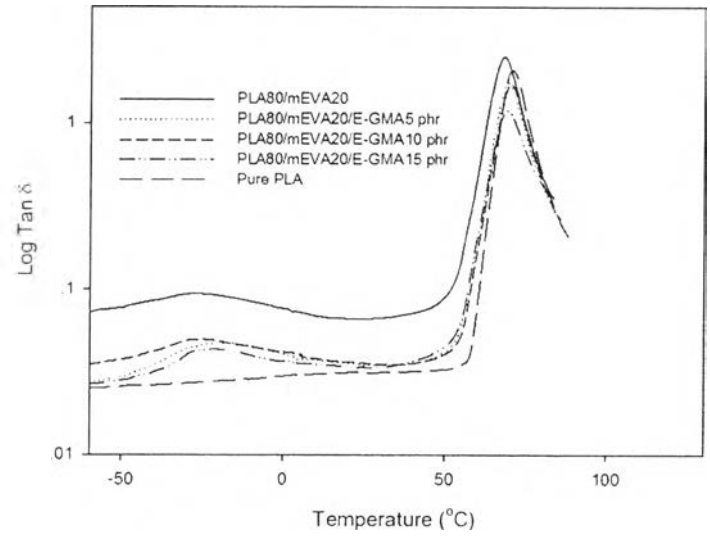

Figure 6.22 Tan δ of PLA/mEVA (80/20 w/w) blends at various E-GMA contents.

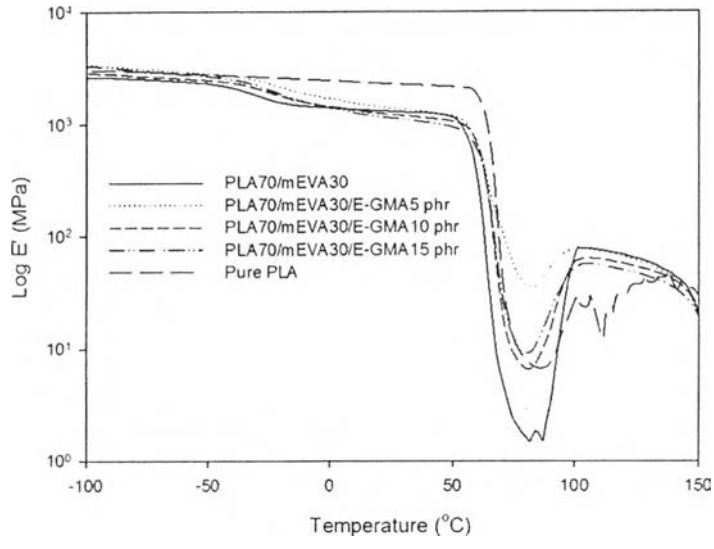

Figure 6.23 Tan δ of PLA/mEVA (70/30 w/w) blends at various E-GMA contents.

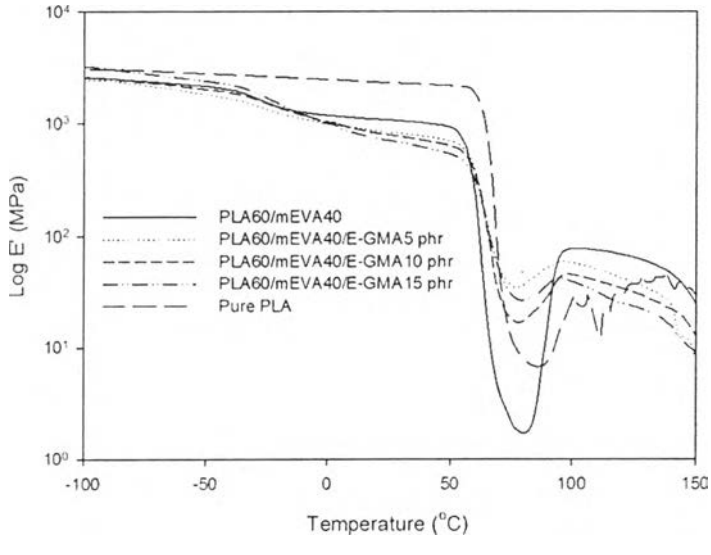

Figure 6.24 Tan δ of PLA/mEVA (60/40 w/w) blends at various E-GMA contents.

Table 6.6 Dynamic mechanical properties of pure PLA, pure mEVA, PLA/mEVA binary blends and PLA/mEVA/E-GMA blends

Blend composition	Tan $\delta_{max,1}$ (Tg_1, °C)	Tan $\delta_{max,2}$ (Tg_2, °C)	30 °C E′ (MPa)
PLA	70.1	-	2280
mEVA	-20	-	12
PLA90/mEVA10	-26.9	70	2208
E-GMA 5 phr	-23.7	70.2	1910
E-GMA 10 phr	-23.7	70.3	1520
E-GMA 15 phr	-25.7	70.5	1610
PLA80/mEVA20	-27.8	68.2	1364
E-GMA 5 phr	-25.7	70.2	1540
E-GMA 10 phr	-25.7	70.2	1460
E-GMA 15 phr	-21.5	70.3	1340
PLA70/mEVA30	-27.8	66.6	1290
E-GMA 5 phr	-21.8	66	1363
E-GMA 10 phr	-25.6	70.3	1194
E-GMA 15 phr	-21.5	70.1	1102
PLA60/mEVA40	-28.6	66.4	1048
E-GMA 5 phr	-23.5	66.4	811
E-GMA 10 phr	-26.1	66.5	758
E-GMA 15 phr	-21.8	66.5	669

6.6.1.5 Morphology

FE-SEM images of the cryogenic fracture of PLA/mEVA (70/30 w/w) blends with different E-GMA contents are presented in Figures 6.25a.-6.25d. In Figure 6.25a, the spherulites are the mEVA in PLA/mEVA blend [4] and the binary blend exhibits two-phase structure of mEVA domain and PLA matrix. On the other hand, Figures 6.25b-6.25d (blends with E-GMA compatibilizer) show better compatibility between mEVA and PLA matrix. With the incorporation of E-GMA compatibilizer, the mEVA domain sizes are decrease that confirms E-GMA can act as the effective compatibilizer in PLA/mEVA blends.

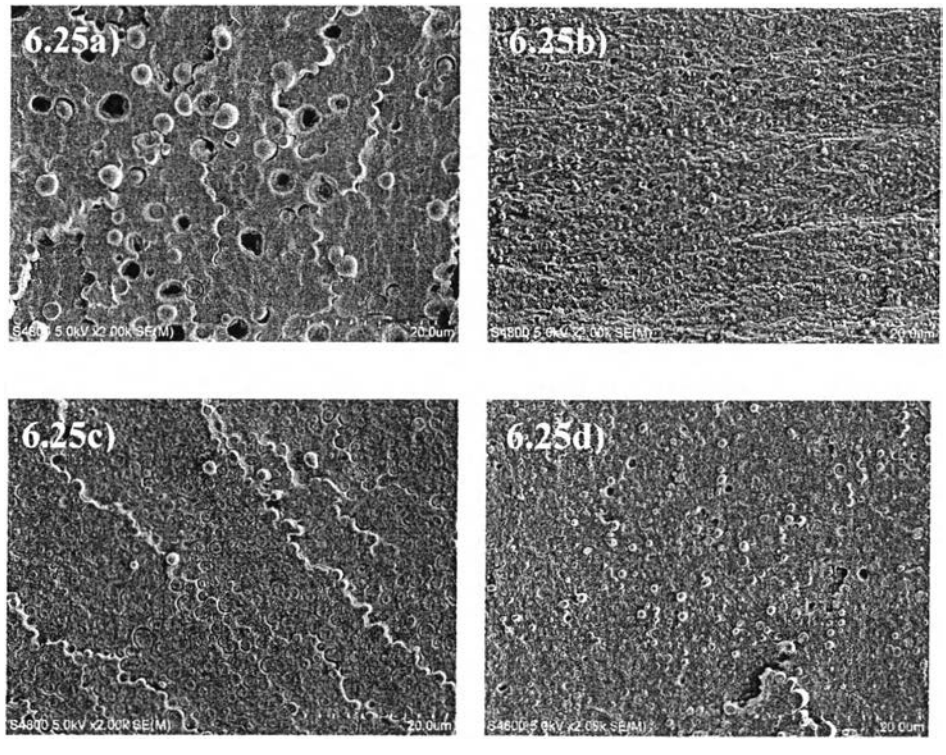

Figure 6.25 SEM images of the fracture of the blends (a) PLA/mEVA (70/30 w/w) blend (b) PLA/mEVA/E-GMA5 phr blend (c) PLA/mEVA/E-GMA10 phr blend (d) PLA/mEVA/E-GMA15 phr blend.

6.6.1.6 Mechanical properties

The effect of E-GMA compatibilizer on the tensile properties is exhibited in Figures 6.26-6.28. With the incorporation of E-GMA compatibilizer, the Young's modulus and tensile strength of the binary blends decrease; however elongation at break increases due to the enhancement in the interfacial adhesion between PLA and mEVA phase occurred via the reaction between epoxy group of GMA and hydroxyl group of PLA [1]. According to the elongation at break of all the blends depending only the amount of E-GMA contents, an excess amount of E-GMA (15 phr) leads to the lower tensile properties because of the agglomeration of E-GMA particles induced to the weak point of PLA/mEVA/E-GMA blends. From these results, the PLA/mEVA/E-GMA blends with the lowest compatibilizer content (10 phr of E-GMA) is obviously obtained the optimum elongation at break.

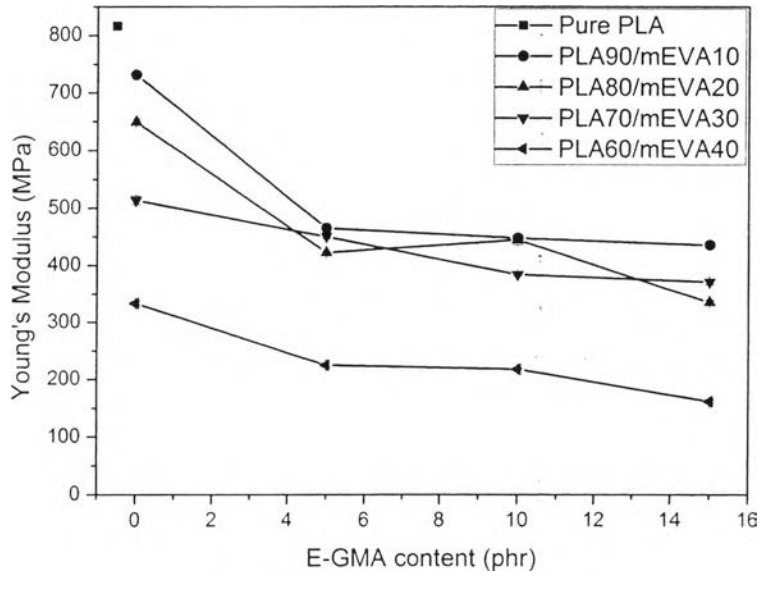

Figure 6.26 Young's modulus of PLA/mEVA blends at various E-GMA contents.

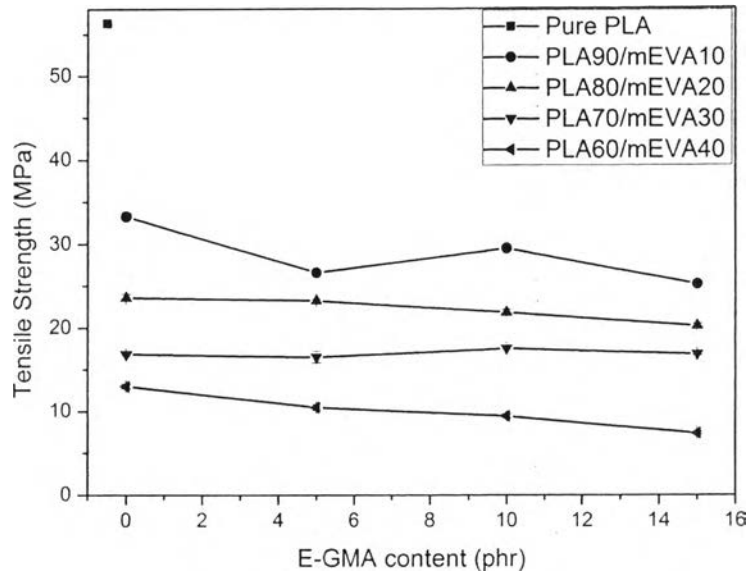

Figure 6.27 Tensile strength of PLA/mEVA blends at various E-GMA contents.

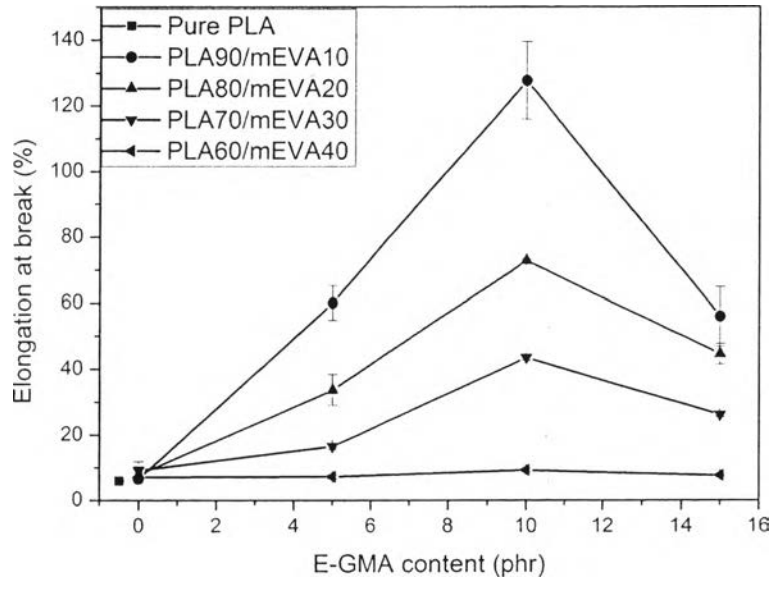

Figure 6.28 Elongation at break of PLA/mEVA blends at various E-GMA contents.

6.6.1.7 Melt flow index (MFI)

MFI values of PLA/mEVA/E-GMA blends with various E-GMA contents are represented in Figure 6.29. The addition of E-GMA in the PLA/mEVA blends leads to a reduction of the MFI values. These MFI results are confirming that reaction between E-GMA compatibilizer and PLA/mEVA blends restricts the polymer chain mobility and also enhances the polymer viscosity [2].

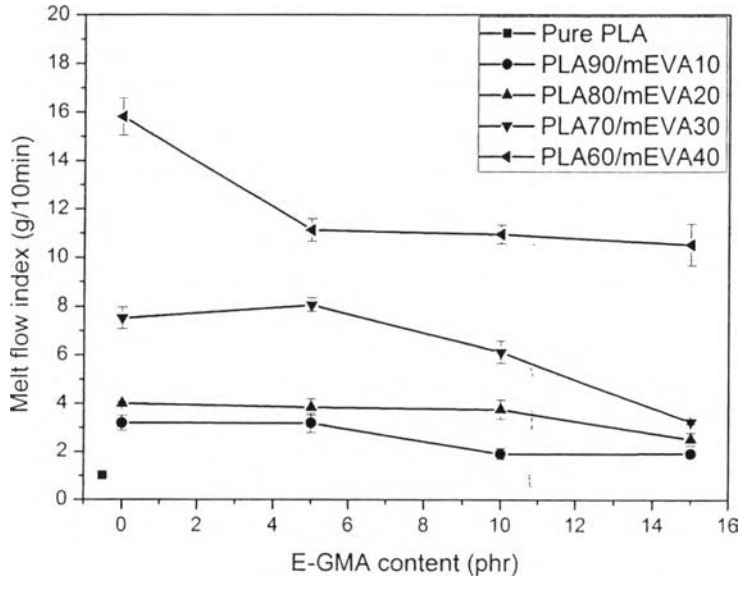

Figure 6.29 MFI values of PLA/mEVA blends at various E-GMA contents.

6.6.1.8 Biodegradability

The biodegradability refers to weight loss of pure PLA, PLA/mEVA binary blends and PLA/mEVA with various E-GMA contents are represented in Figure 6.30. With the incorporation of E-GMA compatibilizer, the weight loss of PLA/mEVA/E-GMA blends is slightly lower than that of PLA/mEVA binary blend and decreases with increasing of E-GMA contents. This suggests that E-GMA retard biodegradable property of PLA blends.

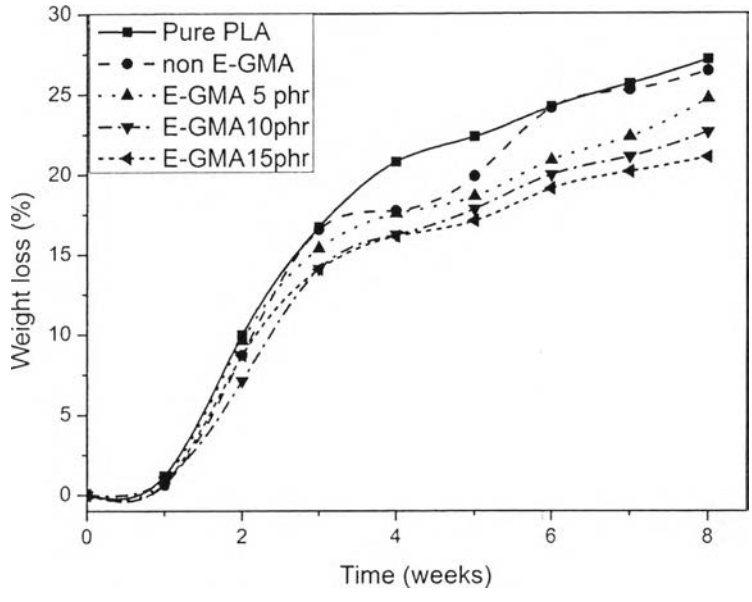

Figure 6.30 Weight loss of PLA/mEVA (90/10 w/w) blends at various E-GMA contents.

6.6.2 Ethylene-methyl acrylate-glycidyl methacrylate terpolymer (T-GMA)

6.6.2.1 Chemical analysis

Epoxy group of T-GMA compatibilizer reacts with the carboxylic end group or hydroxyl end group of PLA and hydroxyl group of mEVA to form ester linkage which is shown in Figure 6.31-6.32. From this reaction, it is the cause of decrease of epoxy, carboxylic and hydroxyl groups. On the other hand, increasing of ester group of the blends is occurring.

FTIR spectra of Pure PLA and PLA/mEVA/T-GMA blends with different T-GMA contents are exhibited in Figures 6.33. FTIR spectra and Table 6.8 show the characteristic peak of pure PLA which compose of C=O stretching at 1730 cm^{-1} corresponding to carboxylic group and carbonyl group of PLA, O-H stretching at 3500 cm^{-1} corresponding to hydroxyl group and C-H stretching at 2850 cm^{-1} corresponding to CH_2 and CH aliphatic, the characteristic peak of mEVA which compose of C=O stretching at 1730 cm^{-1} corresponding to carbonyl group of vinyl acetate, O-H stretching at 3500 cm^{-1} corresponding to

hydroxyl group and C-H stretching at 2850 cm^{-1} corresponding to CH_2 and CH aliphatic and the characteristic peak of T-GMA which compose of C-O stretching at 910 cm^{-1} corresponding to epoxy group, C=O stretching at 1730 cm^{-1} corresponding to carbonyl group and C-H stretching at 2850 cm^{-1} corresponding to CH_2 and CH aliphatic. From Table 6.7, the absorbance ratio of the peak at 910/2850 cm^{-1} which is attributed to the epoxy group of T-GMA and the absorbance ratio of the peak at 1200/2850 cm^{-1} which is attributed to the ester linkage of the blend[22,23]. For PLA/mEVA/T-GMA blends, the disappearance of the characteristic peak of the epoxy group of T-GMA at 910/2850 cm^{-1}, the increment of the absorbance ratio at 1200/2850 cm^{-1} and the reduction of the absorbance ratio at 1730/2850 cm^{-1} and 3500/2850 cm^{-1} which is shown in Table 6.7. All these changes confirm the reactions occurring between the epoxy groups of T-GMA and carboxylic end groups of PLA or hydroxyl end group of PLA and hydroxyl group of mEVA to from ester linkage [23].

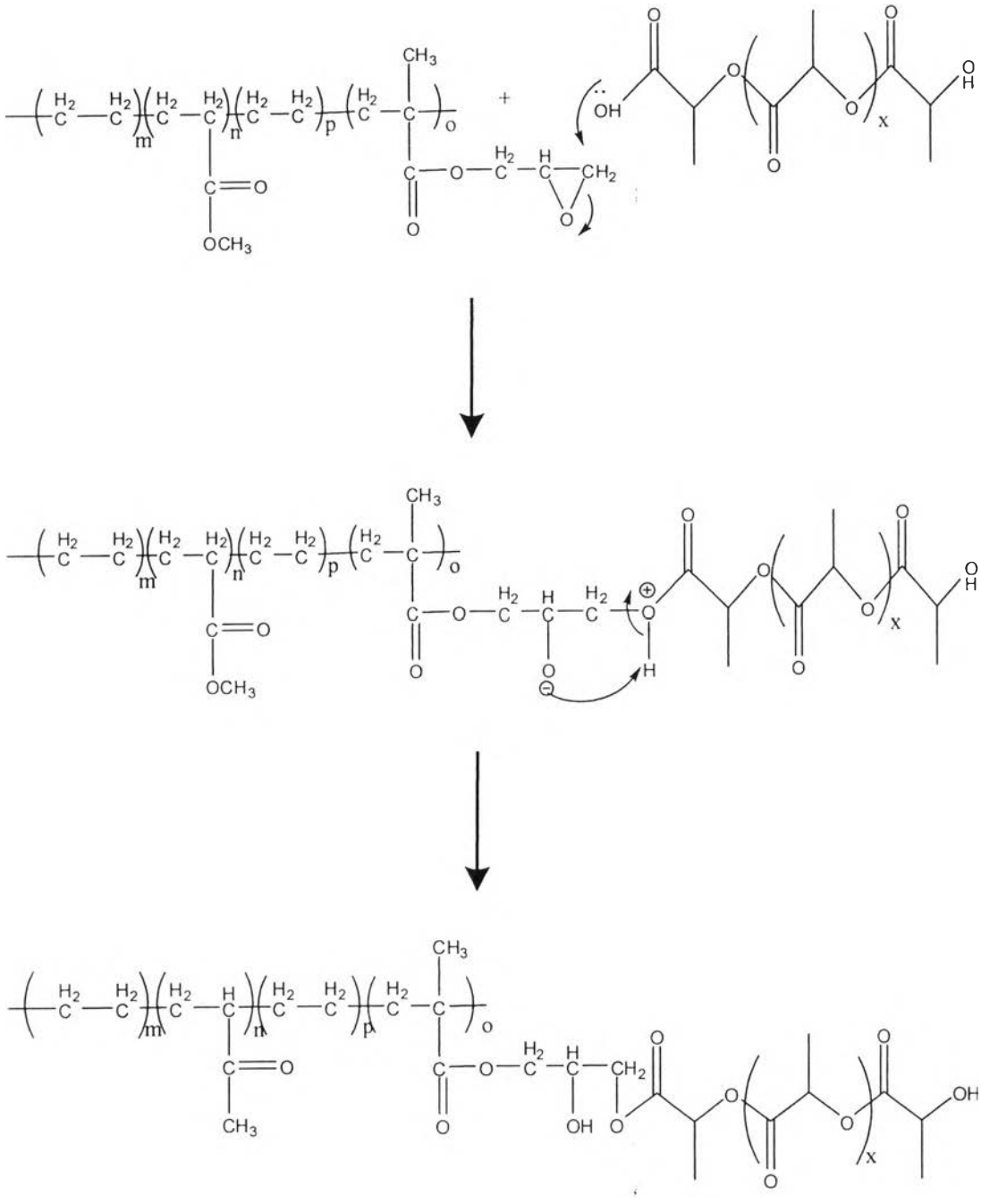

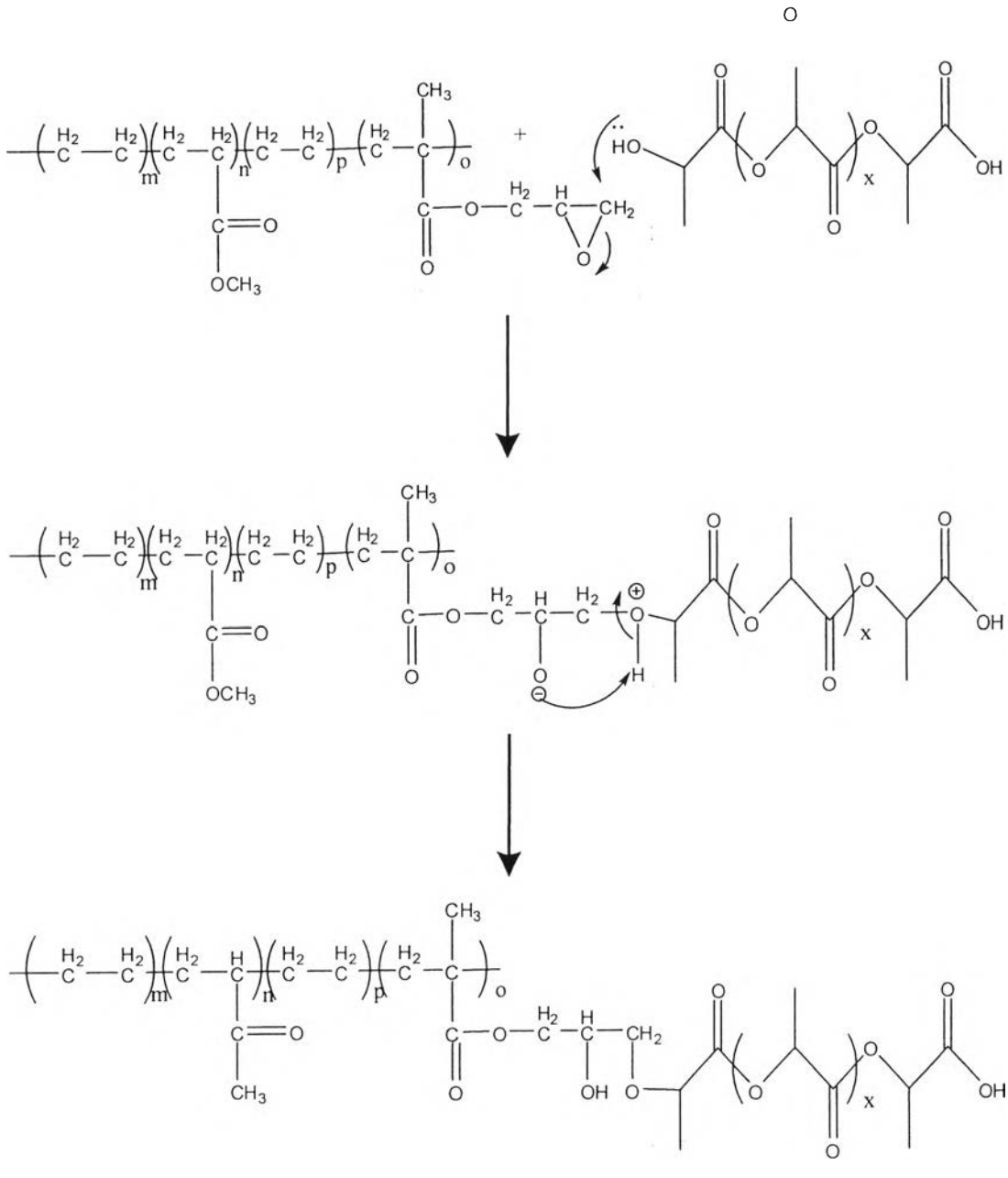

Figure 6.31 Reaction of –COOH and -OH groups of PLA with GMA unit of T-GMA compatibilizer.

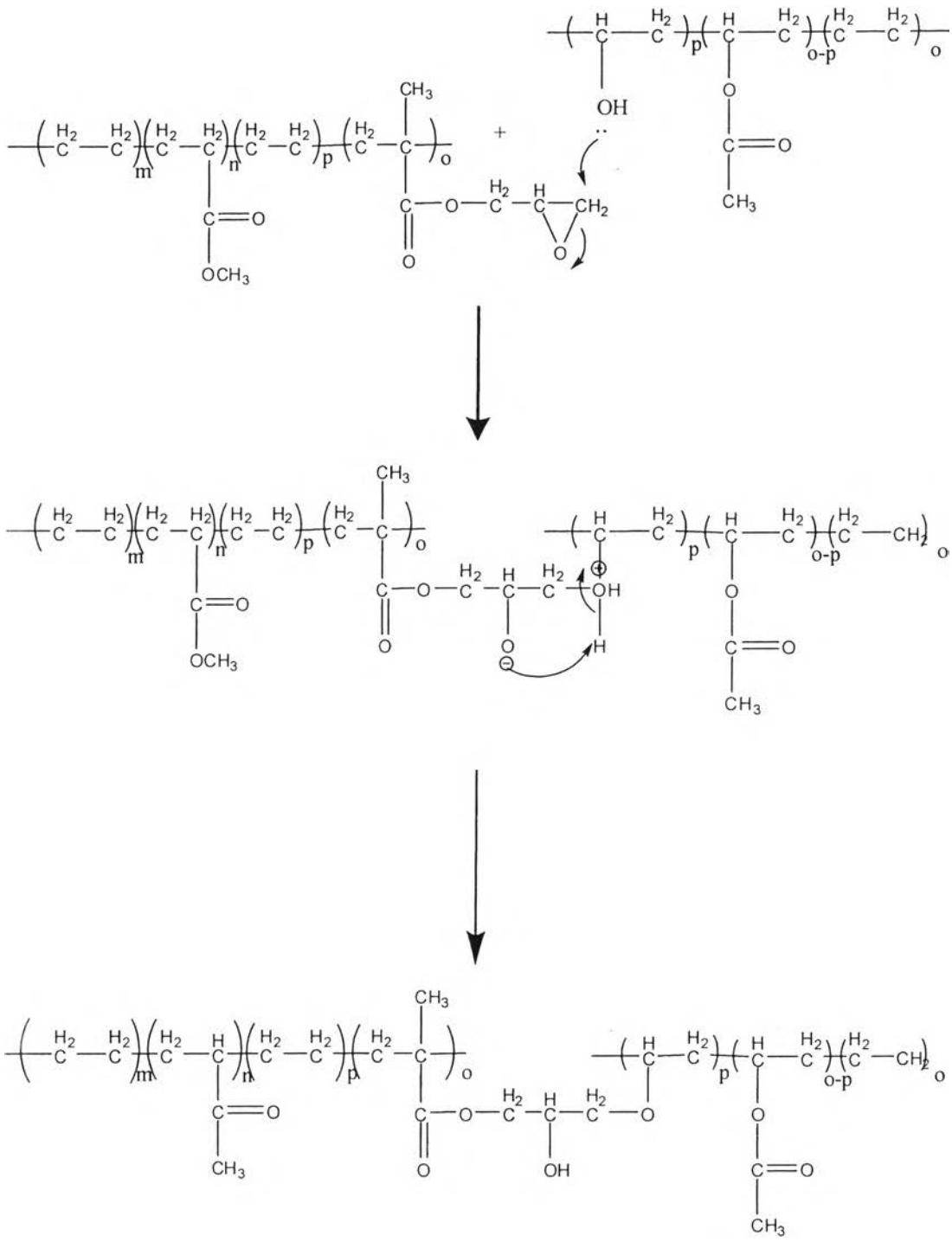

Figure 6.32 Reaction of –OH groups of mEVA with GMA unit of T-GMA compatibilizer.

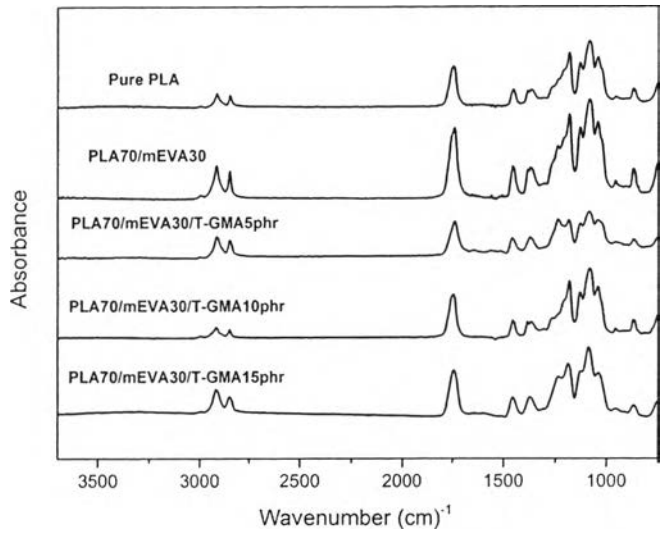

Figure 6.33 FTIR spectra of PLA/mEVA (70/30 w/w) blends at various T-GMA contents.

Table 6.7 Absorbance ratio of pure PLA, PLA/mEVA binary blends and PLA/mEVA/T-GMA blends

absorbance ratio	Pure PLA	PLA/mEVA	PLA/mEVA/ T-GMA 5 phr	PLA/mEVA/ T-GMA 10 phr	PLA/mEVA/ T-GMA 15 phr
910/2850 peak	0.57	0.62	0.72	0.69	0.70
1200/2850 peak	0.81	0.89	0.91	0.95	0.93
1730/2850 peak	0.87	0.89	0.88	0.82	0.78
3500/2850 peak	0.77	0.78	0.73	0.69	0.71

Table 6.8 Assignment of absorbance of PLA, mEVA and T-GMA

Materials	Absorbance (cm^{-1})	Assignment
PLA	1200	C-O stretching of Ester group
	1730	C=O stretching of Carbonyl group and Carboxylic group
	2850	C-H stretching of CH_2 and CH aliphatic
	3500	O-H (H-bonded), usually broad of Hydroxyl group
mEVA	1200	C-O stretching of Ester group
	1730	C=O stretching of Carbonyl group
	2850	C-H stretching of CH_2 and CH aliphatic
	3500	O-H (H-bonded), usually broad of Hydroxyl group
T-GMA	910	C-O stretching of epoxy group
	1200	C-O stretching of Ester group
	1730	C=O stretching of Carbonyl group
	2850	C-H stretching of CH_2 and CH aliphatic

6.6.2.2 Thermal stability

TGA thermograms of PLA/mEVA/T-GMA blends with the different T-GMA contents (Figures 6.34-6.37) shows the two steps of degradation which are simply displayed in Table 6.9. The decomposition temperatures of PLA/mEVA/T-GMA blends are higher than those of PLA/mEVA binary blend due to chemical reactions, an ester linkage, between epoxy group and hydroxyl group [5]. However, the thermal stability of all blends depended on the amount of T-GMA content that excess T-GMA content (15 phr) turns to lower thermal stability.

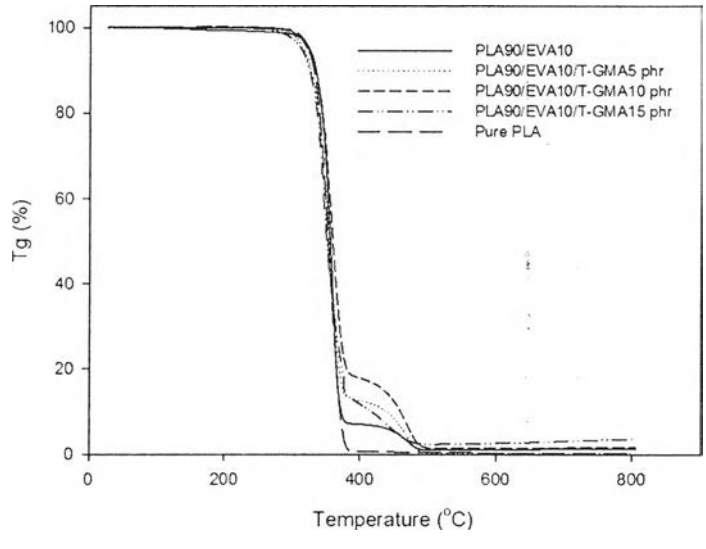

Figure 6.34 TGA thermograms of PLA/mEVA (90/10 w/w) blends at various T-GMA contents.

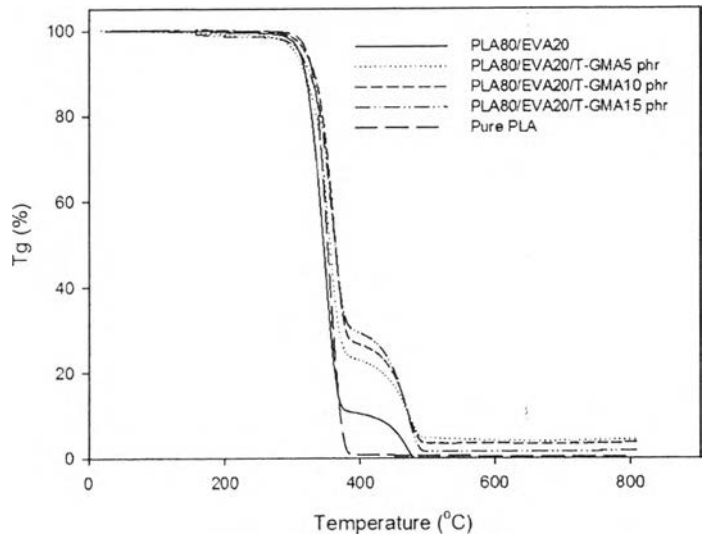

Figure 6.35 TGA thermograms of PLA/mEVA (80/20 w/w) blends at various T-GMA contents.

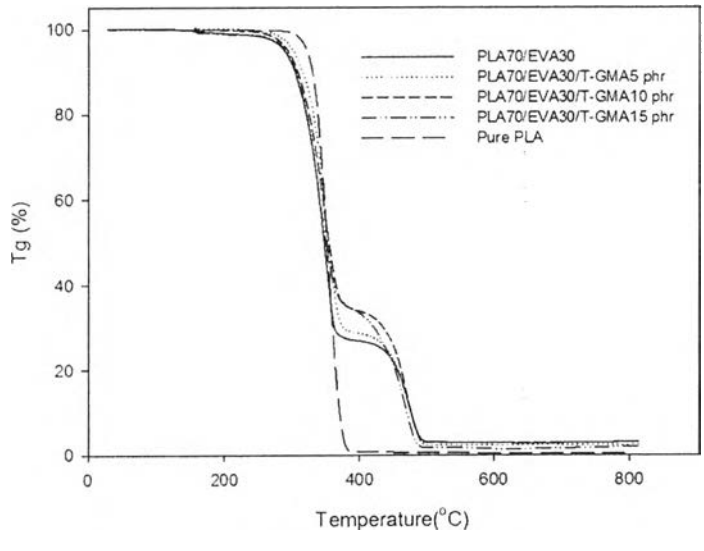

Figure 6.36 TGA thermograms of PLA/mEVA (70/30 w/w) blends at various T-GMA contents.

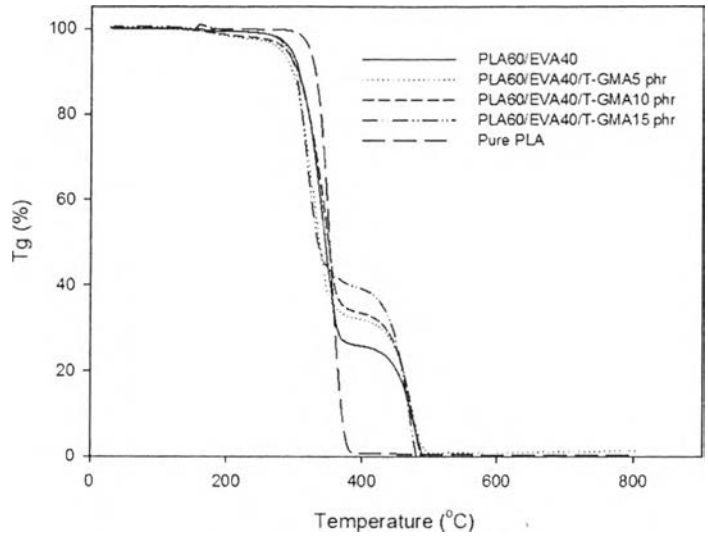

Figure 6.37 TGA thermograms of PLA/mEVA (60/40 w/w) blends at various T-GMA contents.

Table 6.9 Decomposition temperatures of pure PLA, pure mEVA, PLA/mEVA binary blends and PLA/mEVA/T-GMA blends

Blend composition	Decomposition Temperature (°C)	
	1st	2nd
PLA	332.8	-
mEVA	351.5	468.0
PLA90/mEVA10	351.2	471.0
T-GMA 5 phr	354.6	467.7
T-GMA 10 phr	356.1	467.2
T-GMA 15 phr	348.7	443.8
PLA80/mEVA20	351.3	472.1
T-GMA 5 phr	356.3	472.6
T-GMA 10 phr	359.5	467.3
T-GMA 15 phr	356.6	465.4
PLA70/mEVA30	342.9	471.0
T-GMA 5 phr	347.6	468.8
T-GMA 10 phr	347.8	470.2
T-GMA 15 phr	333.4	452.2
PLA60/mEVA40	334.6	469.7
T-GMA 5 phr	334.7	472.8
T-GMA 10 phr	346.2	473.6
T-GMA 15 phr	317.4	465.3

ต้นฉบับ หน้าขาดหาย

6.6.2.2 Thermal properties

DSC curves of PLA/mEVA blends with different T-GMA contents are represented in Figures 6.38-6.41 In addition, the melting temperature (T_m), cold crystallization temperature (T_{cc}), degree of crystallization (χ_c) and two glass transition temperatures (around -25 °C for mEVA and around 60 °C for PLA) of the PLA/mEVA/T-GMA blends are indicated in Table 6.10 The result emphasizes that PLA/mEVA blends are two-phase system or immiscible blends. Furthermore, the glass transition temperatures of PLA/mEVA/T-GMA blends are enhanced with the additional T-GMA and also higher than that of PLA/mEVA binary blends suggested that the epoxy groups of T-GMA could react with hydroxyl or carboxylic groups of PLA, probably leading to the limitation of molecular chain motion. The presences of T-GMA compatibilizer in the blends do not show any appreciable change in melting transition. The cold crystallization temperature and degree of crystallization increase with increasing the amount of T-GMA.

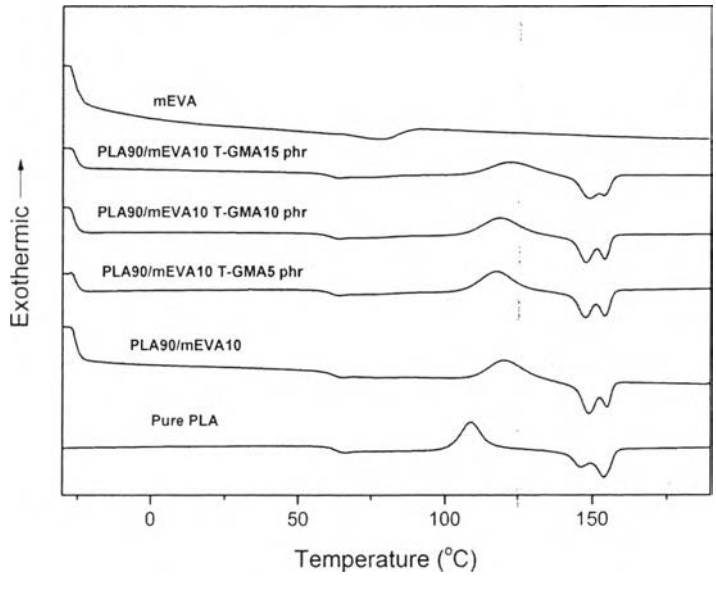

Figure 6.38 DSC thermograms of PLA/mEVA (90/10 w/w) blends at various T-GMA contents.

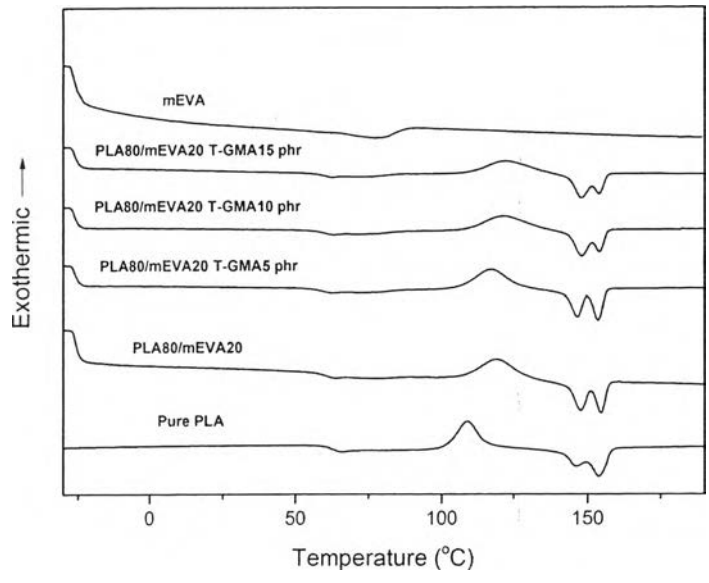

Figure 6.39 DSC thermograms of PLA/mEVA (80/20 w/w) blends at various T-GMA contents.

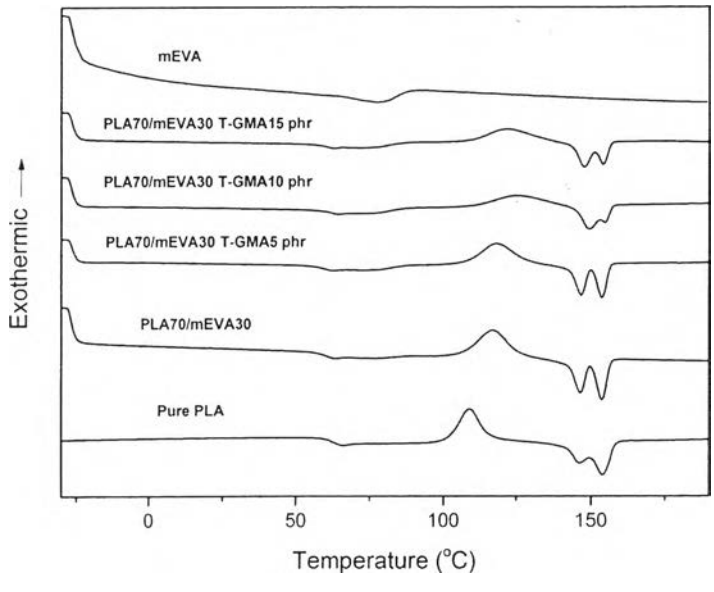

Figure 6.40 DSC thermograms of PLA/mEVA (70/30 w/w) blends at various T-GMA contents.

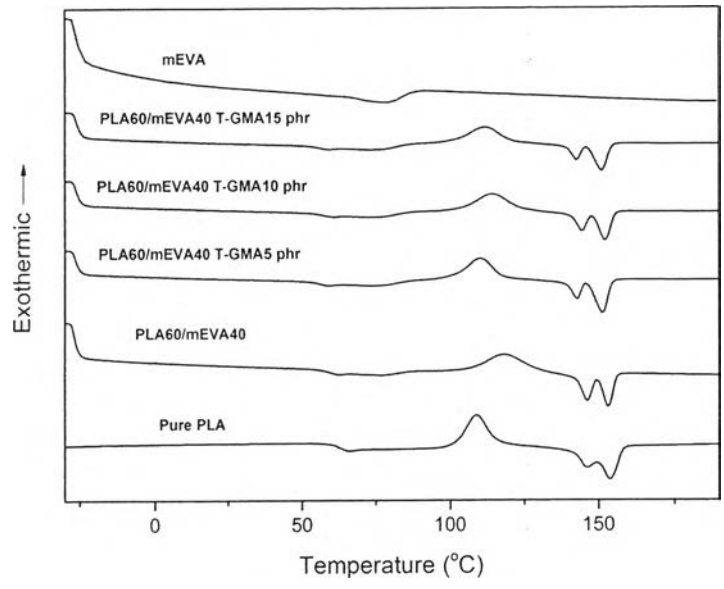

Figure 6.41 DSC thermograms of PLA/mEVA (60/40 w/w) blends at various T-GMA contents.

Table 6.10 Thermal properties of pure PLA, PLA/mEVA binary blends and PLA/mEVA/T-GMA blends

Sample	T_{g1} (°C)	T_{g2} (°C)	T_{cc} (°C)	T_{m1} (°C)	T_{m2} (°C)	ΔH_{cc} (J/g)	ΔH_m (J/g)	$\%\chi_c$
Pure PLA	-	57.9	103.0	146.8	153.7	19.4	24.5	5.45
PLA90/mEVA10	-26.8	58.6	120.3	148.9	154.8	26.9	28.3	1.72
T-GMA5 phr	-26.9	58.3	117.5	147.9	154.0	26.0	27.0	1.18
T-GMA10 phr	-27.5	58.0	118.6	147.8	153.8	24.5	25.9	1.71
T-GMA15 phr	-25.9	57.7	122.3	148.9	153.8	21.2	23.3	2.61
PLA80/mEVA20	-26.6	57.0	119.3	147.8	154.4	26.9	27.9	1.34
T-GMA5 phr	-27.1	55.2	117.2	146.7	153.5	25.6	26.3	0.93
T-GMA10 phr	-27.3	56.8	121.3	148.0	153.9	22.9	23.7	1.15
T-GMA15 phr	-27.1	57.3	122.1	147.9	153.8	20.0	21.2	1.54
PLA70/mEVA30	-27.7	56.4	117.0	146.6	153.7	27.2	27.9	1.15
T-GMA5 phr	-27.4	56.2	118.3	146.7	153.5	22.8	23.8	1.41
T-GMA10 phr	-27.6	58.8	124.1	149.4	154.6	15.8	16.7	1.46
T-GMA15 phr	-27.3	57.4	121.3	147.9	153.9	17.3	18.5	1.89
PLA60/mEVA40	-27.8	55.9	118.3	146.2	159.2	22.3	22.9	1.06
T-GMA5 phr	-27.5	53.1	118.0	142.8	151.4	21.0	21.7	1.29
T-GMA10 phr	-27.1	54.4	114.3	144.6	152.2	19.2	20.0	1.29
T-GMA15 phr	-27.1	52.4	112.0	142.6	151.1	17.7	18.4	1.32

6.6.2.3 Dynamic mechanical properties

The effect of T-GMA contents on the storage modulus and loss modulus as mentioned in Figures 6.42-6.49 and Table 6.11, it is explicited that the storage modulus of all blend compositions diminishes with the increase in T-GMA content especially at room temperature (30 °C) because of the addition of the rubbery polyethylene of terpolymer into the PLA/mEVA blends [6]. From these results, the PLA/mEVA/T-GMA blends at 5 phr T-GMA show the optimum storage modulus with the lowest compatibilizer content.

For Tan δ result indicated in Figures 6.50-6.53 and Table 6.11, the glass transition temperature increases with the incorporation of T-GMA compatibilizer because of the hindrance in the movement of polymer chains which is

occurred via the addition of T-GMA compatibilizer [2]. As a result, the glass transition temperatures of PLA/mEVA/T-GMA blend increase.

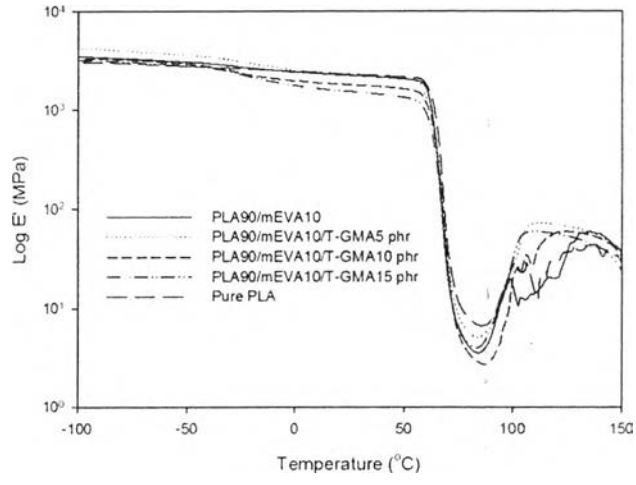

Figure 6.42 Storage Modulus of PLA/mEVA (90/10 w/w) blends at various T-GMA contents.

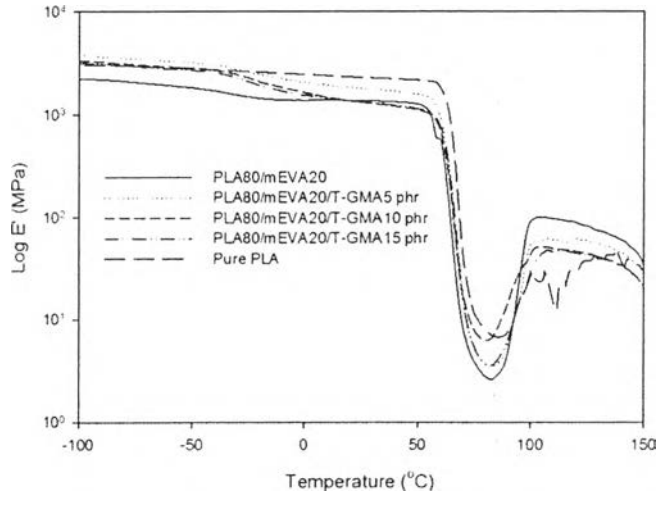

Figure 6.43 Storage Modulus of PLA/mEVA (80/20 w/w) blends at various T-GMA contents.

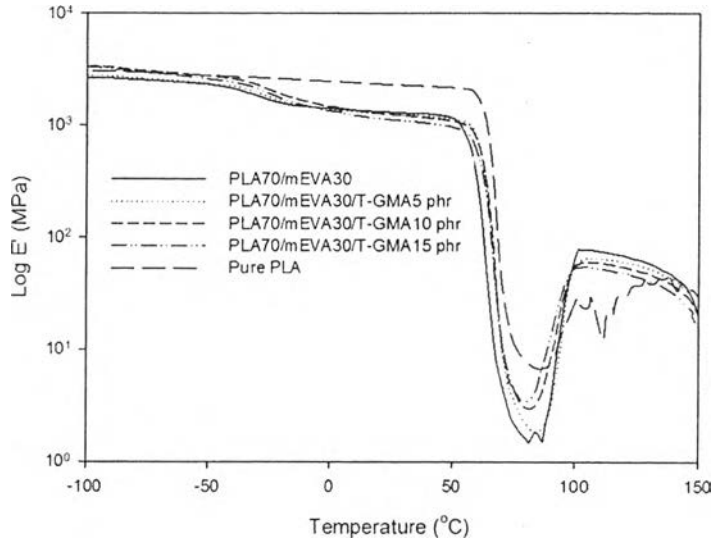

Figure 6.44 Storage Modulus of PLA/mEVA (70/30 w/w) blends at various T-GMA contents.

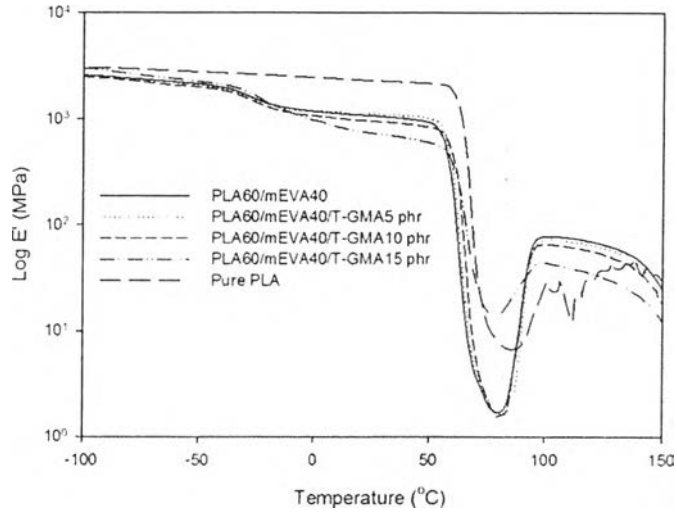

Figure 6.45 Storage Modulus of PLA/mEVA (60/40 w/w) blends at various T-GMA contents.

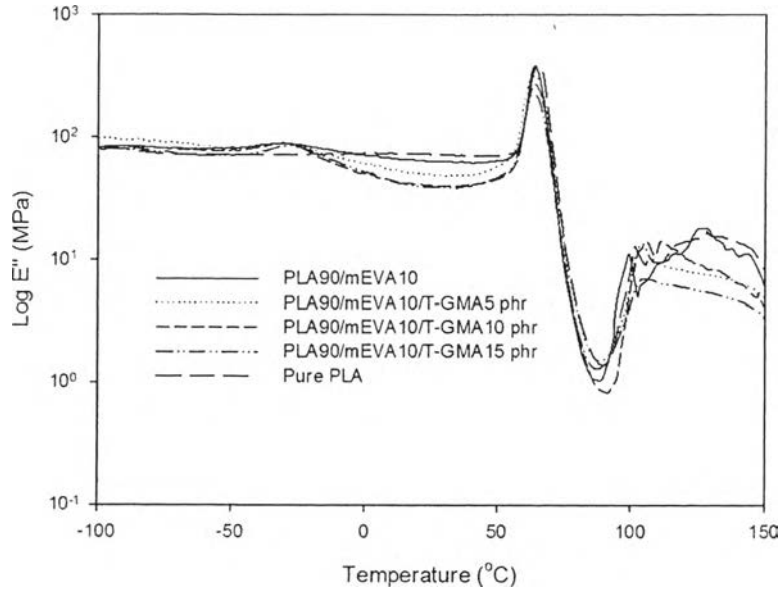

Figure 6.46 Loss Modulus of PLA/mEVA blends (90/10 w/w) at various T-GMA contents.

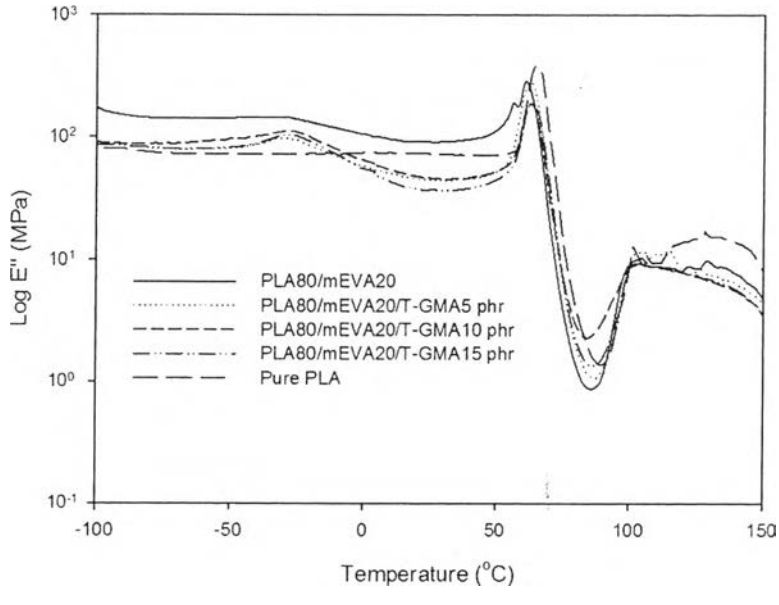

Figure 6.47 Loss Modulus of PLA/mEVA blends (80/20 w/w) at various T-GMA contents.

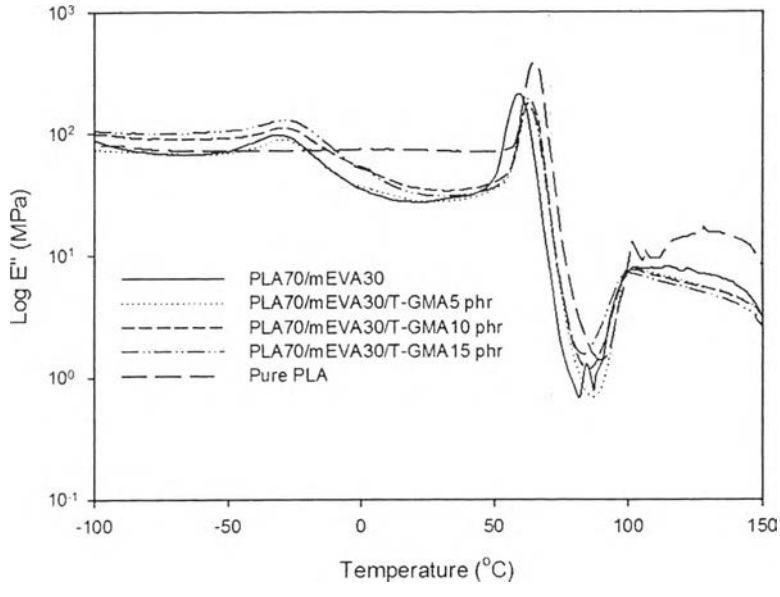

Figure 6.48 Loss Modulus of PLA/mEVA blends (70/30 w/w) at various T-GMA contents.

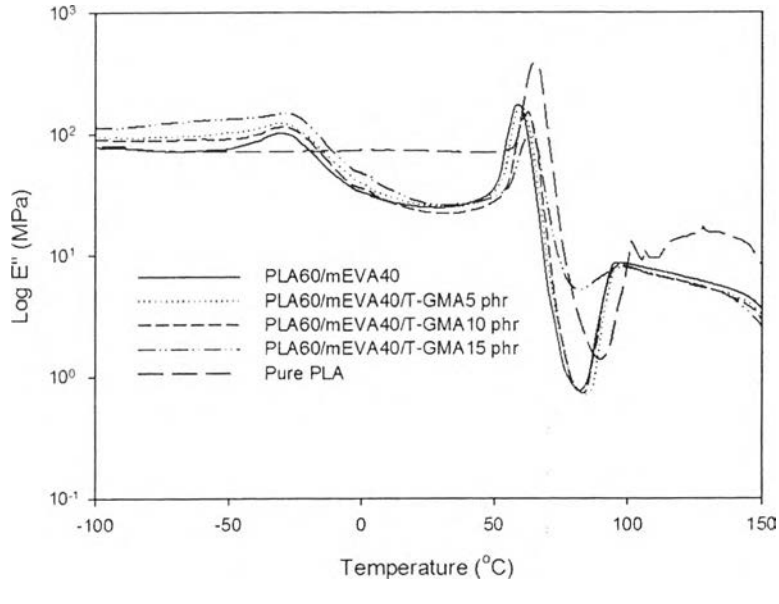

Figure 6.49 Loss Modulus of PLA/mEVA blends (60/40 w/w) at various T-GMA contents.

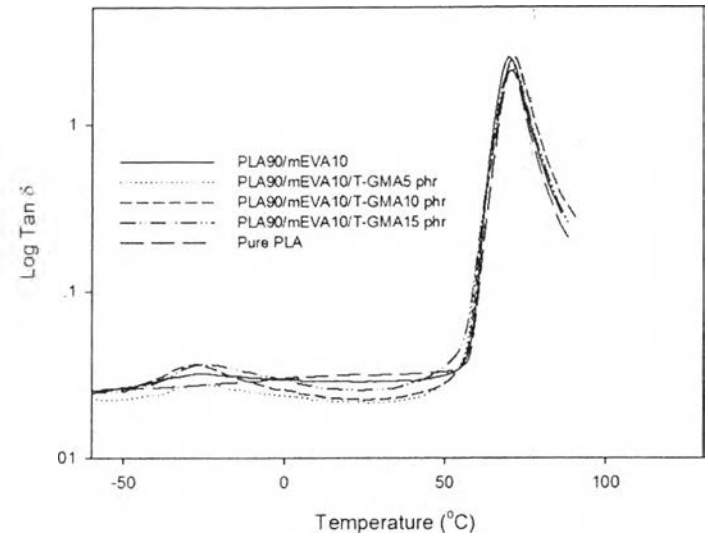

Figure 6.50 Tan δ of PLA/mEVA (90/10 w/w) blends at various T-GMA contents.

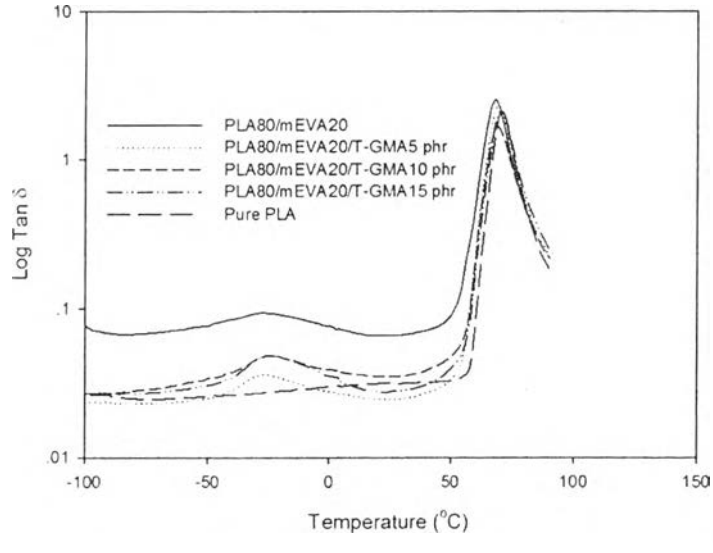

Figure 6.51 Tan δ of PLA/mEVA (80/20 w/w) blends at various T-GMA contents.

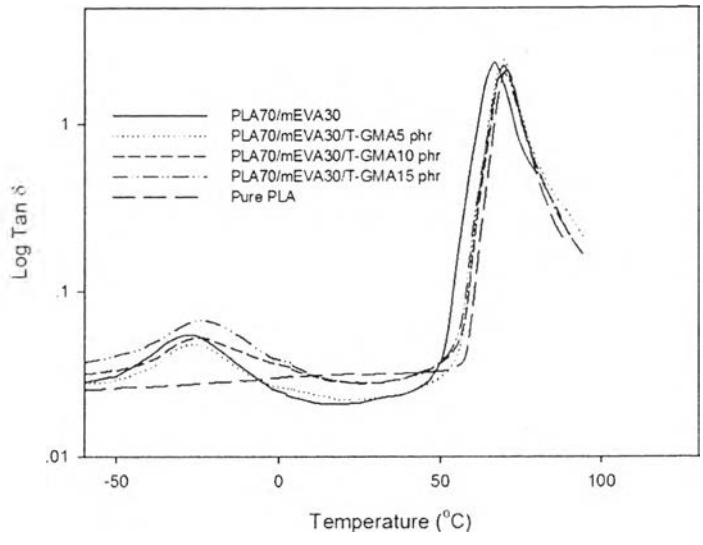

Figure 6.52 Tan δ of PLA/mEVA (70/30 w/w) blends at various T-GMA contents.

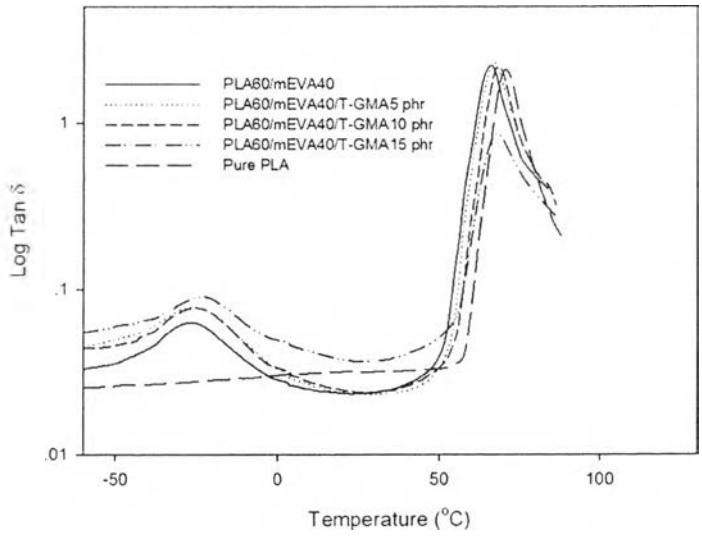

Figure 6.53 Tan δ of PLA/mEVA (60/40 w/w) blends at various T-GMA contents.

Table 6.11 Dynamic mechanical properties of pure PLA, pure mEVA, PLA/mEVA binary blends and PLA/mEVA/T-GMA blends

Blend composition	Tan δ_{max1} (Tg_1, °C)	Tan δ_{max2} (Tg_2, °C)	30 °C
			E′ (MPa)
PLA	-	70.1	2280
mEVA	-20	-	12
PLA90/mEVA10	-26.9	70	2208
T-GMA 5 phr	-24.7	70.1	2201
T-GMA 10 phr	-27.6	72.3	1779
T-GMA 15 phr	-25.8	70.2	1503
PLA80/mEVA20	-27.8	68.2	1364
T-GMA 5 phr	-26.7	70.2	1362
T-GMA 10 phr	-23.8	70.3	1284
T-GMA 15 phr	-23.8	70.3	1295
PLA70/mEVA30	-27.8	66.6	1290
T-GMA 5 phr	-25.5	70.3	1234
T-GMA 10 phr	-24.6	70.4	1216
T-GMA 15 phr	-23.5	70.5	1093
PLA60/mEVA40	-28.6	66.4	1048
T-GMA 5 phr	-26.0	67.3	1008
T-GMA 10 phr	-25.6	67.9	934
T-GMA 15 phr	-23.5	68.2	708

6.6.2.4 Morphology

FE-SEM images of the cryogenic fracture of PLA/mEVA (70/30 w/w) blends with various T-GMA contents are shown in Figures 6.54a.-6.54d. The two-phase structure of mEVA domain and PLA matrix in the binary blend is presented in Figure 6.54a. Likewise, the spherulites are the mEVA in the PLA/mEVA blend [4] and the voids are occurred by debonding between the PLA and mEVA during fracture in the liquid nitrogen [1]. Comparing to Figures 6.54b.-6.54d., with the incorporation of T-GMA (5, 10 and 15 phr), the blends show smaller size of mEVA domains than those in the PLA/mEVA binary blend. Moreover, the increasing of T-GMA content led to the decrease of amount of voids and dispersed phase size. These results obviously confirm that the addition of T-GMA improves the compatibility between PLA and mEVA successfully. On the other hand, mEVA particles in PLA/mEVA blend with the excess T-GMA content (15 phr) large than the blend with T-GMA 10 phr due to aggregation of the mEVA particles.

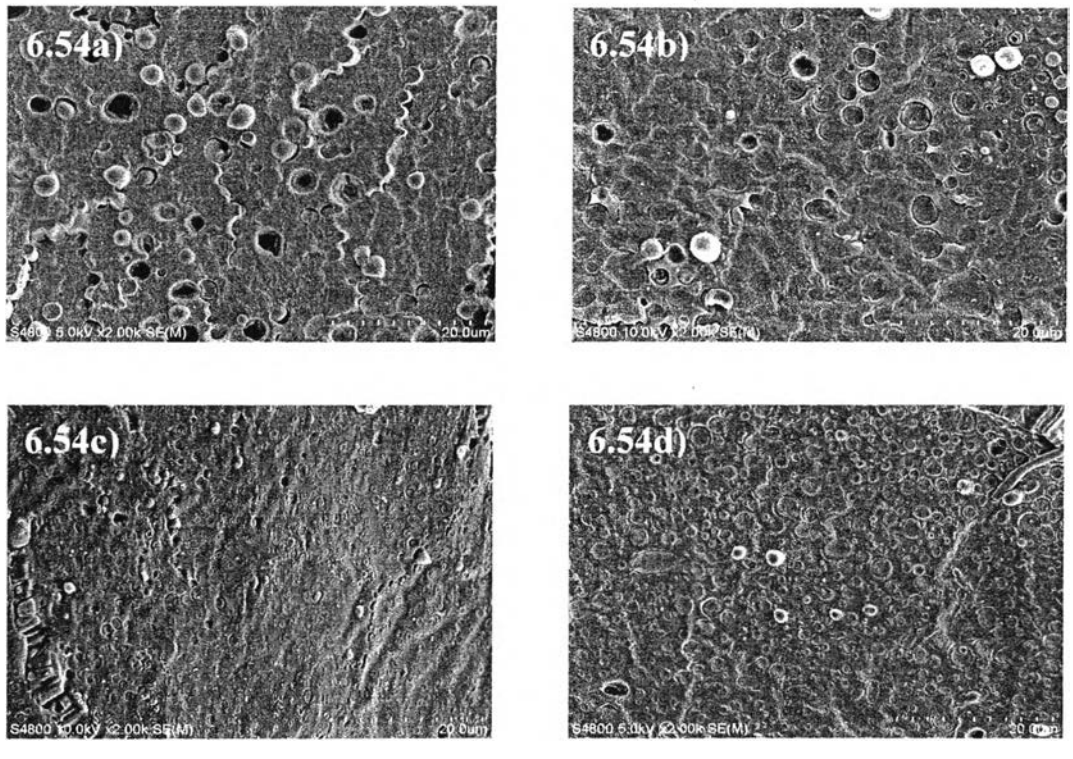

Figure 6.54 SEM images of the fracture of the blends (a) PLA/mEVA (70/30 w/w) blend (b) PLA/mEVA/T-GMA5 phr blend (c) PLA/mEVA/T-GMA10 phr blend (d) PLA/mEVA/T-GMA15 phr blend.

6.6.2.5 Mechanical properties

The tensile properties of pure PLA, PLA/mEVA binary blends, and PLA/mEVA with various T-GMA contents are shown in Figures 6.55-6.57. With the addition of T-GMA compatibilizer, the Young's modulus and tensile strength are dropped; however the enrichment in elongation at break of the binary blends is observed. This confirms that the interaction between T-GMA and PLA matrix can occur resulting in higher elongation at break. The excess amount of T-GMA compatibilizer (15 phr) causes a decrease in tensile properties of the all blends composition corresponding to the discussion in morphology section. From these results, the PLA/mEVA/T-GMA blends at 10 phr of T-GMA show the optimum elongation at break with the lowest compatibilizer content.

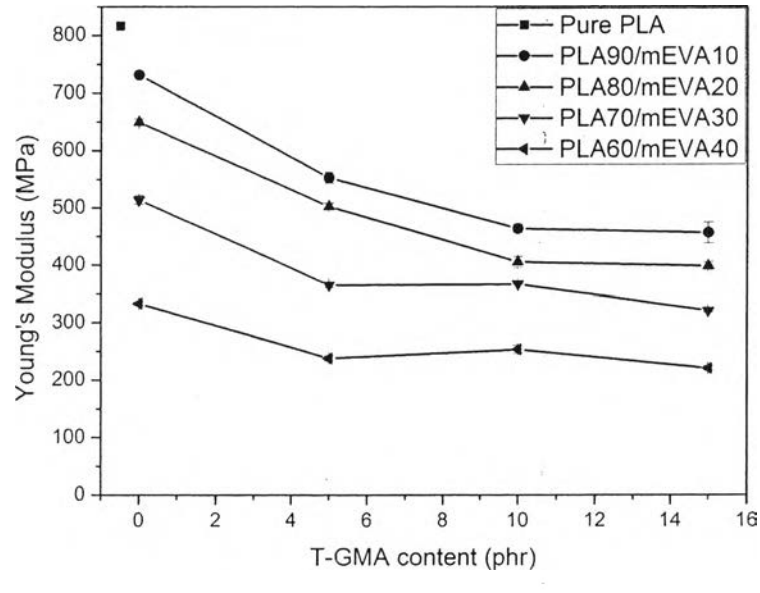

Figure 6.55 Young's modulus of PLA/mEVA blends at various T-GMA contents.

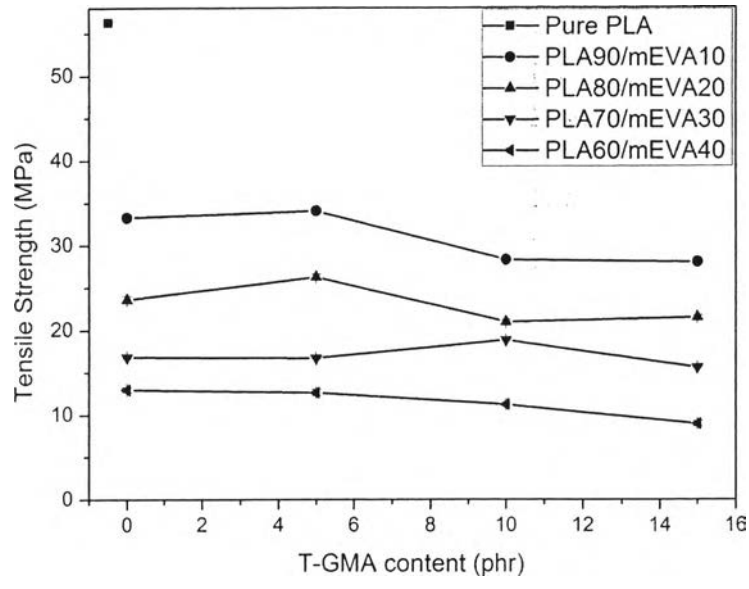

Figure 6.56 Tensile strength of PLA/mEVA blends at various T-GMA contents.

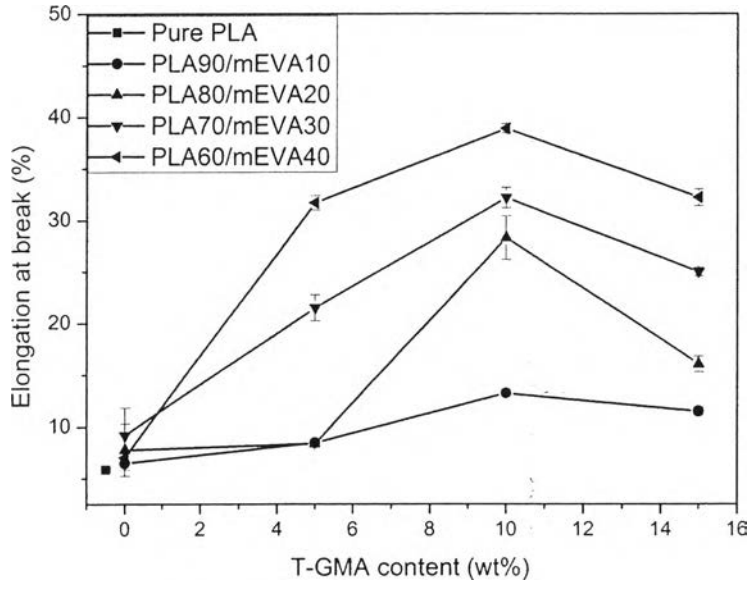

Figure 6.57 Elongation at break of PLA/mEVA blends at various T-GMA contents.

6.6.2.6 Melt flow index

In Figure 6.58, MFI values of PLA/mEVA/T-GMA blends with different T-GMA contents are lower than those of PLA/mEVA binary blends with respect to the improvement in an interfacial interaction between both phases of the blends [7]. Moreover, the MFI values of PLA/mEVA/T-GMA blends also decrease with the increasing of T-GMA contents implied that the reaction increases with the T-GMA content [8].

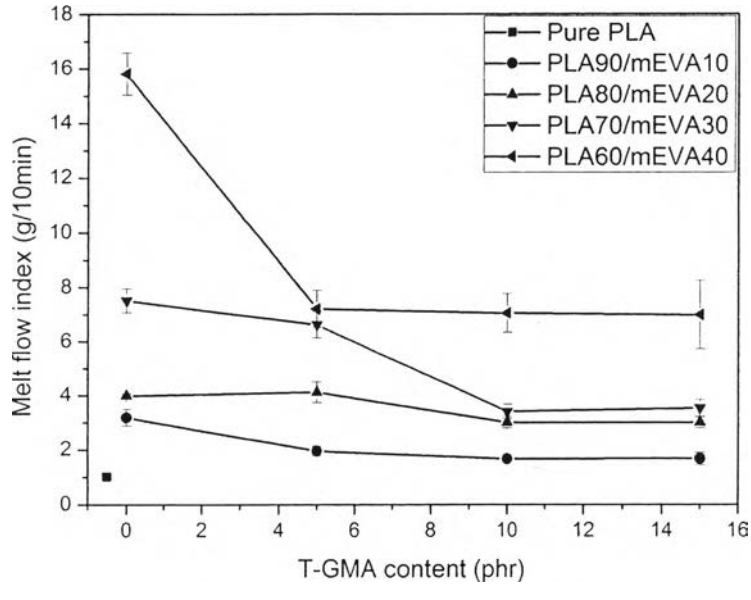

Figure 6.58 MFI values of PLA/mEVA blends at various T-GMA contents.

6.6.2.7 Biodegradability

The biodegradability is relevant to weight loss of pure PLA, PLA/mEVA binary blends and PLA/mEVA with various T-GMA contents. The weight loss is demonstrated in Figure 6.59. After the addition of T-GMA compatibilizer, the weight loss of PLA/mEVA/T-GMA blends is slightly lower than that of PLA/mEVA binary blend and decreases with increasing of T-GMA contents.

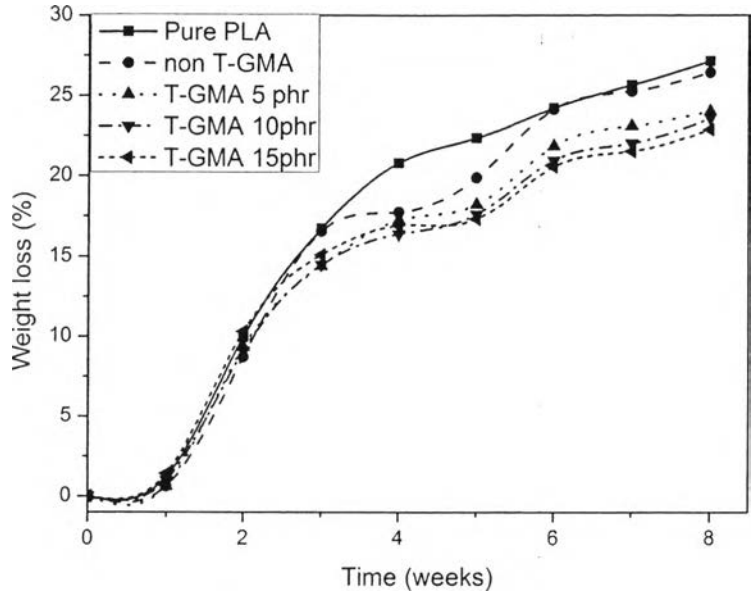

Figure 6.59 Weight loss of PLA/mEVA (90/10 w/w) blends at various T-GMA contents.

6.6.3 Ethylene-acrylic acid copolymer (PE-AA)

6.6.3.1 Chemical analysis

Carboxylic group of PE-AA compatibilizer reacts with the hydroxyl end group of PLA and mEVA to form ester linkage which is shown in Figure 6.60-6.61. From this reaction, it is the cause of decrease of hydroxyl and carboxylic groups. On the contrary, the increment of ester group is observed in the blends.

FTIR spectra of Pure PLA and PLA/mEVA/PE-AA blends with difference PE-AA contents are shown in Figures 6.62. FTIR spectra and Table 6.13 show the characteristic peak of pure PLA which compose of C=O stretching at 1730 cm^{-1} corresponding to carboxylic group and carbonyl group of PLA, O-H stretching at 3500 cm^{-1} corresponding to hydroxyl group and C-H stretching at 2850 cm^{-1} corresponding to CH_2 and CH aliphatic, the characteristic peak of mEVA which compose of C=O stretching at 1730 cm^{-1} corresponding to carbonyl group of vinyl acetate, O-H stretching at 3500 cm^{-1} corresponding to hydroxyl group and C-H

stretching at 2850 cm^{-1} corresponding to CH_2 and CH aliphatic and the characteristic peak of PE-AA which compose of C=O stretching at 1730 cm^{-1} corresponding to carboxylic group, C-H stretching at 2850 cm^{-1} corresponding to CH_2 and CH aliphatic and O-H stretching at 3500 cm^{-1} corresponding to hydroxyl group. From Table 6.12, the absorbance ratio of the peak at 1200/2850 cm^{-1} which is attributed to the ester linkage of the blend. The increasing of the absorbance ratio of the peak at 1200/2850 cm^{-1} and the decreasing of the absorbance ratio of the peak at 3500/2850 cm^{-1} confirm the chemical reactions between the carboxylic groups of PE-AA and hydroxyl end groups of PLA and mEVA to from ester linkage.

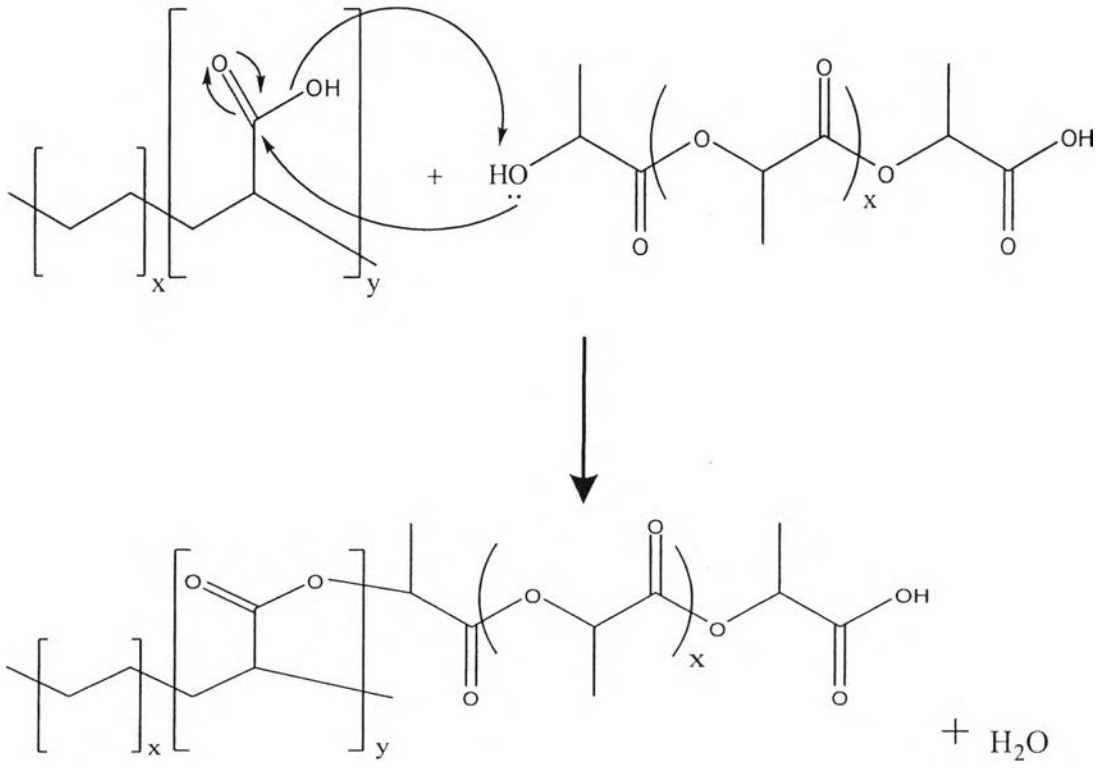

Figure 6.60 Reaction of –OH group of PLA with carboxylic group of PE-AA compatibilizer.

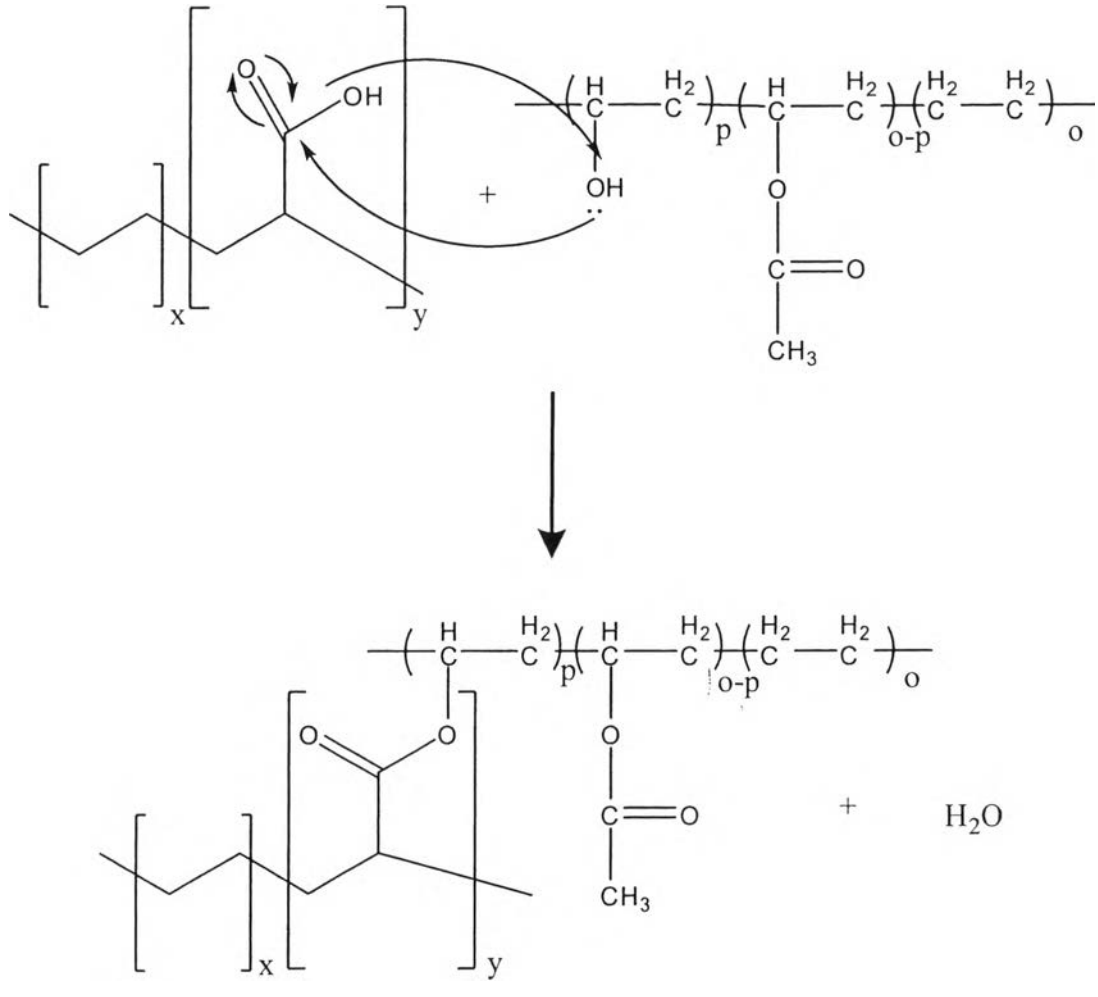

Figure 6.61 Reaction of –OH group of mEVA with carboxylic group of PE-AA compatibilizer.

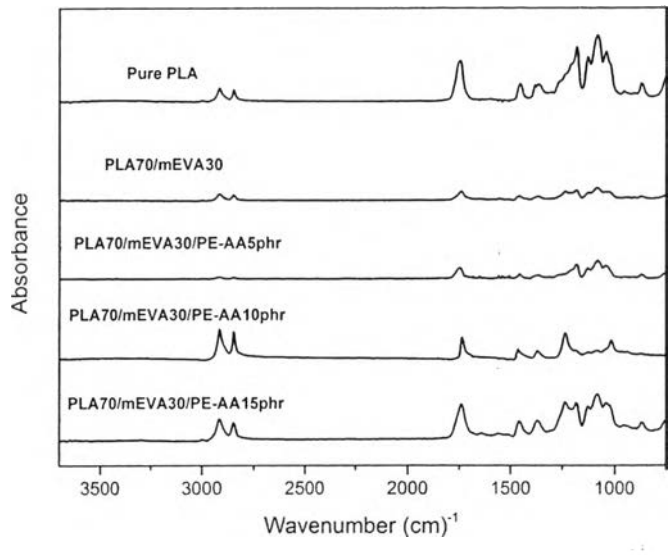

Figure 6.62 FTIR spectra of PLA/mEVA (70/30 w/w) blends at various PE-AA contents.

Table 6.12 Absorbance ratio of pure PLA, PLA/mEVA binary blends and PLA/mEVA/PE-AA blends

absorbance ratio	Pure PLA	PLA/mEVA	PLA/mEVA/ PE-AA 5 phr	PLA/mEVA/ PE-AA 10 phr	PLA/mEVA/ PE-AA 15 phr
1730/2850 peak	0.87	0.89	0.85	0.82	0.81
1200/2850 peak	0.81	0.89	0.98	1.07	0.99
3500/2850 peak	0.77	0.78	0.74	0.71	0.70

Table 6.13 Assignment of absorbance of PLA, mEVA and PE-AA

Materials	Absorbance (cm^{-1})	Assignment
PLA	1200	C-O stretching of Ester group
	1730	C=O stretching of Carbonyl group and Carboxylic group
	2850	C-H stretching of CH_2 and CH aliphatic
	3500	O-H (H-bonded), usually broad of Hydroxyl group
mEVA	1200	C-O stretching of Ester group
	1730	C=O stretching of Carbonyl group
	2850	C-H stretching of CH_2 and CH aliphatic
	3500	O-H (H-bonded), usually broad of Hydroxyl group
PE-AA	1730	C=O stretching of Carboxylic group
	2850	C-H stretching of CH_2 and CH aliphatic
	3500	O-H (H-bonded), usually broad of Hydroxyl group

6.6.3.1 Thermal stability

TGA thermograms of PLA/mEVA/PE-AA blends with different PE-AA contents are represented in Figures 6.63-6.66. The PLA/mEVA/PE-AA blends evidently exhibit two steps of degradation as shown in Table 6.14. With the incorporation of PE-AA compatibilizer, the decomposition temperatures of PLA/mEVA/PE-AA blends are higher than those of PLA/mEVA binary blend due to chemical interaction and physical entanglement between the two constituents [9]. Consequently, the decomposition temperatures of PLA/mEVA/PE-AA blends also increase with the supplement of PE-AA contents. As the effect of blend ratios, the results show the reducing in the decomposition temperatures with increasing mEVA content owing to the phase separation of PLA and mEVA.

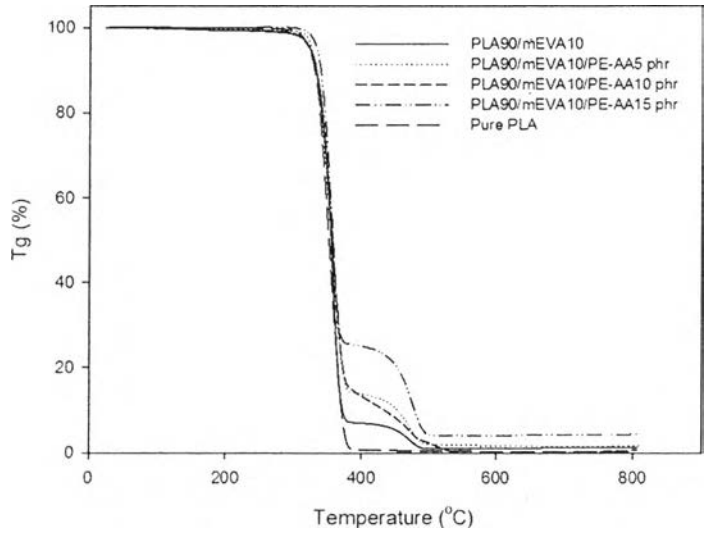

Figure 6.63 TGA thermograms of PLA/mEVA (90/10 w/w) blends at various PE-AA contents.

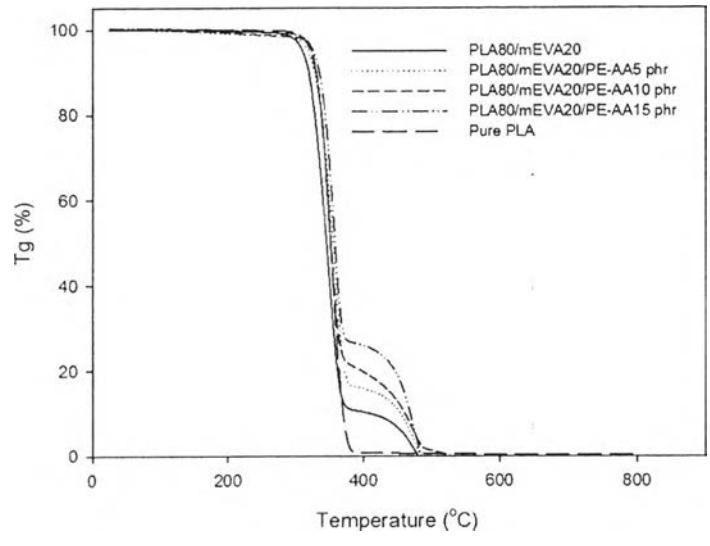

Figure 6.64 TGA thermograms of PLA/mEVA (80/20 w/w) blends at various PE-AA contents.

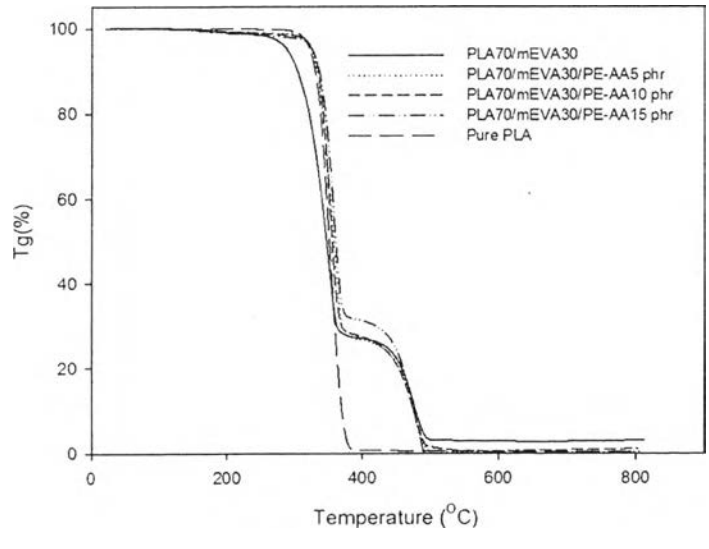

Figure 6.65 TGA thermograms of PLA/mEVA (70/30 w/w) blends at various PE-AA contents.

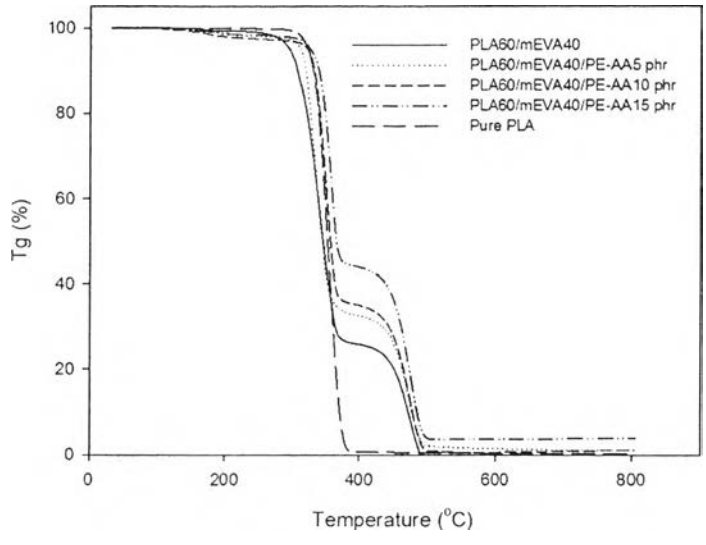

Figure 6.66 TGA thermograms of PLA/mEVA (60/40 w/w) blends at various PE-AA contents.

Table 6.14 Decomposition temperatures of pure PLA, pure mEVA, PLA/mEVA binary blends and PLA/mEVA/PE-AA blends

Blend composition	Decomposition Temperature (°C)	
	1st	2nd
PLA	332.8	-
mEVA	351.5	468.0
PLA90/mEVA10	351.2	471.0
PE-AA 5 phr	361.5	472.8
PE-AA 10 phr	362.3	471.5
PE-AA 15 phr	357.6	475.4
PLA80/mEVA20	351.3	472.1
PE-AA 5 phr	353.9	471.8
PE-AA 10 phr	359.4	470.3
PE-AA 15 phr	358.3	471.9
PLA70/mEVA30	342.9	471.0
PE-AA 5 phr	356.3	475.0
PE-AA 10 phr	361.5	476.7
PE-AA 15 phr	362.6	477.7
PLA60/mEVA40	334.6	469.7
PE-AA 5 phr	340.7	472.3
PE-AA 10 phr	352.2	474.9
PE-AA 15 phr	357.3	474.7

6.6.3.2 Thermal properties

In Figures 6.67-6.70, the thermal properties of PLA/mEVA/PE-AA blends with difference PE-AA contents are inspected via DSC curves in which the melting temperature (T_m), cold crystallization temperature (T_{cc}), degree of crystallization (χ_c) and two glass transition temperature (around -25 °C for mEVA and around 60 °C for PLA) are presented in Table 6.15. The DSC curves exhibit the glass transition temperature of PLA/mEVA/PE-AA blends are higher than those of the binary blends due to reaction between PE-AA compatibilizer and PLA blend restrict the mobility of polymer chain. Furthermore, this result shows only one peak of the melting temperature result from better compatibility than the binary blends. However, no shift of T_m in PLA/mEVA is found, indicating the added of PE-AA does not have an effect on the lamellar structure of PLA or mEVA [10]. On the other hand, cold crystallization temperature and degree of crystallization is generally reduced with the increment of PE-AA. This suggests that PE-AA constrain the crystallization of PLA and mEVA to some extent by interaction between PLA and PE-AA [10].

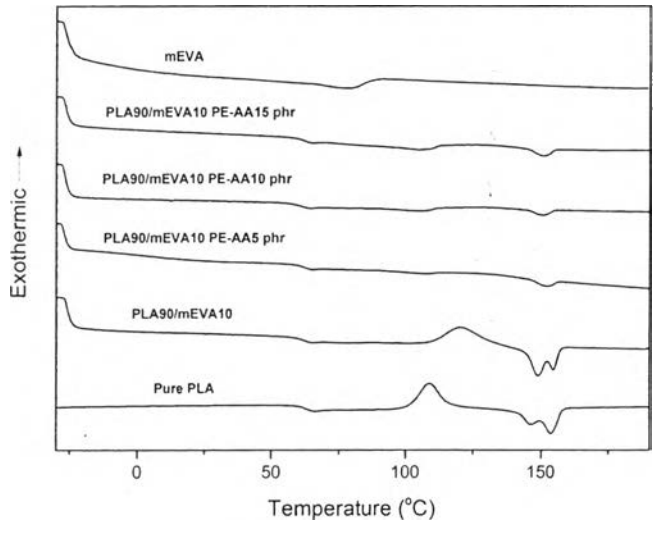

Figure 6.67 DSC thermograms of PLA/mEVA (90/10 w/w) blends at various PE-AA contents.

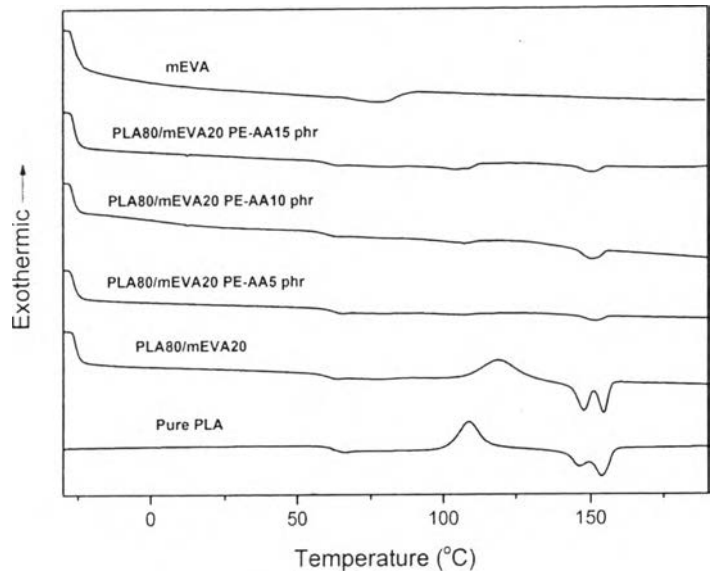

Figure 6.68 DSC thermograms of PLA/mEVA (80/20 w/w) blends at various PE-AA contents.

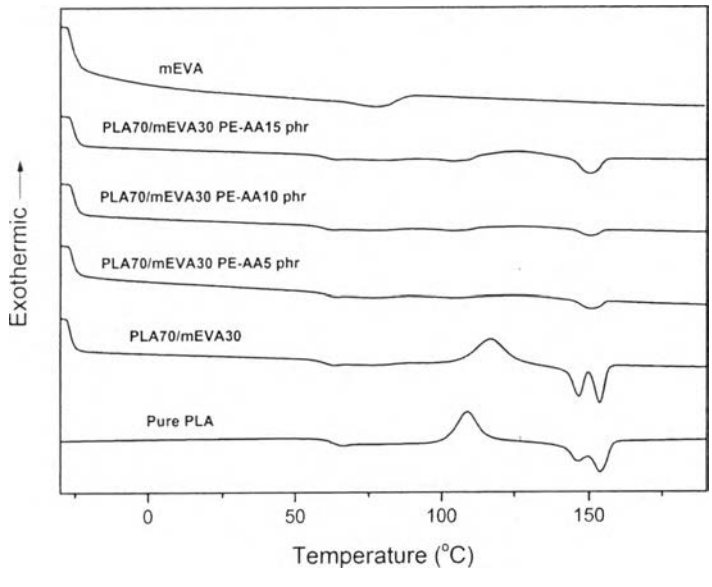

Figure 6.69 DSC thermograms of PLA/mEVA (70/30 w/w) blends at various PE-AA contents.

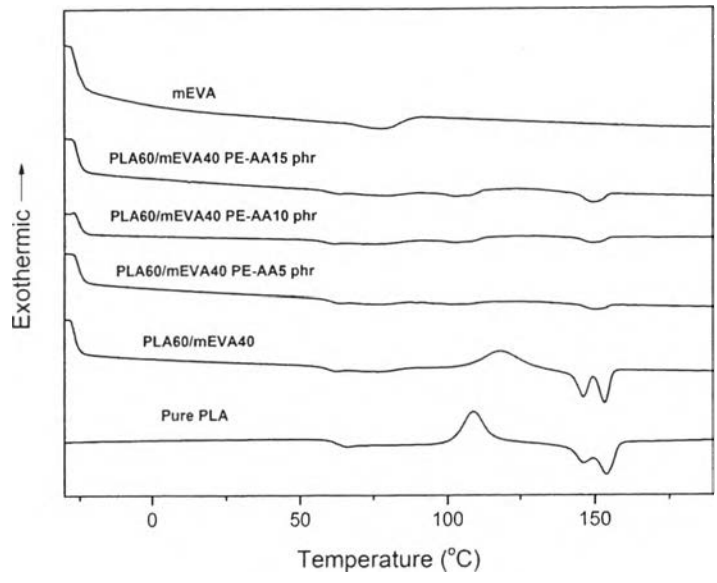

Figure 6.70 DSC thermograms of PLA/mEVA (60/40 w/w) blends at various PE-AA contents.

Table 6.15 Thermal properties of pure PLA, PLA/mEVA binary blends and PLA/mEVA/PE-AA blends

Sample	T_{g1} (°C)	T_{g2} (°C)	T_{cc} (°C)	T_{m1} (°C)	T_{m2} (°C)	ΔH_{cc} (J/g)	ΔH_m (J/g)	$\%\chi_c$
Pure PLA	-	57.9	103.0	146.8	153.7	19.4	24.5	5.45
PLA90/mEVA10	-26.8	58.6	120.3	148.9	154.8	26.9	28.3	1.72
PE-AA 5 phr	-28.0	58.5	128.2	-	151.8	2.6	4.0	1.72
PE-AA 10phr	-27.6	57.4	126.6	-	150.5	3.9	4.4	0.62
PE-AA15 phr	-27.3	58.7	120.3	-	150.8	4.9	5.2	0.32
PLA80/mEVA20	-26.6	57.0	119.3	147.8	154.4	26.9	27.9	1.34
PE-AA 5 phr	-27.5	56.5	130.6	-	151.5	1.7	3.1	1.88
PE-AA 10phr	-27.5	56.1	123.9	-	150.2	6.9	7.4	0.77
PE-AA15 phr	-27.2	57.1	115.2	-	150.0	4.0	4.4	0.46
PLA70/mEVA30	-27.7	56.4	117.0	146.6	153.7	27.2	27.9	1.15
PE-AA 5 phr	-27.0	56.8	125.9	-	150.5	5.2	5.8	0.94
PE-AA 10phr	-26.7	56.9	125.1	-	150.3	3.7	4.1	0.61
PE-AA15 phr	-26.7	57.5	125.2	-	150.3	10.1	10.7	0.80
PLA60/mEVA40	-27.8	55.9	118.3	146.2	159.2	22.3	22.9	1.06
PE-AA 5 phr	-26.6	54.3	121.9	-	149.8	5.6	5.9	0.39
PE-AA 10phr	-26.5	54.9	125.8	-	149.5	3.5	3.5	0.11
PE-AA15 phr	-26.9	57.3	122.5	-	149.0	3.2	3.3	0.11

6.6.3.3 Dynamic mechanical properties

The effect of an additional PE-AA on the storage modulus and loss modulus of PLA/mEVA/PE-AA blends at room temperature (30 °C) is indicated in Figures 6.71-6.78 and Table 6.16. The result is insisted that the storage modulus of all blends declines with increasing in PE-AA contents. The improvement in flexibility is attributed to the incorporation of the rubbery polyethylenic chains into the PLA matrix [11]. Subsequently, the optimum storage modulus with the lowest compatibilizer content is observed at 5 phr of PE-AA adding in the PLA/mEVA/ PE-AA blends. In the effect of blend ratios, the storage modulus of both PLA/mEVA binary blends and PLA/mEVA/PE-AA blends at the same PE-AA content decline with the additional mEVA content due to a high flexibility of mEVA.

Beyond the storage modulus, Tan δ value in the presence of PE-AA compatibilizer in PLA/mEVA blends, as shown in Figures 6.79-6.82 and Table 6.16, exhibits the increasing in T_g because of the chemical reaction between acrylic acid groups of PE-AA and hydroxyl groups of PLA in order to form ester linkages, resulting in the obstruction of molecular chain motion. As a result, the glass transition temperatures of PLA/mEVA/ PE-AA blend increase.

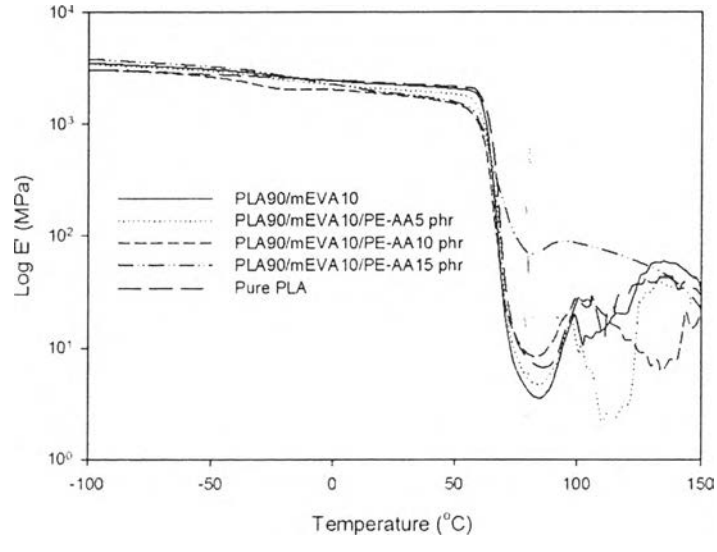

Figure 6.71 Storage Modulus of PLA/mEVA (90/10 w/w) blends at various PE-AA contents.

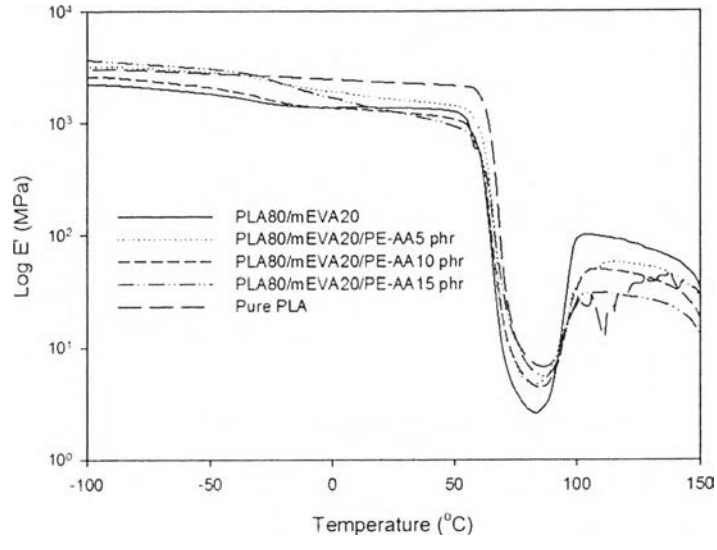

Figure 6.72 Storage Modulus of PLA/mEVA (80/20 w/w) blends at various PE-AA contents.

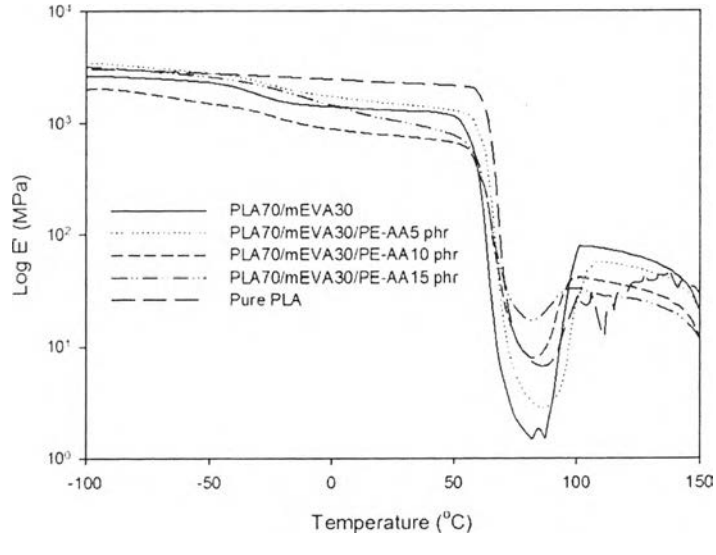

Figure 6.73 Storage Modulus of PLA/mEVA (70/30 w/w) blends at various PE-AA contents.

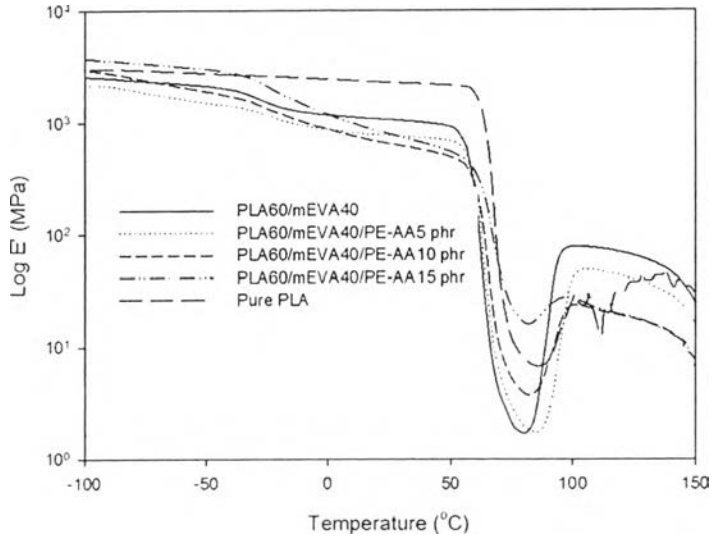

Figure 6.74 Storage Modulus of PLA/mEVA (60/40 w/w) blends at various PE-AA contents.

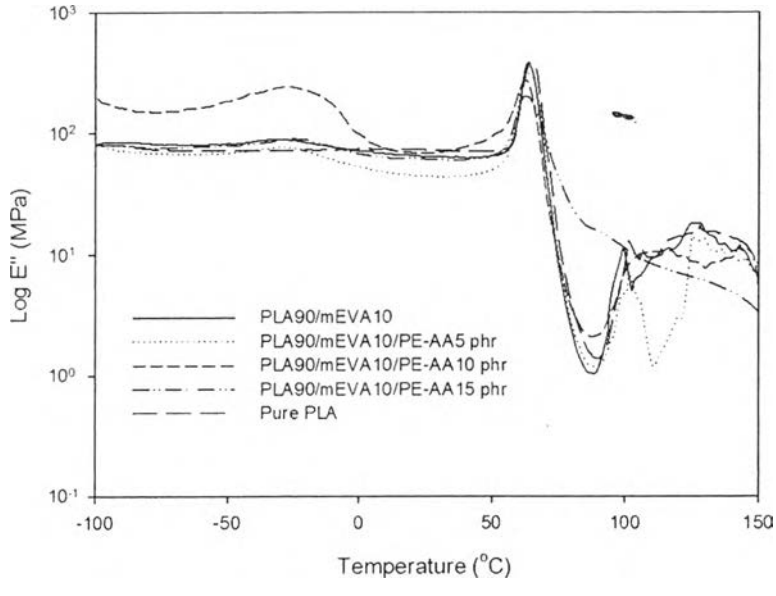

Figure 6.75 Loss Modulus of PLA/mEVA blends (90/10 w/w) at various PE-AA contents.

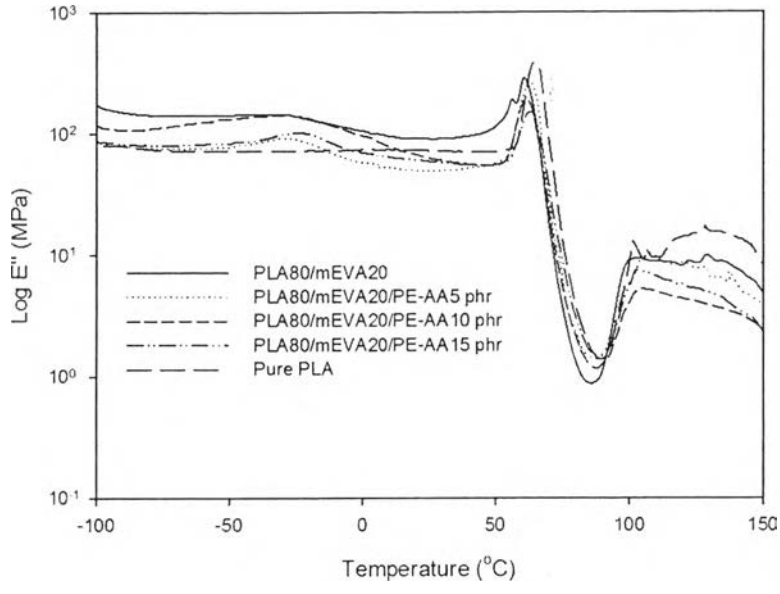

Figure 6.76 Loss Modulus of PLA/mEVA blends (80/20 w/w) at various PE-AA contents.

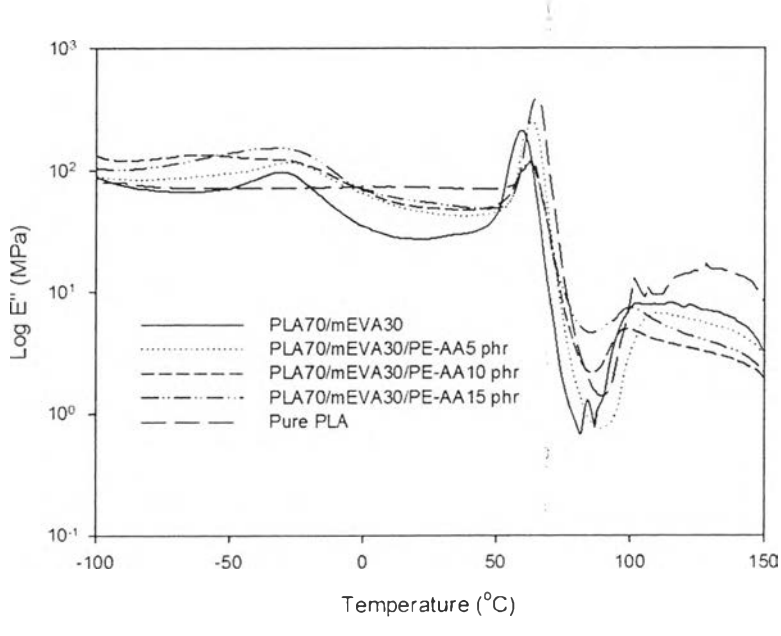

Figure 6.77 Loss Modulus of PLA/mEVA blends (70/30 w/w) at various PE-AA contents.

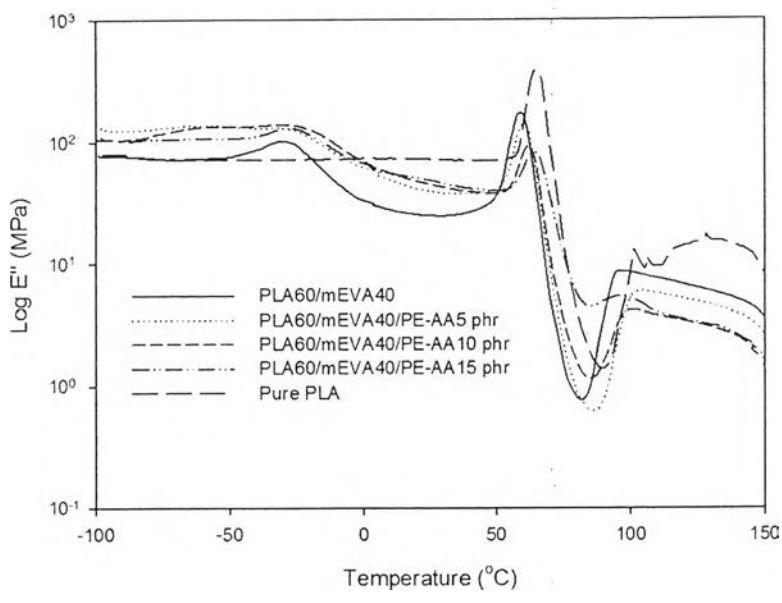

Figure 6.78 Loss Modulus of PLA/mEVA blends (60/40 w/w) at various PE-AA contents.

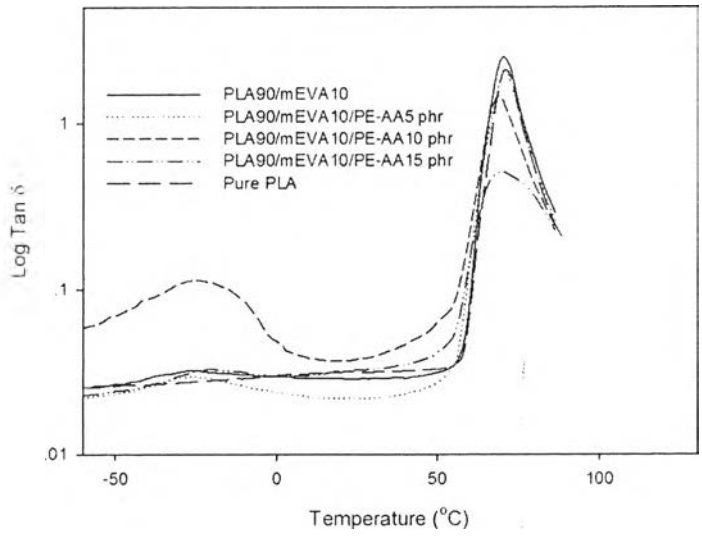

Figure 6.79 Tan δ of PLA/mEVA (90/10 w/w) blends at various PE-AA contents.

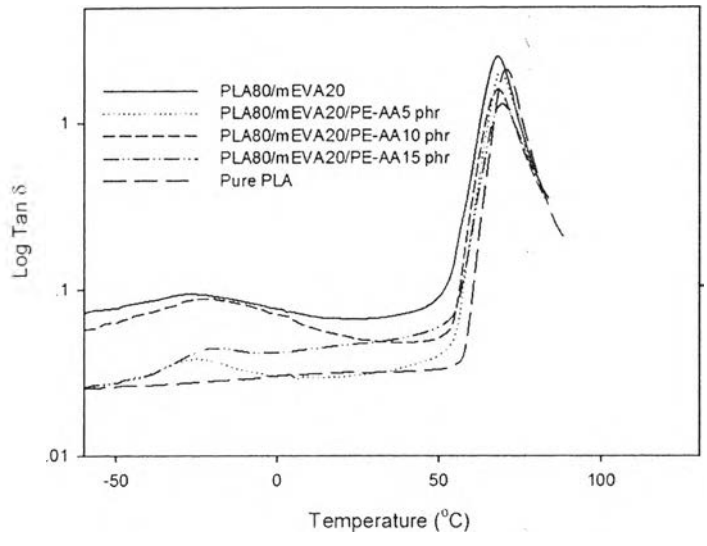

Figure 6.80 Tan δ of PLA/mEVA (80/20 w/w) blends at various PE-AA contents.

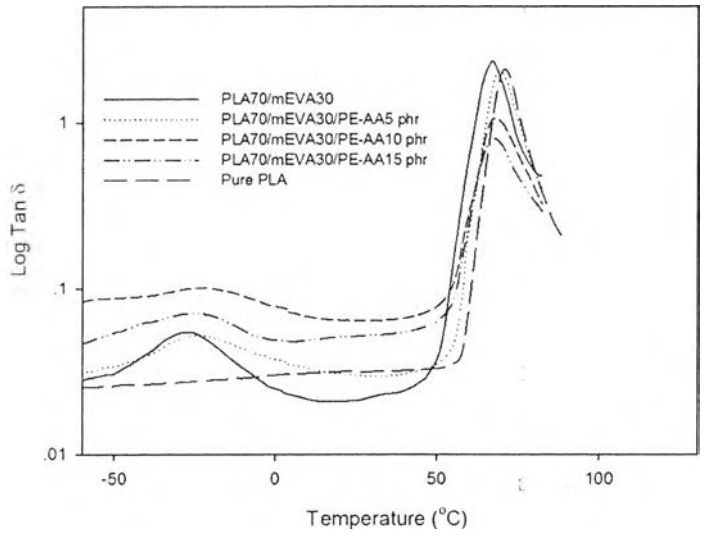

Figure 6.81 Tan δ of PLA/mEVA (70/30 w/w) blends at various PE-AA contents.

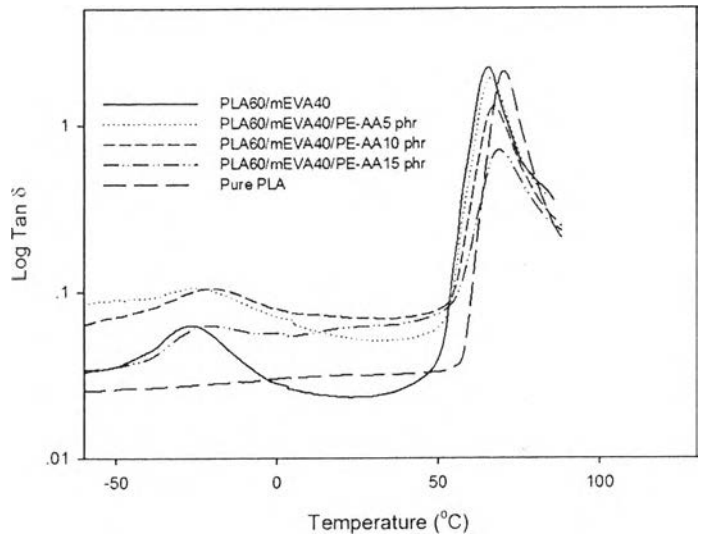

Figure 6.82 Tan δ of PLA/mEVA (60/40 w/w) blends at various PE-AA contents.

Table 6.16 Dynamic mechanical properties of pure PLA, pure mEVA, PLA/mEVA binary blends and PLA/mEVA/PE-AA blends

Blend composition	Tan δ_{max1} (Tg_1, °C)	Tan δ_{max2} (Tg_2, °C)	30 °C
			E′ (MPa)
PLA	70.1	-	2280
mEVA	-20	-	12
PLA90/mEVA10	-26.9	70	2208
PE-AA 5 phr	-25.7	70.5	1998
PE-AA 10 phr	-25.7	70.2	1828
PE-AA 15 phr	-19.9	70.6	1768
PLA80/mEVA20	-27.8	68.2	1364
PE-AA 5 phr	-25.7	70.2	1592
PE-AA 10 phr	-23.7	70.4	1229
PE-AA 15 phr	-19.6	70.4	1195
PLA70/mEVA30	-27.8	66.6	1290
PE-AA 5 phr	-23.5	70	1464
PE-AA 10 phr	-23.6	70	1009
PE-AA 15 phr	-25.6	70.7	758
PLA60/mEVA40	-28.6	66.4	1048
PE-AA 5 phr	-25.7	66.5	752
PE-AA 10 phr	-19.7	68	738
PE-AA 15 phr	-21.6	70.3	619

6.6.3.4 Morphology

FE-SEM images (Figures 6.83a-6.83d) of the cryogenic fracture of PLA/mEVA (70/30 w/w) blends with different PE-AA contents display the binary blend between the two-phase structure of mEVA domain and PLA matrix especially in Figure 6.83a. As a result, the spherulites are the mEVA in the PLA/mEVA blend [4]. The diameter of mEVA phase reduces with the addition of PE-AA compatibilizer in all blend compositions expected as the function of acrylic acid which exists in the structure of compatibilizer. Moreover, there is a fine dispersion and homogeneity of mEVA in the matrix of the blends. This better dispersion arises from the formation of ester linkage caused by reaction of the carboxyl groups of acrylic acid with the hydroxyl groups of PLA [12].

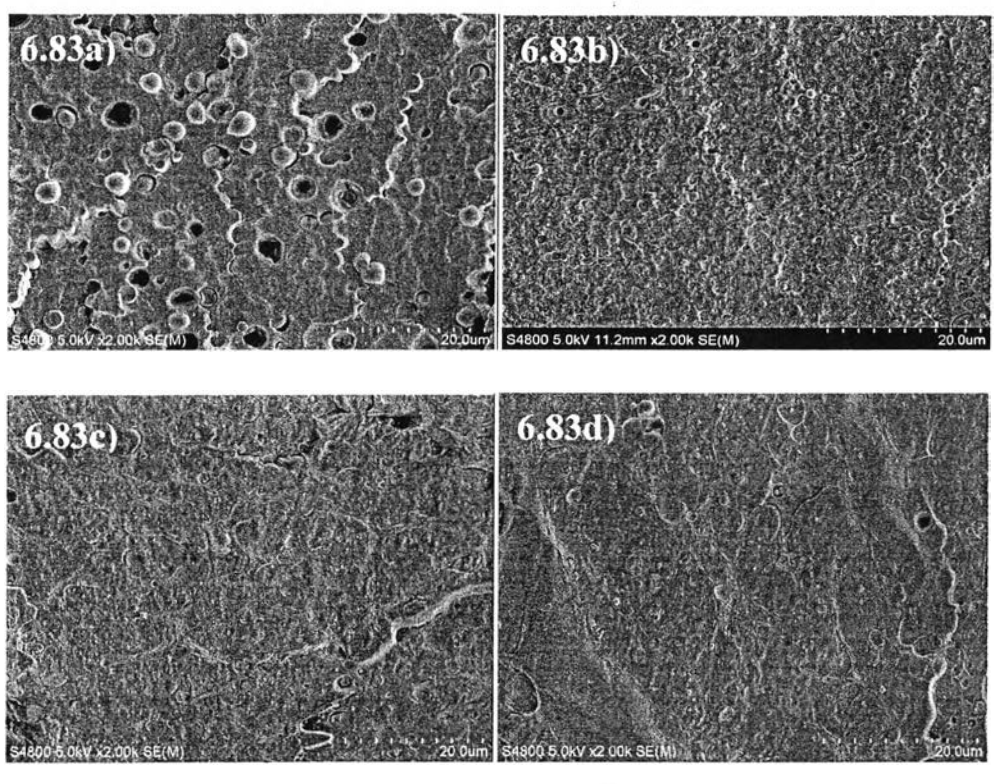

Figure 6.83 SEM images of the fracture of the blends (a) PLA/mEVA (70/30 w/w) blend (b) PLA/mEVA/PE-AA5 phr blend (c) PLA/mEVA/PE-AA10 phr blend (d) PLA/mEVA/PE-AA15 phr blend.

6.6.3.5 Mechanical properties

The effect of PE-AA compatibilizer on the tensile properties of pure PLA, PLA/mEVA binary blends, and PLA/mEVA/PE-AA blend as mentioned in Figures 6.84-6.86. The all compositions of the ternary blends exhibit a reduction in the Young's modulus and tensile strength as the PE-AA content increase especially in the excess additional PE-AA. In contrast, the elongation at break of PLA/mEVA/PE-AA blends improves suggested that the compatibility in ternary blend is better than that of the binary blend. From these results, the PLA/mEVA/PE-AA blends at 10 phr of E-GMA present the optimum elongation at break with the lowest compatibilizer content.

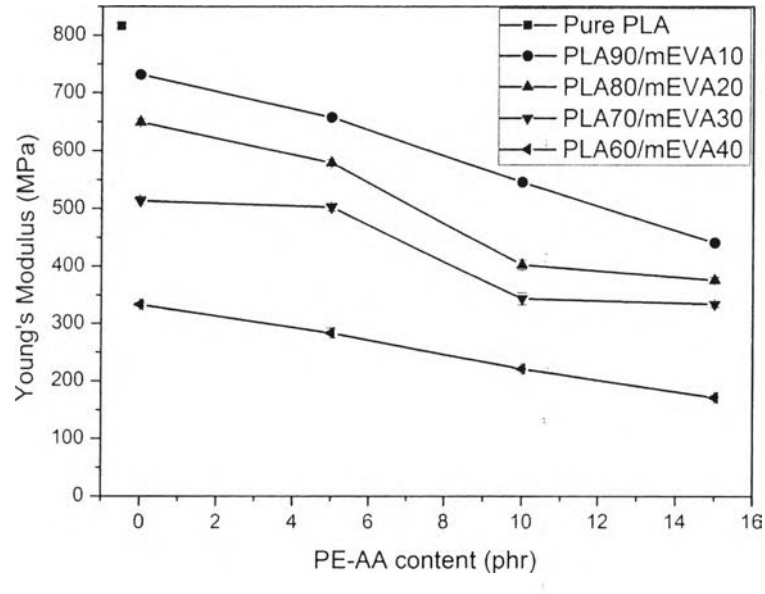

Figure 6.84 Young's modulus of PLA/mEVA blends at various PE-AA contents.

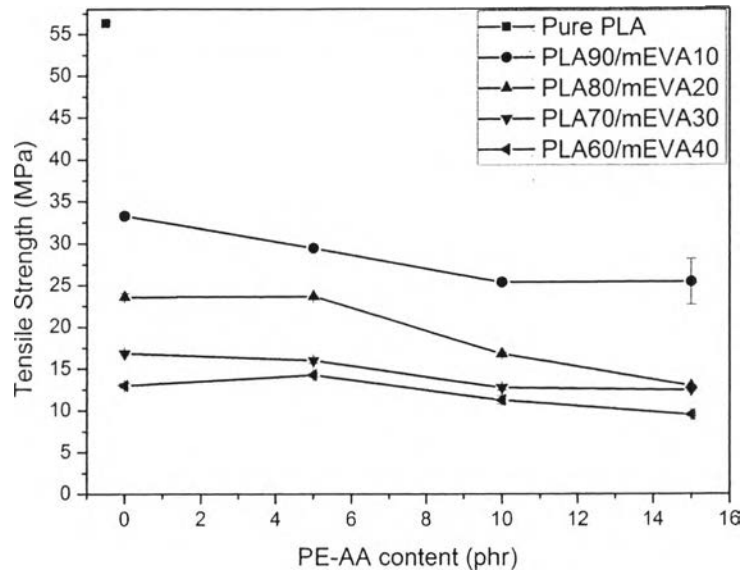

Figure 6.85 Tensile strength of PLA/mEVA blends at various PE-AA contents.

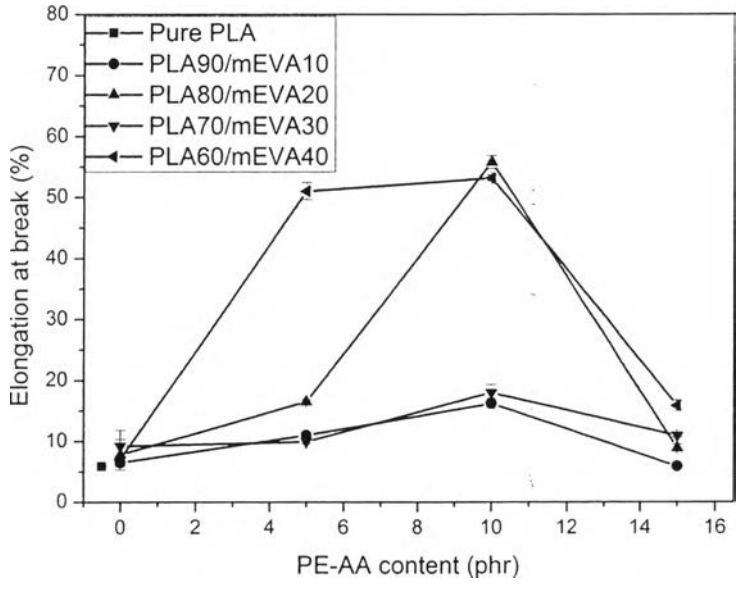

Figure 6.86 Elongation at break of PLA/mEVA blends at various PE-AA contents.

6.6.3.6 Melt flow index (MFI)

MFI values of PLA/mEVA/PE-AA blends with various PE-AA contents are shown in Figure 6.87. With the incorporation of PE-AA compatibilizer, the MFI values are lower than those of PLA/mEVA binary blends because of the obstruction effect on chain motion through the reaction between PE-AA compatibilizer and PLA/mEVA blends. The MFI values are enhanced with increasing in PE-AA contents in all blend compositions suggested that PE-AA is not only acting as a compatibilizer but also improving in processability.

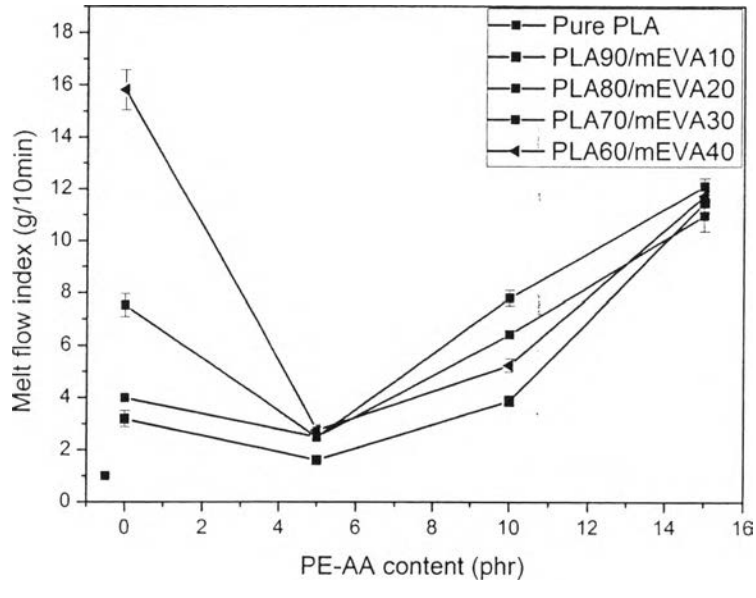

Figure 6.87 MFI values of PLA/mEVA blends at various PE-AA contents.

6.6.3.7 Biodegradability

In Figure 6.88, weight loss of pure PLA, PLA/mEVA binary blends and PLA/mEVA with various PE-AA contents can refer to biodegradable property. The first stage (1-4 weeks) weight loss of PLA/mEVA/PE-AA is lower than that of PLA/mEVA binary blend. After 4 week, weight loss of PLA/mEVA/PE-AA is higher than that of PLA/mEVA binary blend.

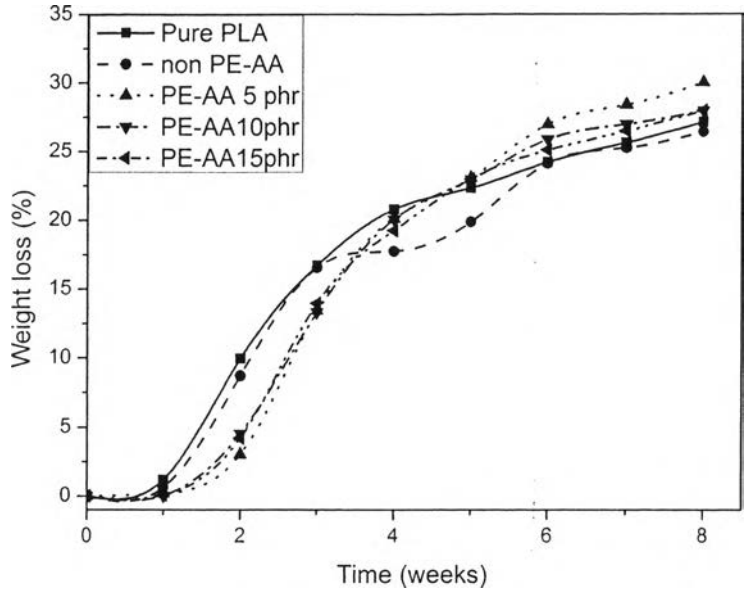

Figure 6.88 Weight loss of PLA/mEVA(90/10 w/w) blends at various PE-AA contents.

6.6.4 Poly(2-Ethyl-2-Oxazoline)

6.6.4.1 Chemical analysis

Oxazoline group of Oxa compatibilizer reacts with the carboxylic end group or hydroxyl end group of PLA and hydroxyl group of mEVA to form amide linkage which is shown in figure 6.89-6.90. From this reaction, it is the cause of decrease of oxazoline, hydroxyl and carboxylic groups. On the other hand, the increasing of amide group of the blends is observed.

FTIR spectra of Pure PLA and PLA/mEVA/Oxa blends with various Oxa contents are shown in Figures 6.91. FTIR spectra and Table 6.18 show the characteristic peak of pure PLA which compose of C=O stretching at 1730 cm^{-1} corresponding to carboxylic group and carbonyl group of PLA, O-H stretching at 3500 cm^{-1} corresponding to hydroxyl group and C-H stretching at 2850 cm^{-1} corresponding to CH_2 and CH aliphatic, the characteristic peak of mEVA which compose of C=O stretching at 1730 cm^{-1} corresponding to carbonyl group of vinyl acetate, O-H stretching at 3500 cm^{-1} corresponding to hydroxyl group and C-H

stretching at 2850 cm^{-1} corresponding to CH_2 and CH aliphatic and the characteristic peak of Oxa which compose of C-O stretching at 1200 cm^{-1}, C-N stretching at 1685 cm^{-1} and C-H stretching at 2850 cm^{-1} corresponding to CH_2 and CH aliphatic. For PLA/mEVA/Oxa blends, the oxazoline group reacts with carboxyl group or hydroxyl group of PLA forming oxamide group shown as amide I (C-N stretching) bands at 1685 cm^{-1} and N-H stretching at 3300 cm^{-1} [24]. Table 6.17 show the absorbance ratio of pure PLA, PLA/mEVA binary blends and PLA/mEVA/Oxa blends. The absorbance ratio of the peak at 1730/2850 cm^{-1} and 3500/2850 cm^{-1} decrease however, the absorbance ratio of the peak at 1685/2850 cm^{-1} and 3300/2850 cm^{-1} increase with the increasing of Oxa contents which confirms the reactions between the oxazoline group and carboxylic end groups of PLA or hydroxyl end group of PLA and mEVA to from amide linkage.

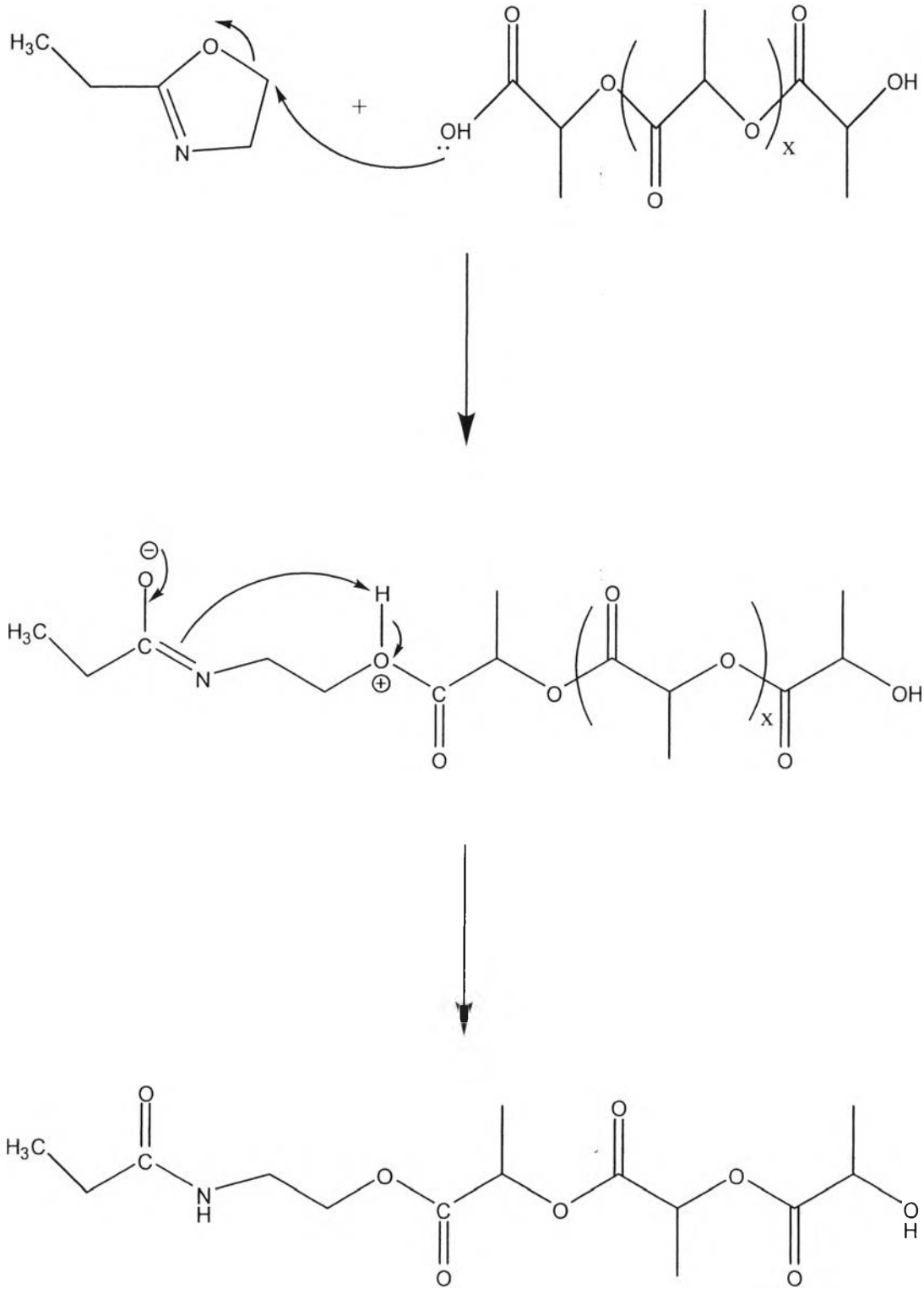

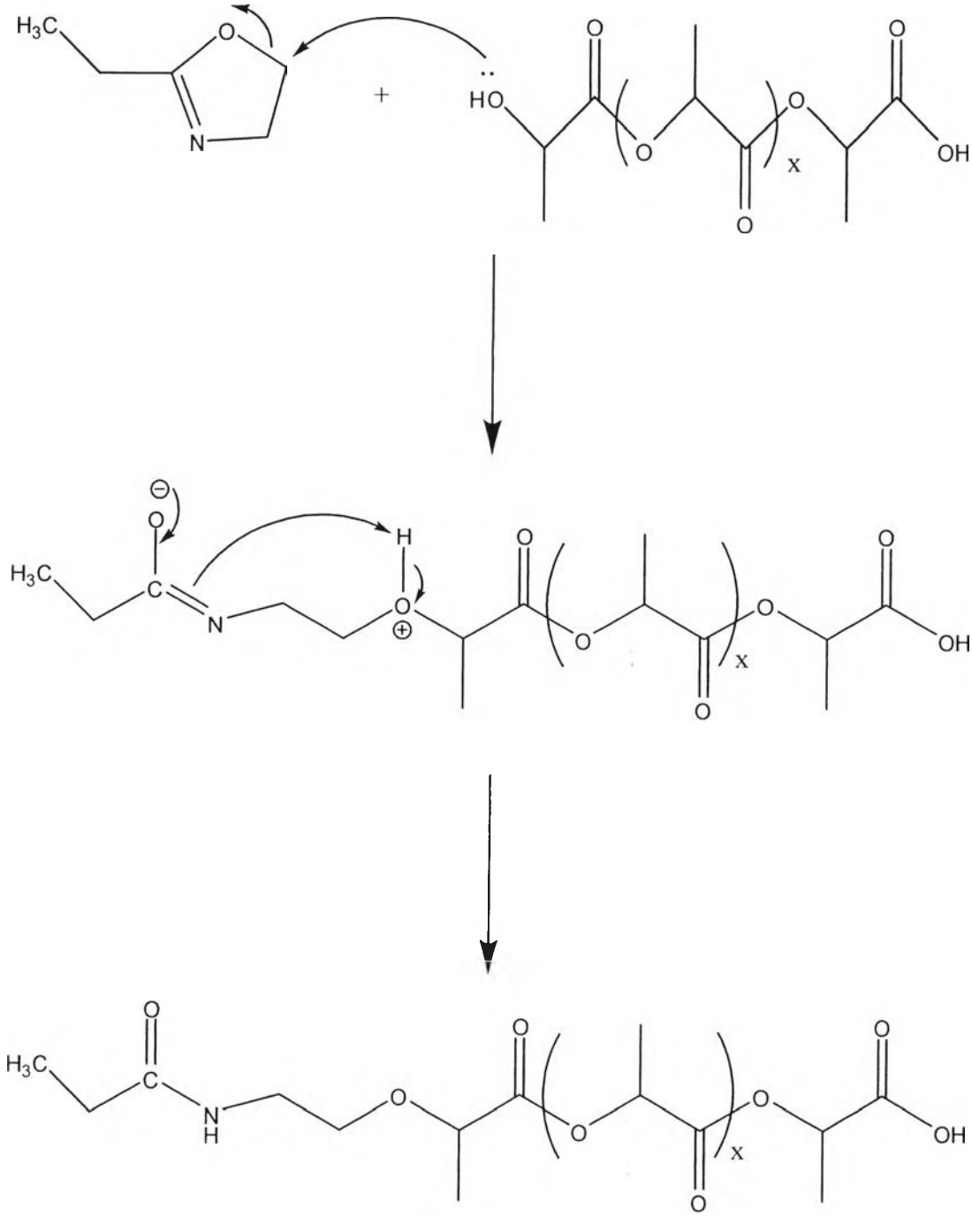

Figure 6.89 Reaction of –COOH and -OH groups of PLA with oxazoline group of Oxa compatibilizer.

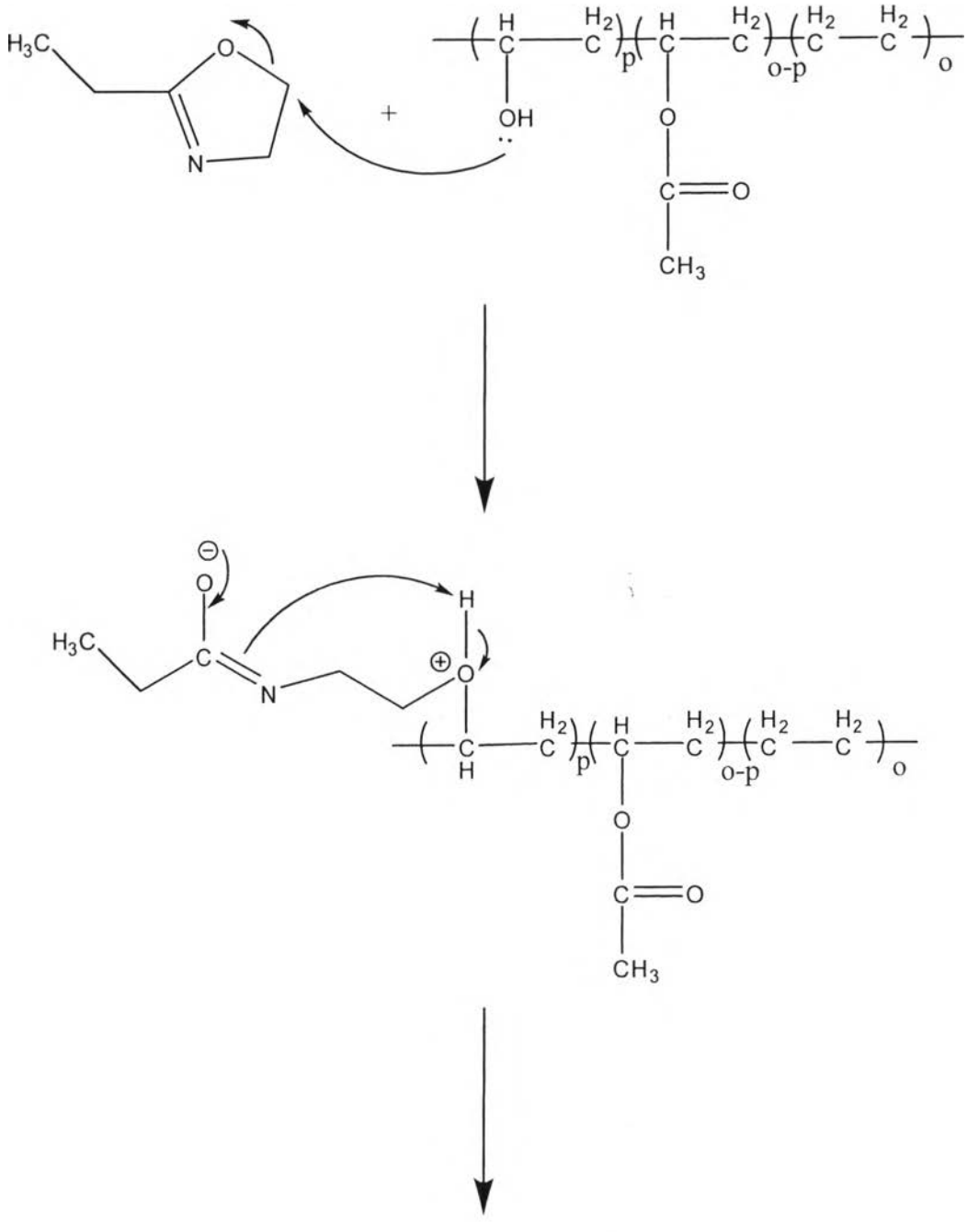

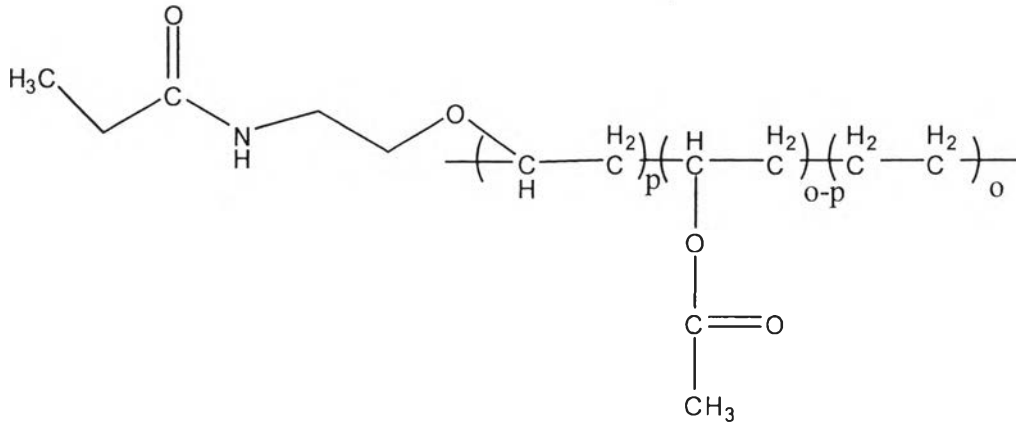

Figure 6.90 Reaction of –OH groups of mEVA with oxazoline group of Oxa compatibilizer.

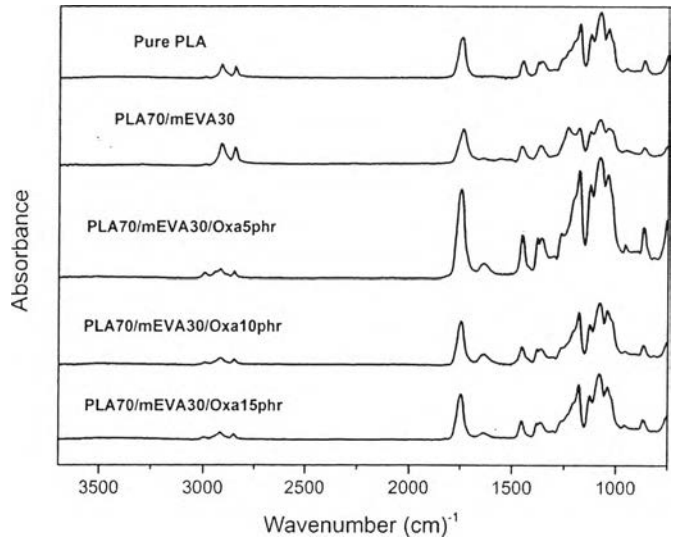

Figure 6.91 FTIR spectra of PLA/mEVA (70/30 w/w) blends at various Oxa contents.

Table 6.17 Absorbance ratio of pure PLA, PLA/mEVA binary blends and PLA/mEVA/Oxa blends

absorbance ratio	Pure PLA	PLA/mEVA	PLA/mEVA/ Oxa 5 phr	PLA/mEVA/ Oxa 10 phr	PLA/mEVA/ Oxa 15 phr
1200/2850 peak	0.81	0.89	0.94	0.96	0.90
1685/2850 peak	0.54	0.56	0.72	0.69	0.65
3300/2850 peak	0.60	0.61	0.76	0.87	0.78
3500/2850 peak	0.77	0.78	0.75	0.73	0.72

Table 6.18 Assignment of absorbance of PLA, mEVA and Oxa

Materials	Absorbance (cm^{-1})	Assignment
PLA	1200	C-O stretching of Ester group
	1730	C=O stretching of Carbonyl group and Carboxylic group
	2850	C-H stretching of CH_2 and CH aliphatic
	3500	O-H (H-bonded), usually broad of Hydroxyl group
mEVA	1200	C-O stretching of Ester group
	1730	C=O stretching of Carbonyl group
	2850	C-H stretching of CH_2 and CH aliphatic
	3500	O-H (H-bonded), usually broad of Hydroxyl group
Oxa	1200	C-O stretching
	1685	C-N stretching
	2850	C-H stretching of CH_2 and CH aliphatic

6.6.4.2 Thermal stability

TGA thermograms of PLA/mEVA/Oxa blends with different Oxa contents (Figures 6.92-6.95) shows the two steps of degradation which are exhibited in Figure 6.92-6.95 and Table 6.19. For the effect of Oxa compatibilizer, the decomposition temperatures of PLA/mEVA/Oxa blends are lower than those of PLA/mEVA binary blends. Therefore, the decomposition temperatures of PLA/mEVA/Oxa blends also decrease with the increment of Oxa contents.

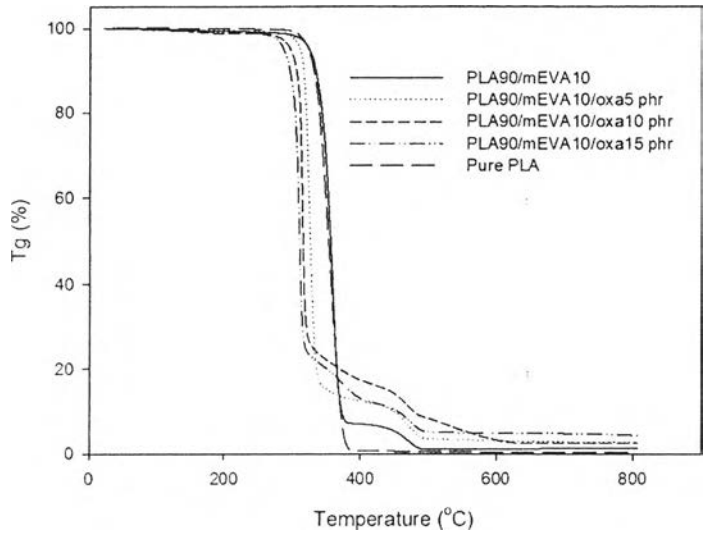

Figure 6.92 TGA thermograms of PLA/mEVA (90/10 w/w) blends at various Oxa contents.

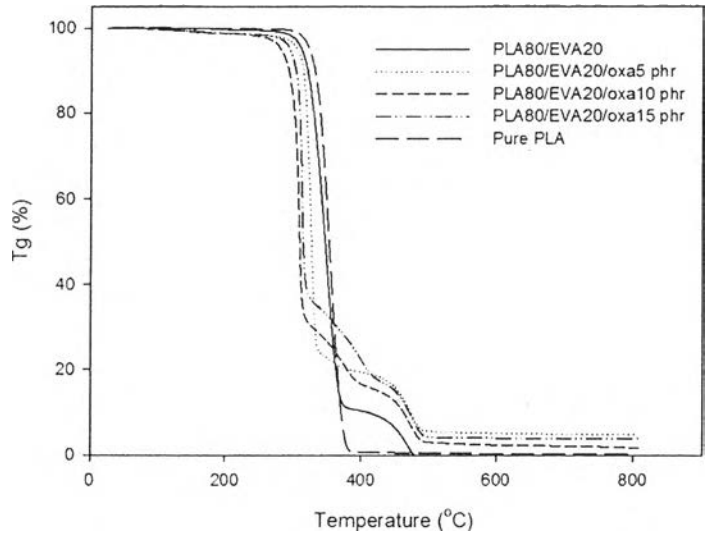

Figure 6.93 TGA thermograms of PLA/mEVA (80/20 w/w) blends at various Oxa contents.

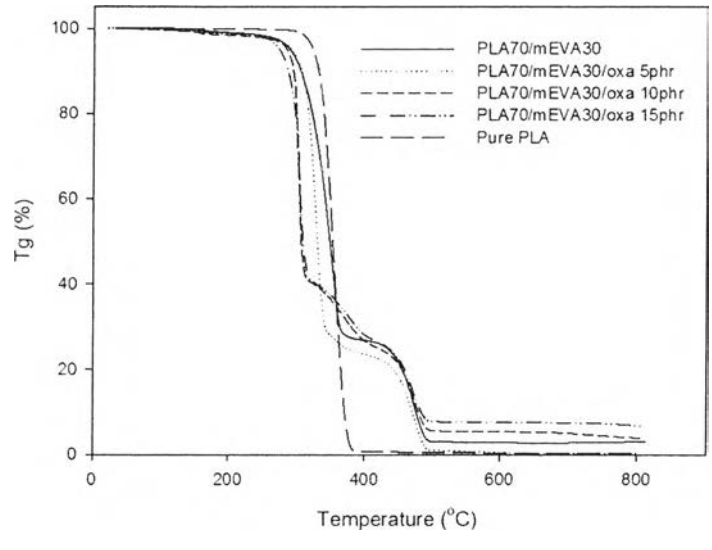

Figure 6.94 TGA thermograms of PLA/mEVA (70/30 w/w) blends at various Oxa contents.

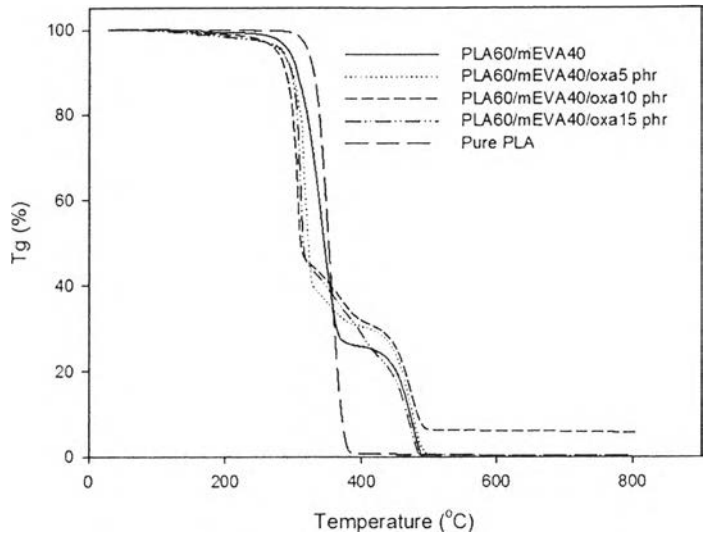

Figure 6.95 TGA thermograms of PLA/mEVA (60/40 w/w) blends at various Oxa contents.

Table 6.19 Decomposition temperatures of pure PLA, pure mEVA, PLA/mEVA binary blends and PLA/mEVA/Oxa blends

Blend composition	Decomposition Temperature (°C)	
	1st	2nd
PLA	332.8	-
mEVA	351.5	468.0
PLA90/mEVA10	351.2	471.0
Oxa 5 phr	328.0	474.6
Oxa 10 phr	315.1	472.7
Oxa 15 phr	311.1	479.5
PLA80/mEVA20	351.3	472.1
Oxa 5 phr	325.0	473.5
Oxa 10 phr	308.4	474.7
Oxa 15 phr	313.9	477.1
PLA70/mEVA30	342.9	471.0
Oxa 5 phr	325.6	474.3
Oxa 10 phr	305.0	477.2
Oxa 15 phr	301.3	474.8
PLA60/mEVA40	334.6	469.7
Oxa 5 phr	319.5	475.1
Oxa 10 phr	308.0	475.0
Oxa 15 phr	310.3	471.8

6.6.4.2 Thermal properties

DSC curves of PLA/mEVA/Oxa with various Oxa contents are exhibited in Figures 6.96-6.99. Moreover, the melting temperature (T_m), cold crystallization temperature (T_{cc}), degree of crystallization (χ_c) and two glass transition temperature (around -25 °C for mEVA and around 60 °C for PLA) are presented in Table 6.20. The glass transition temperature of PLA/mEVA/Oxa blends increase with the increment of Oxa contents because of reaction between Oxazoline groups of Oxa compatibilizer and carboxylic end groups of PLA [13]. The addition of Oxa compatibilizer not effect with the melting temperature of the PLA/mEVA blends. However, cold crystallization temperature and degree of crystallization increase with the supplement of Oxa contents. This indicates that Oxa not only compatibilizer but also act as nucleating agent.

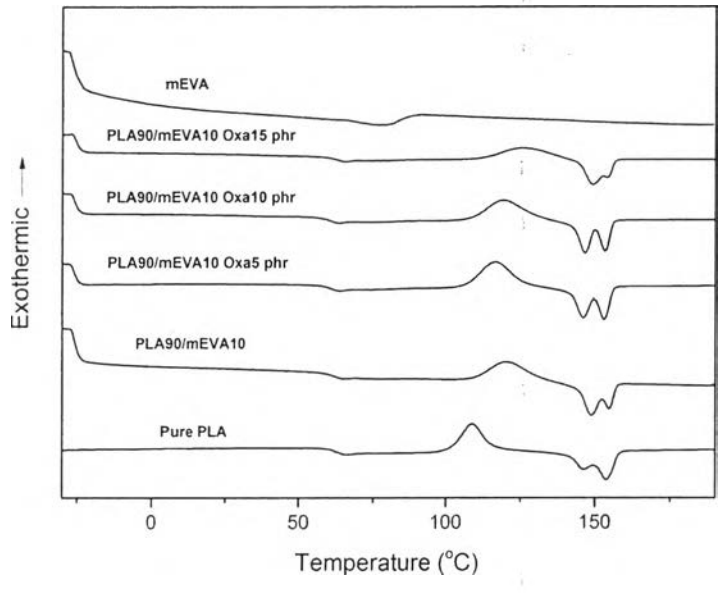

Figure 6.96 DSC thermograms of PLA/mEVA (90/10 w/w) blends at various Oxa contents.

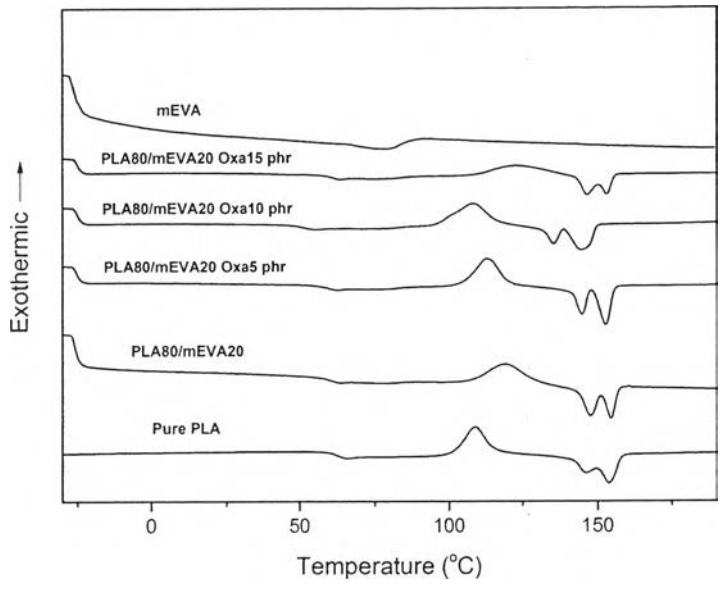

Figure 6.97 DSC thermograms of PLA/mEVA (80/20 w/w) blends at various Oxa contents.

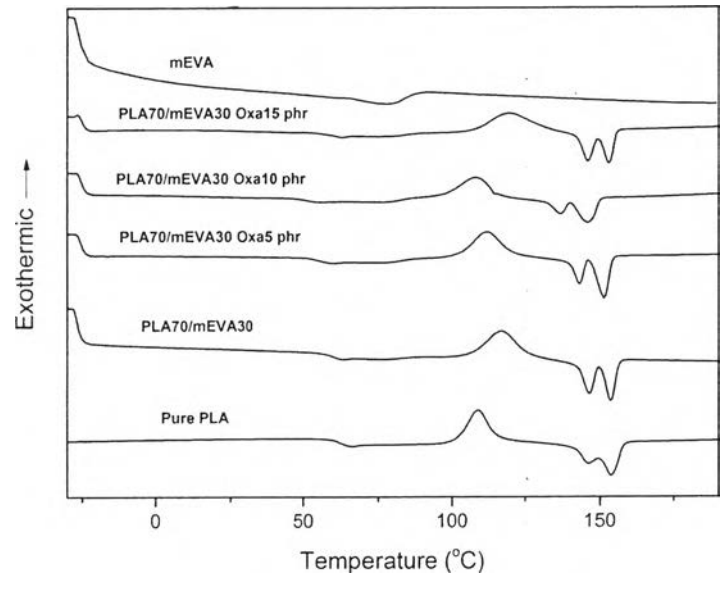

Figure 6.98 DSC thermograms of PLA/mEVA (70/30 w/w) blends at various Oxa contents.

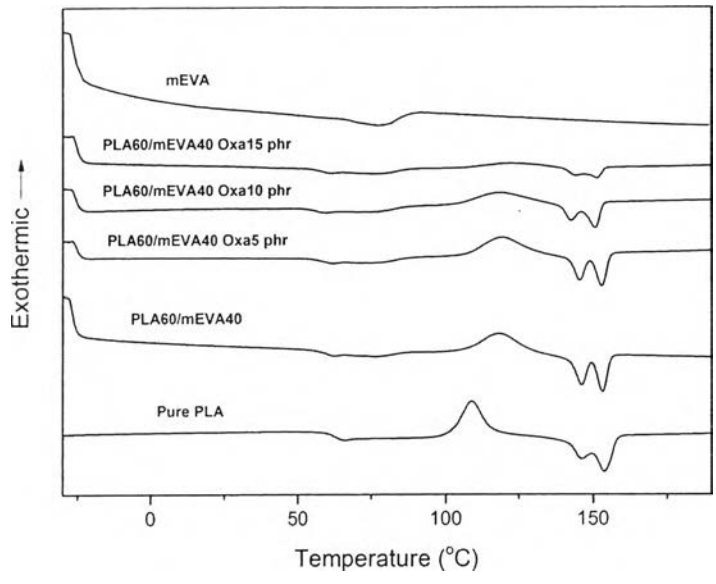

Figure 6.99 DSC thermograms of PLA/mEVA (60/40 w/w) blends at various Oxa contents.

Table 6.20 Thermal properties of pure PLA, PLA/mEVA binary blends and PLA/mEVA/Oxa blends

Sample	T_{g1} (°C)	T_{g2} (°C)	T_{cc} (°C)	T_{m1} (°C)	T_{m2} (°C)	ΔH_{cc} (J/g)	ΔH_m (J/g)	$\%\chi_c$
Pure PLA	-	57.9	103.0	146.8	153.7	19.4	24.5	5.45
PLA90/mEVA10	-26.8	58.6	120.3	148.9	154.8	26.9	28.3	1.72
Oxa5 phr	-27.1	57.1	116.5	146.1	152.9	30.0	31.2	1.46
Oxa 10phr	-26.9	56.7	119.2	146.7	153.1	27.0	28.6	1.87
Oxa15 phr	-26.3	59.4	125.8	149.2	154.6	18.8	19.9	1.31
PLA80/mEVA20	-26.6	57.0	119.3	147.8	154.4	26.9	27.9	1.34
Oxa5 phr	-26.4	55.6	113.1	145.0	152.6	28.5	29.6	1.42
Oxa 10phr	-26.2	57.5	108.2	135.4	152.5	16.1	17.6	2.03
Oxa15 phr	-26.2	57.5	122.7	146.7	153.0	27.1	28.6	2.09
PLA70/mEVA30	-27.7	56.4	117.0	146.6	153.7	27.2	27.9	1.15
Oxa5 phr	-26.6	51.9	121.3	143.2	151.3	20.9	21.5	0.84
Oxa 10phr	-26.4	50.0	115.5	136.8	151.9	25.7	26.5	1.20
Oxa15 phr	-26.3	56.3	132.9	146.1	152.9	23.1	24.3	1.83
PLA60/mEVA40	-27.8	55.9	118.3	146.2	159.2	22.3	22.9	1.06
Oxa5 phr	-26.4	55.0	119.5	145.6	152.9	6.5	7.1	1.06
Oxa 10phr	-26.8	52.6	118.3	142.8	152.6	15.0	16.3	2.24
Oxa15 phr	-26.3	54.5	121.8	145.2	152.0	20.0	21.5	2.67

6.6.4.3 Dynamic mechanical properties

The effect of Oxa contents on the storage modulus and loss modulus of PLA/mEVA/Oxa blends as mentioned on Figures 6.100-6.107 and Table 6.21, it is obvious that the storage modulus of all blend compositions decreases with the increase in Oxa content especially at room temperature (30 °C) due to the decrease in the strength of the blends.

For Tan δ result shown in Figures 6.108-6.111 and Table 6.21, the glass transition temperature increases with the addition of Oxa compatibilizer suggested that the reaction between Oxazoline group and carboxylic group. This reaction also leads to form bonding between Oxa compatibilizer and PLA, which resulting in the glass transition temperatures of PLA/mEVA/ PE-AA blend increase.

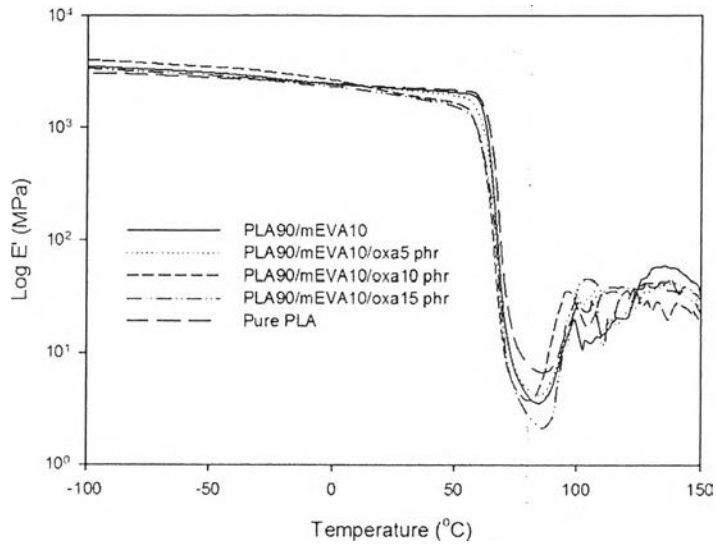

Figure 6.100 Storage Modulus of PLA/mEVA (90/10 w/w) blends at various Oxa contents.

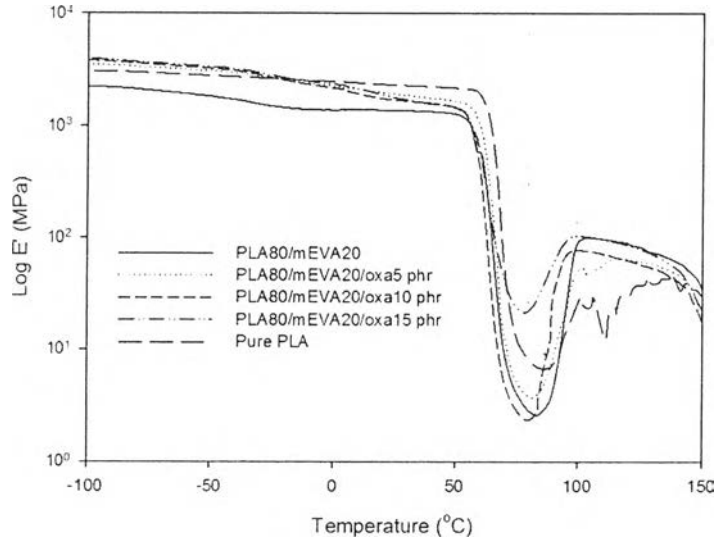

Figure 6.101 Storage Modulus of PLA/mEVA (80/20 w/w) blends at various Oxa contents.

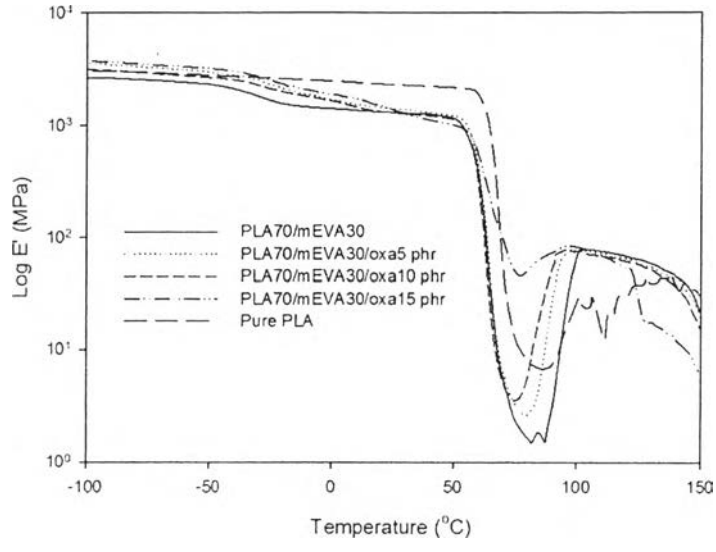

Figure 6.102 Storage Modulus of PLA/mEVA (70/30 w/w) blends at various Oxa contents.

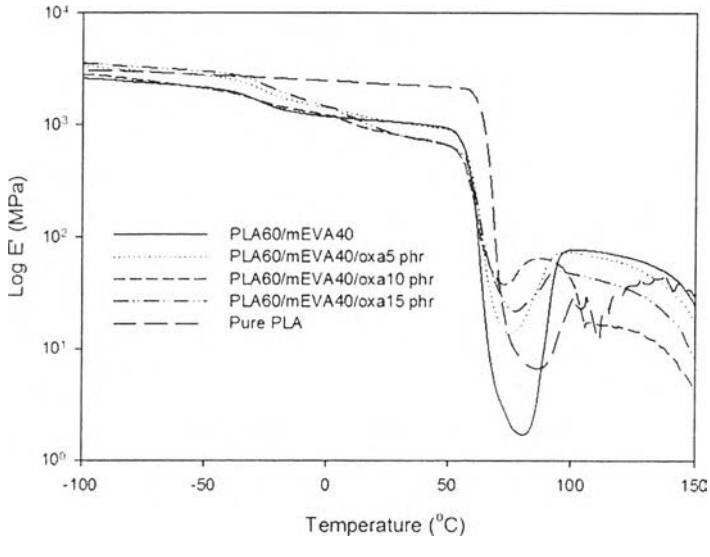

Figure 6.103 Storage Modulus of PLA/mEVA (60/40 w/w) blends at various Oxa contents.

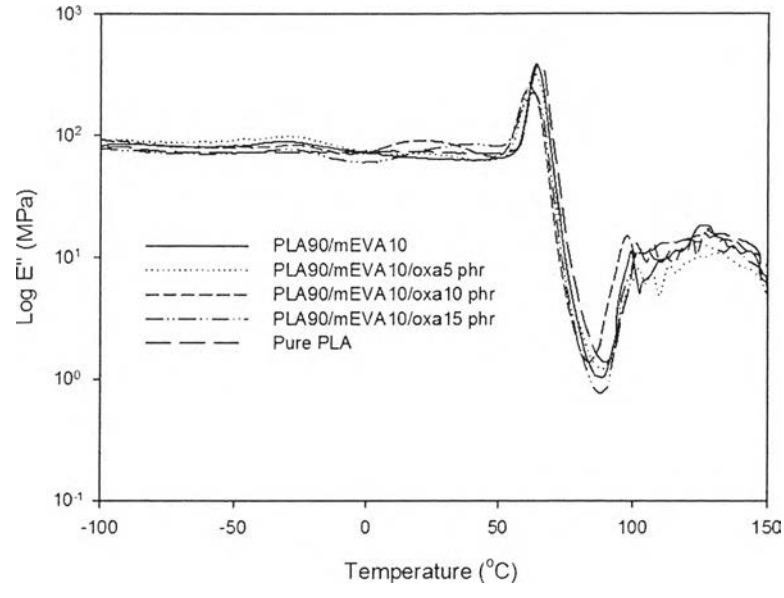

Figure 6.104 Loss Modulus of PLA/mEVA blends (90/10 w/w) at various Oxa contents.

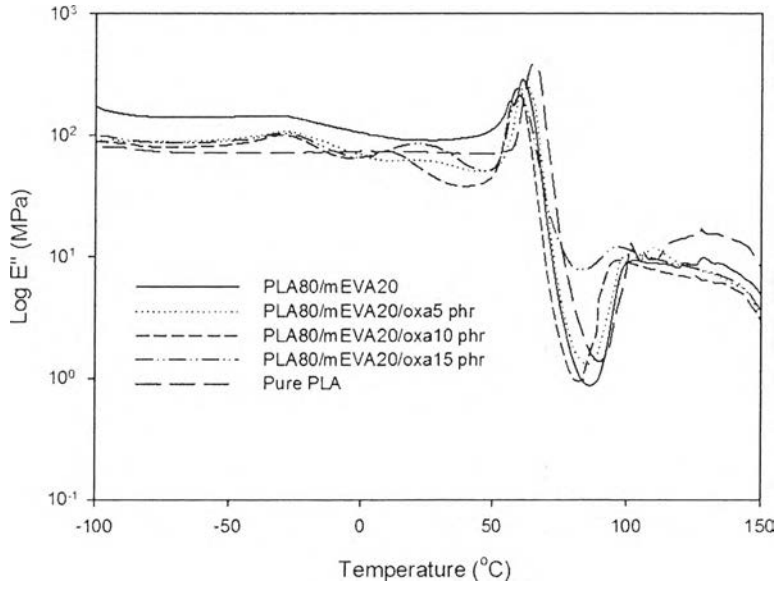

Figure 6.105 Loss Modulus of PLA/mEVA blends (80/20 w/w) at various Oxa contents.

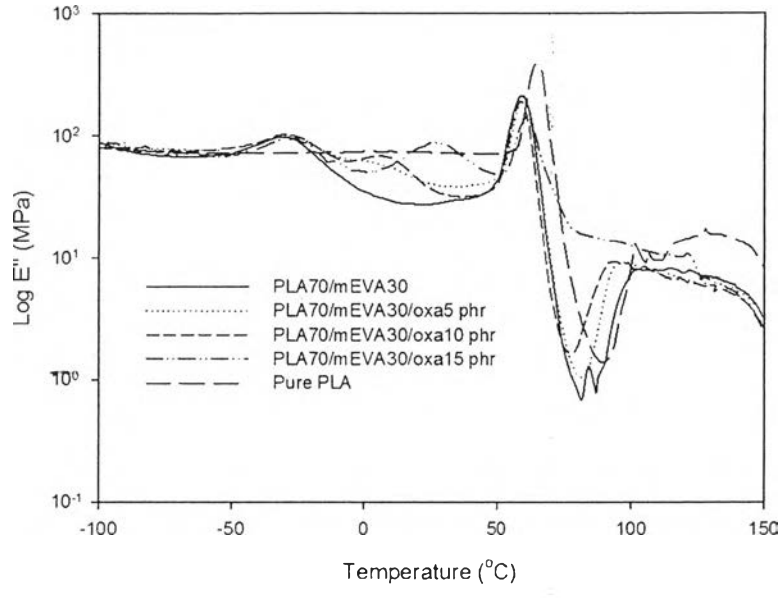

Figure 6.106 Loss Modulus of PLA/mEVA blends (70/30 w/w) at various Oxa contents.

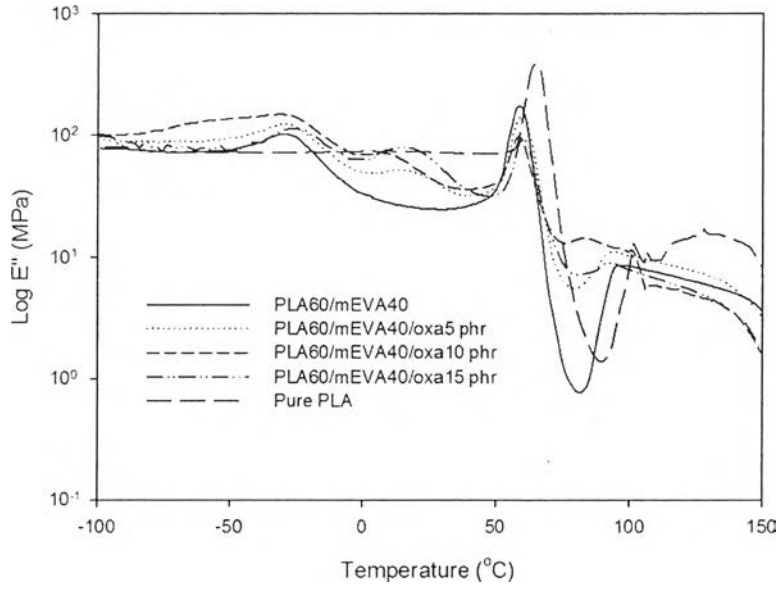

Figure 6.107 Loss Modulus of PLA/mEVA blends (60/40 w/w) at various Oxa contents.

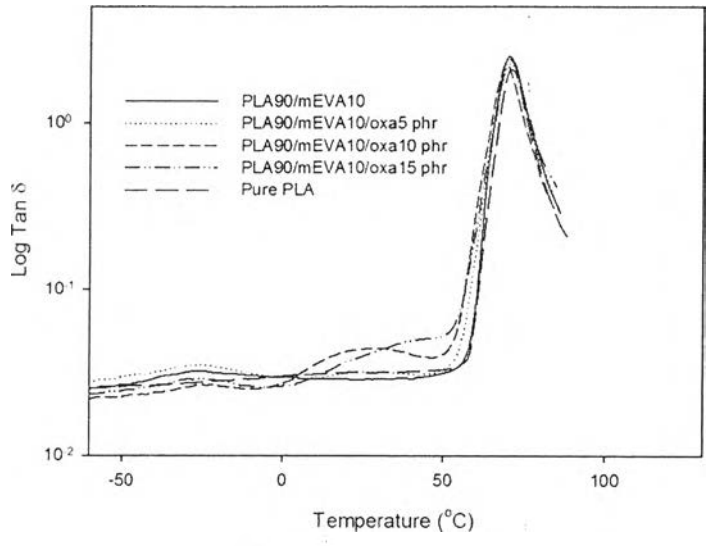

Figure 6.108 Tan δ of PLA/mEVA (90/10 w/w) blends at various Oxa contents.

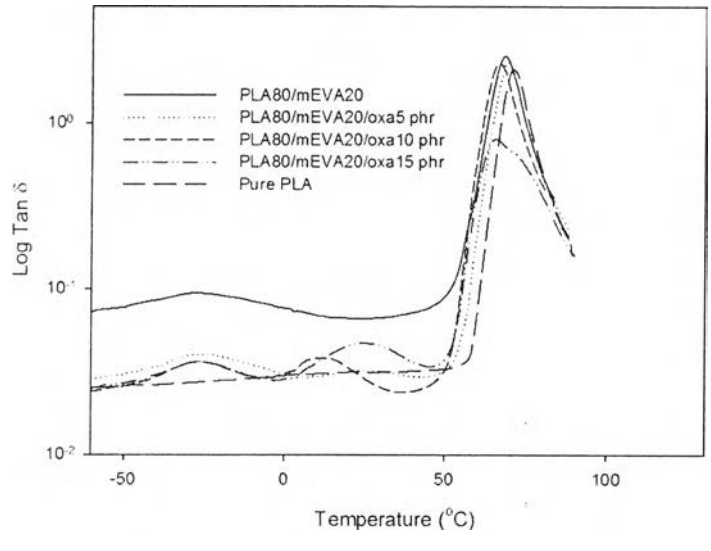

Figure 6.109 Tan δ of PLA/mEVA (80/20 w/w) blends at various Oxa contents.

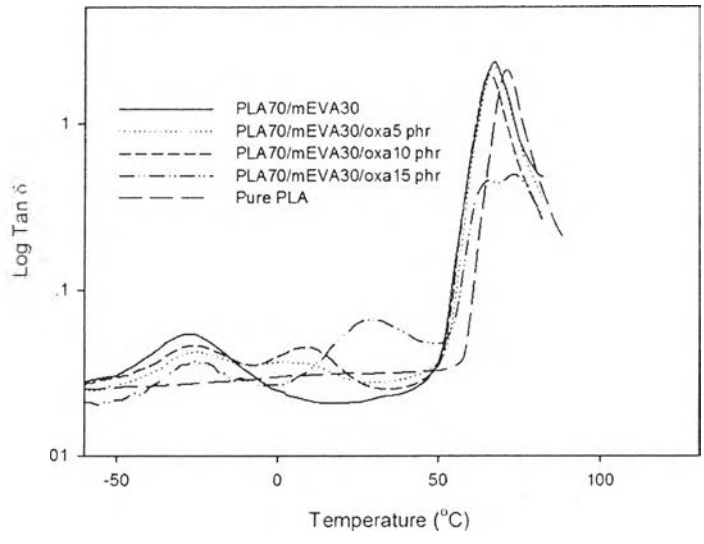

Figure 6.110 Tan δ of PLA/mEVA (70/30 w/w) blends at various Oxa contents.

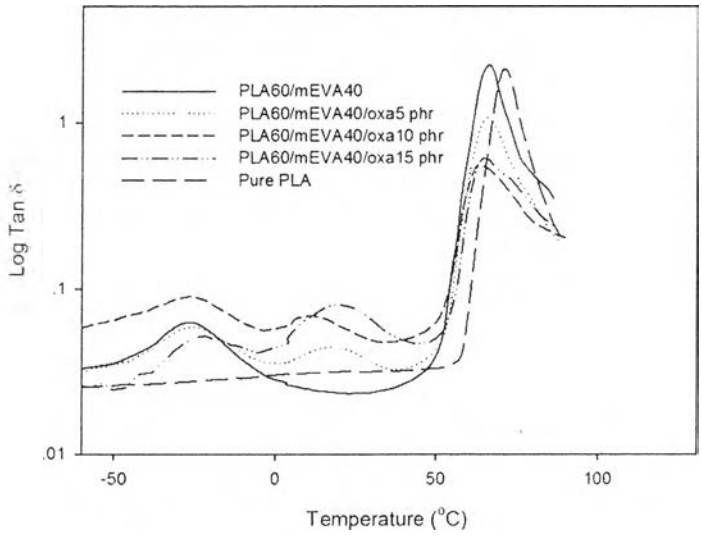

Figure 6.111 Tan δ of PLA/mEVA (60/40 w/w) blends at various Oxa contents.

Table 6.21 Dynamic mechanical properties of pure PLA, pure mEVA, PLA/mEVA binary blends and PLA/mEVA/Oxa blends

Blend composition	Tan δ_{max1} (Tg_1, °C)	Tan δ_{max2} (Tg_2, °C)	30 °C
			E′ (MPa)
PLA	70.1	-	2280
mEVA	-20	-	12
PLA90/mEVA10	-26.9	70	2208
Oxa 5 phr	-25.8	70.5	2144
Oxa 10 phr	-25.7	70.1	1964
Oxa 15 phr	-25.7	70	1888
PLA80/mEVA20	-27.8	68.2	1364
Oxa 5 phr	-25.7	68.4	1863
Oxa 10 phr	-25.8	66.3	1659
Oxa 15 phr	-25.5	66.1	1693
PLA70/mEVA30	-27.8	66.6	1290
Oxa 5 phr	-25.7	68	1385
Oxa 10 phr	-25.8	66.3	1273
Oxa 15 phr	-25.9	66.3	1278
PLA60/mEVA40	-28.6	66.4	1048
Oxa 5 phr	-25.9	66.6	1043
Oxa 10 phr	-25.8	64.1	802
Oxa 15 phr	-21.7	64.2	800

6.6.4.4 Morphology

FE-SEM images of the cryogenic fracture of PLA/mEVA (70/30 w/w) blends with various Oxa contents are shown in Figures 6.112a.-6.112d. The two-phase structure of mEVA domain and PLA matrix in the binary blend is shown in Figure 6.112a. Moreover, the spherulites are the mEVA in PLA/mEVA blend [4].With the incorporation of Oxa compatibilizer, the particles of the mEVA disperse phase becomes much more uniform and much reduce in size, as mentioned in Figures 6.112b-6.112d. The mEVA particles are smaller than PLA/mEVA binary blend for all compatibilized blends and much more firmly embed in the PLA matrix.

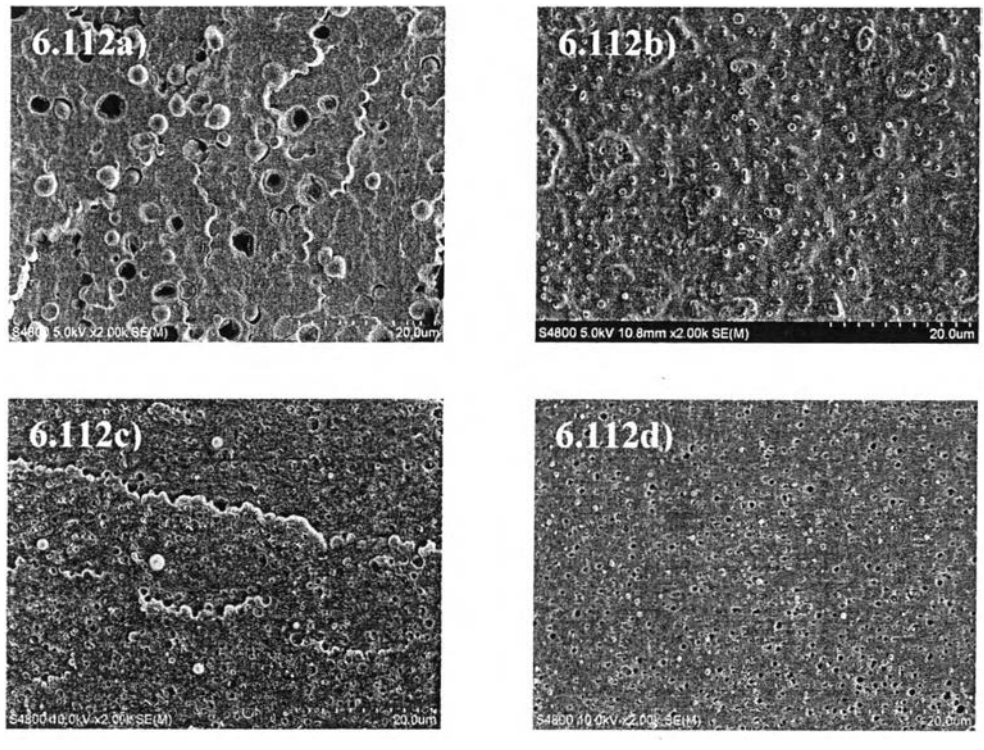

Figure 6.112 SEM images of the fracture of the blend (a) PLA/mEVA (70/30 wt%) blend (b) PLA/mEVA/ Oxa5phr blend (c) PLA/mEVA/Oxa10 phr blend (d) PLA/mEVA/ Oxa 15 phr blend.

6.6.4.5 Mechanical properties

The tensile properties of pure PLA, PLA/mEVA binary blends, and PLA/mEVA with various Oxa contents are represented in Figures 6.113-6.115. PLA/mEVA/Oxa ternary blends indicates a lower in the Young's modulus and tensile strength but higher elongation at break compared to PLA/mEVA binary blends at all compositions. Moreover, the increasing in the Oxa contents from 5 to 15 phr enhances the elongation at break of PLA/mEVA/Oxa ternary blends. This confirms that Oxa actually act as the effective compatibilizer in PLA/mEVA blends. From these results, the PLA/mEVA/Oxa blends at 15 phr of Oxa show the optimum elongation at break with the lowest compatibilizer content.

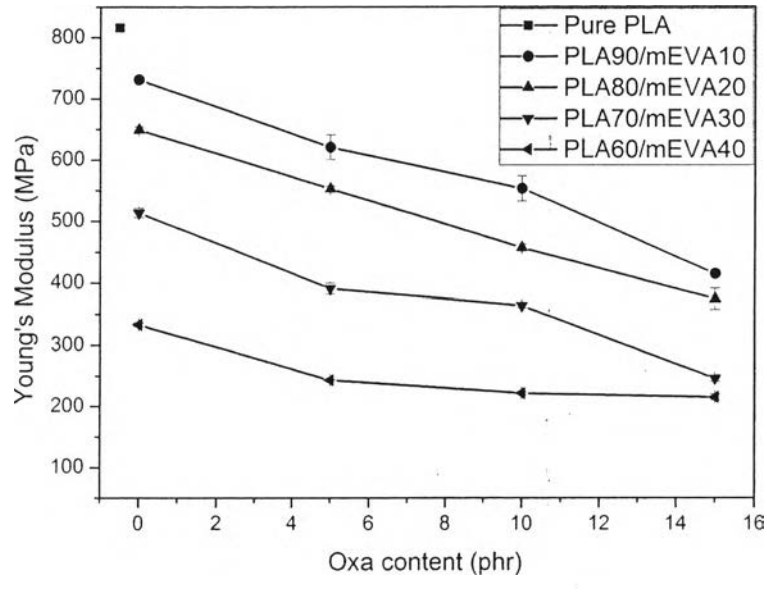

Figure 6.113 Young's modulus of PLA/mEVA blends at various Oxa contents.

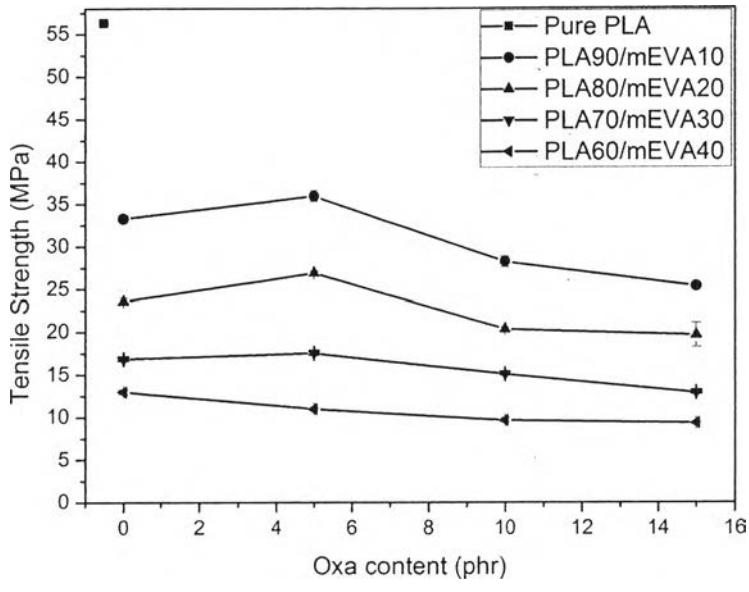

Figure 6.114 Tensile strength of PLA/mEVA blends at various Oxa contents.

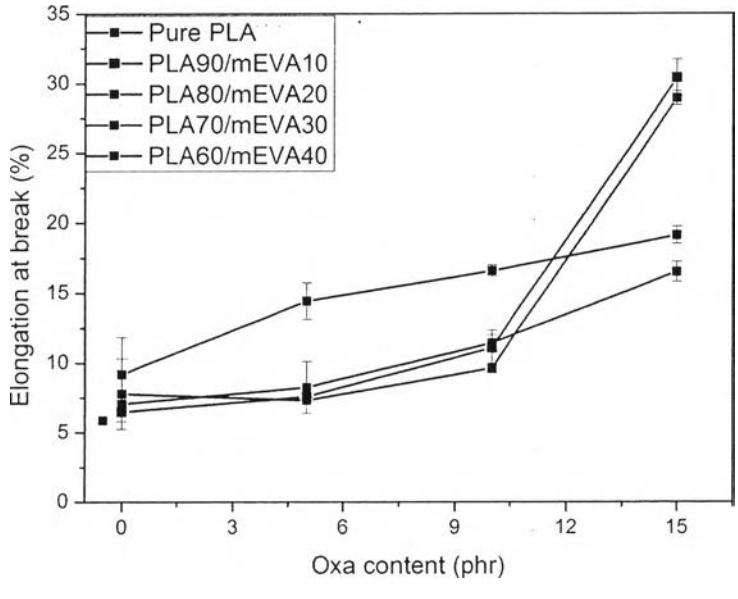

Figure 6.115 Elongation at break of PLA/mEVA blends at various Oxa contents.

6.6.4.6 Melt flow index (MFI)

In Figure 6.116, MFI values of PLA/mEVA/Oxa blends with various Oxa contents are higher than those of PLA/mEVA binary blends and also increase with the increasing of Oxa contents. This suggests that PLA/mEVA/Oxa to be more easily process than PLA/mEVA binary blends.

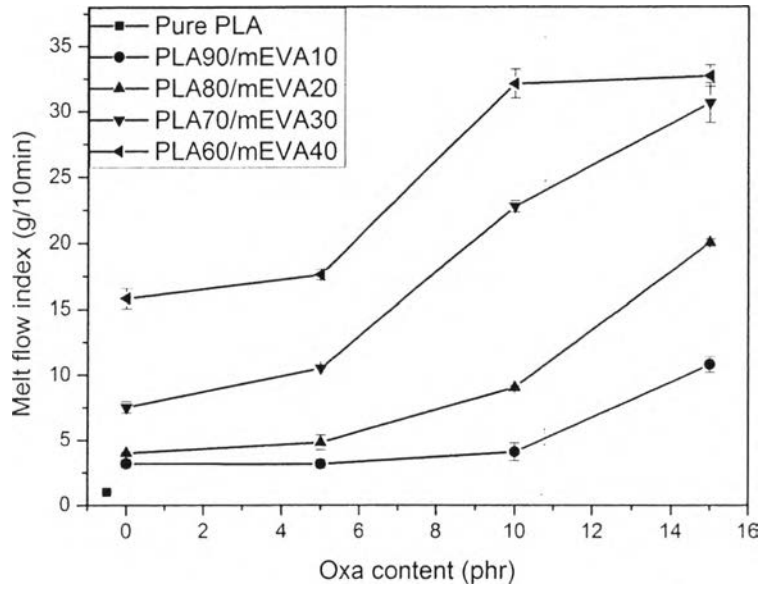

Figure 6.116 MFI values of PLA/mEVA blends at various Oxa contents.

6.6.4.7 Biodegradibility

In Figure 6.117, the biodegradability is relative to weight loss of pure PLA, PLA/mEVA binary blends and PLA/mEVA with various Oxa contents. The result shows weight loss of PLA/mEVA/Oxa increase with the increment of Oxa contents. This is proposed that Oxa enhance biodegradability of PLA blends.

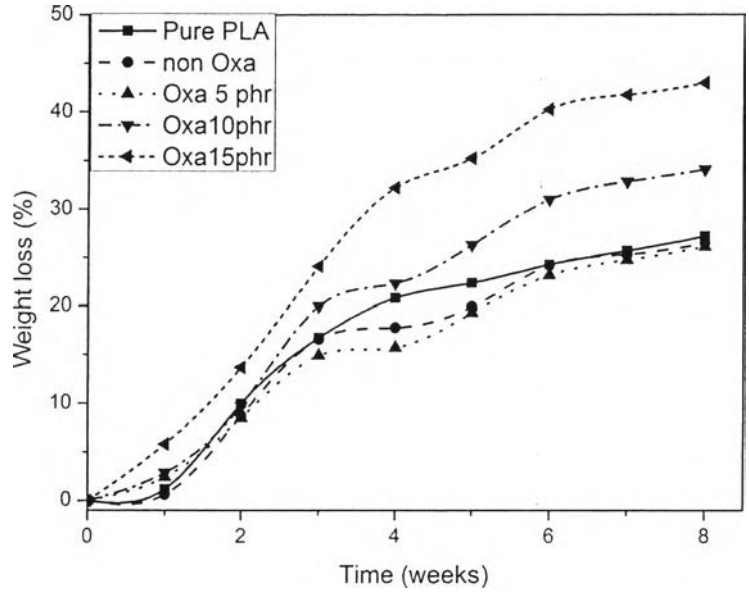

Figure 6.117 Weight loss of PLA/mEVA (90/10 w/w) blends at various Oxa contents.

6.7 Conclusion

The PLA/mEVA/compatibilizers blends were produced by a 20 mm diameter co-rotating twin-screw extruder with 40:1 L/D ratio and screw speed at 30 rpm with various compatibilizers contents. The result from FTIR revealed that the decreasing of the absorbance ratio at the peak 910/2850, 1730/2850 and 3500/2850 cm^{-1} and the increasing of the absorbance ratio at the peak 1200/2850, 1685/2850 and 3300/2850 cm^{-1} were confirm chemical reactions between compatibilizers and the PLA/mEVA blends. PLA/mEVA blends with all compatibilizers still exhibited the two glass transition temperatures. The increasing in all compatibilizers loading in the PLA/mEVA blends caused an increase in glass transition temperature (T_g). For the DSC results, degree of crystallization decreased with the increment of E-GMA and PE-AA compatibilizers. On the other hand, T-GMA and Oxa compatibilizers enhanced degree of crystallization. Moreover, storage modulus was decreased with the increase of all compatibilizers contents. Morphological interpretation through

FE-SEM revealed the improvement in miscibility of the PLA/mEVA blends in the presence of all compatibilizers. Young's modulus and tensile strength were dropped; however, elongation at break increased with the supplement of all compatibilizers. The addition of E-GMA and T-GMA compatibilizers in the PLA/mEVA blends led to a dramatic reduction of the MFI values of the blends and retarded biodegradable property of PLA blends. On the contrary, The MFI values and biodegradability of the PLA/mEVA blends were enhanced with the incorporation of PE-AA and Oxa compatibilizers. In summation, the PLA/mEVA blends with all compatibilizers could inject into dumbbell-shape specimens by injection molding.

6.8 Acknowledgements

This research is funded from National Research Council of Thailand (NRCT), the Petroleum and Petrochemical College

The author would like to gratefully acknowledge the help of TPI POLENE.Co.Ltd, for the material support.

Finally, I would like to thank the help of Assoc. Prof. Dr. Rathanawan Magaraphan, Asst. Prof. Dr. Manit Nithitanakul and Asst. Prof. Dr. Suparat Rukchonlatee for their suggestion of the experiment.

6.9 References

[1] Kumar, M., Mohanty, S., Nayak, S.K., and Parvaiz, M.R. (2010). Effect of glycidyl methacrylate (GMA) on the thermal, mechanical and morphological property of biodegradable PLA/PBAT blend and its nanocomposites. Bioresource Technology , 101, 8406-8415.

[2] Sirisinha, K., and Somboon, W. (2011). Melt characteristics, mechanical, and thermal properties of blown film from modified blends of poly(butylenes adipate-co-terephthalate) and poly(lactide). Journal of Applied Polymer Science , 124, 4986-4992.

[3] Hippi, U. (2005). Novel functionalized polyolefins as compatibilizers in polyolefin/polyamide 6 blends and polyethylene/metal hydroxide composites. Polymer Technology Publication Series , 27.

[4] Takayama, T., and Todo, M. (2006). Improvement of impact fracture properties of PLA/PCL polymer blend due to LTI addition. J Mater Sci , 41, 4989-4992.

[5] Harada, M., Iida, K., Okamoto, K., Hayashi, H., and Hirano, K. (2008). Reactive compatibilization of biodegradable poly(lactic acid)/poly(ε-caprolactone) blends with reactive processing agents. POLYMER ENGINEERING AND SCIENCE , 1359-1368.

[6] Zhang, N., Wang, Q., Ren, J., and Wang, L. (2009). Preparation and properties of biodegradable poly(lactic acid)/poly(butylene adipate-co-terephthalate) blend with glycidyl methacrylate as reactive processing agent. J Mater Sci , 44, 250-257.

[7] Yildirim, E., and Yurtsever, M. (2012). A comparative study on the efficiencies of polyethylene compatibilizers by using theoretical methods. J Polym Res , 19.

[8] Jang, B. C., Huh, S. Y., Jang, J. G., and Bae, Y. C. (2001). Mechanical properties and morphology of the modified HDPE/starch reactive blend. Journal of Applied Polymer Science , 82, 3313-3320.

[9] Liu, H., Song, W., Chen, F., Guo, L., and Zhang, J. (2001). Interaction of microstructure and interfacial adhesion on impact performance of polylactide (PLA) ternary blends. Macromolecules , 44, 1513-1522.

[10] Kim, S., Park, C. E., and An, J. H. (1997). The effect of functional group content on poly(ethylene terephthalate)/high density polyethylene blends compatibilized with poly(ethylene-co-acrylic acid). Polymer Journal , 29, 274-278.

[11] Otocka, E. P., and Kwei, T. K. (1968). Properties of ethylene-acrylic acid copolymers. Macromolecules , 1, 244-249.

[12] Wu, C. S. (2005). Improving polylactide/starch biocomposites by grafting polylactide with acrylic acid-characterization and biodegradability assessment. Macromol Biosci , 5, 352-361.

[13] Jeziorska, R. (2005). Studies on reactive compatibilisation of polyamide 6/poly(butylene terephthalate) blends by low molecular weight bis-oxazoline. Polymer Degradation and Stability , 90, 224-233.

[14] Shi, Q., Chen, C., Gao, Lei., Jiao, L., Xu, H., and Guo, W. (2011). Physical and degradation properties of binary or ternary blends composed of poly(lactic acid), thermoplastic starch and GMA grafted POE. Polymer Degradation and Stability , 96, 175-182.

[15] Tsuji, H., Sawada, M., and Bouapao, L. (2009). Biodegradable polyesters as crystallization-accelerating agents of poly(L-lactide). Applied Material & Interfaces , 1(8), 1719-1730.

[16] Su, Z., Li, Q., Liu, Y., Hu, G. H., and Wu, C. (2009). Compatibility and phase structure of binary blends of poly(lactic acid) and glycidyl methacrylate grafted poly(ethylene octane). European Polymer Journal , 45, 2428-2433.

[17] Song, W., Liu, H., Chen, F., and Zhang, J. (2012). Effects of ionomer characteristics on reactions and properties of poly(lactic acid) ternary blends prepared by reactive blending. Polymer , 53, 2476-2484.

[18] Righetti, M. C., Cardelli, C., Scalari, M., Tombari, E., and Conti, G. (2002). Thermodynamics of mixing of poly(vinyl chloride) and poly(ethylene-co-vinyl acetate). Polymer , 43, 5035-5042.

[19] Pracella, M., Pazzagli, F., and Galeski, A. (2002). Reactive compatibilization and properties of recycled poly(ethylene terephthalate)/polyethylene blends. Polymer Bulletin , 48, 67-74.

[20] Liu, B., Jiang, L., Liu, H., and Zhang, J. (2010). Synergetic effect of dual compatibilizers on in situ formed poly(lactic acid)/soy protein composites. Ind. Eng. Chem. Res , 49, 6399-6406.

[21] Xu, Y. Q., and Qu, J. P. (2008). Mechanical and rheological properties of epoxidized soybean oil plasticized poly(lactic). Journal of Applied Polymer Science , 112, 3185-3191.

[22] Dongdong, L., Baoqing, S., and Zhixue, W. (2011). Morphology, Rheology, and Mechanical Properties of Polylactide/Poly(Ethylene-co-octene) Blends. Journal of Macromolecular Science, Part B: Physic , 50, 2050-2059.

[23] Souad, D., and Nacereddine, H. (2013). Structural, morphological and mechanical characteristics of polyethylene, poly(lactic acid) and poly(ethylene-co-glycidyl methacrylate) blends. Iran Polym J, 22, 245-257.

[24] Kylma, J., Tuominen, J., Helminen, A., and Seppala, J. (2001). Chain extending of lactic acid oligomers. Effect of 2,2'-bis(2-oxazoline) on 1,6-hexamethylene diisocyanate linking reaction. Polymer, 42, 3333-3343.